The Pennsylvania State University

The Graduate School

Department of Energy and Mineral Engineering

DEVELOPMENT OF ARTIFICIAL EXPERT RESERVOIR CHARACTERIZATION TOOLS FOR UNCONVENTIONAL RESERVOIRS

A Dissertation in

Energy and Mineral Engineering

by

Amir Mohammadnejad Gharehlo

Submitted in Partial Fulfillment
of the Requirements
for the Degree of

Doctor of Philosophy

May 2012

The dissertation of Amir Mohammadnejad Gharehlo was reviewed and approved* by the following:

Turgay Ertekin
Professor of Petroleum and Natural Gas Engineering
Dissertation Co-Advisor
Co-Chair of Committee

Luis F. Ayala H.
Associate Professor of Petroleum and Natural Gas Engineering
Dissertation Co-Advisor
Co-Chair of Committee

R. Larry Grayson
Professor of Energy and Mineral Engineering
Graduate Program Officer of Energy and Mineral Engineering

Zuleima T. Karpyn
Associate Professor of Petroleum and Natural Gas Engineering

Antonio Nieto
Associate Professor of Mining Engineering

Mirna Urquidi-Macdonald
Professor of Engineering Science and Mechanics

*Signatures are on file in the Graduate School

ABSTRACT

With the decline in production from conventional hydrocarbon resources, new focus has been shifted to unconventional resources. However, oil and gas production from these types of hydrocarbon resources is not as easy as producing from the conventional resources because of the complex geological features and lack of new technologies. Soft computing techniques such as artificial neural networks provide new approach as that can be used in the characterization of the complex unconventional reservoirs. In this study, artificial expert systems were developed with the purpose of characterizing an unconventional oil reservoir located in West Texas. These expert systems are capable of generating synthetic well logs, completion parameters, production profiles and performing the task of payzone identification. This study focuses on the generation of synthetic well logs and the identification of payzones using artificial expert systems. Synthetic well log prediction module is divided into low-resolution and high-resolution categories where five different well logs are predicted at desired reservoir locations. While low-resolution well logs are predicted using the averaged seismic data, the high-resolution well logs are predicted using detailed 3D seismic data. Training of the networks to predict high-resolution well logs is found to be more successful than that of low-resolution well logs. Predicted synthetic well logs are then used to predict completion data, production profiles and payzone identification.

The second module of this research involves payzone identification in which the gross thickness of the reservoir is ranked based on its productivity level. Payzone identification is achieved through the implementation of artificial expert systems developed to predict well performance (i.e. oil, water, and gas production profiles). Using a moving-window approach to sample seismic and well log data along the well depth and by feeding the sampled information to the well performance network, it is possible to predict the productivity of each sampled segment. Another outcome of the payzone identification study is the possibility of scrutinizing the

relationship between well log parameters and expected productions. A Fuzzy classification method is used to classify production data in terms of lithology logs. One of the outcomes of this classification is the realization that oil production is expected to be higher in shaly segments of the well than that of carbonate segments.

TABLE OF CONTENTS

LIST OF FIGURES

LIST OF TABLES

ACKNOWLEDGEMENTS

- I have been indebted in the preparation of this thesis to my advisers, Dr. Turgay Ertekin and Dr. Luis Ayala, for their patience, kindness, and thoughtful guidance.
- I would like to express my gratitude to Dr. Zuleima Karpyn for her guidance and excellent comments.
- I am extremely grateful to Chevron Company for providing the financial and intellectual support as well as providing field data for this research.
- I would like to acknowledge my mentor Dr. Farouq Ali for his helps throughout the years.
- I would like to give a special thanks to my family for supporting me. My parents have always encouraged me to pursue my dreams and follow my heart.
- Finally, I would like to thank all of my colleagues in the Department of Energy and Mineral Engineering for their support to write and present my thesis project.

Chapter 1

INTRODUCTION

With the decline in production from conventional hydrocarbon resources, the new focus has been shifted to unconventional resources. Conventional reservoirs are characterized by a high to medium permeability formation and the ability to produce hydrocarbons profitably. Unconventional reservoirs however cannot be produced economically without assistance from special recovery process (Holditch, 2009). Examples of the unconventional resources are tight gas and oil reservoirs, coalbed methane, heavy oil, gas shales, and gas hydrates. The distribution of the unconventional resources is presented in Figure 1.1. Conventional reservoirs are located on the top of the resource triangle while unconventional reservoirs are located near the base of the triangle. The size of unconventional resources is much larger than conventional resources but they are more expensive to produce and require new technologies. Figure 1.2 shows natural gas production in United States. With the growing demand in energy in next decades, unconventional resources such as shale gas, tight gas, and coalbed methane are expected to play an increasingly crucial role in supplying world energy.

Hydrocarbon reservoirs also can be classified in terms of reservoir rock and fluid types as shown in Figure 1.3. If either the reservoir fluid or rock type is unconventional, the reservoir is classified as an unconventional reservoir. Examples of unconventional fluids are: heavy oil, bitumen, immature oil, and immature methane gas with high percentages of H_2S, CO_2, and carbon monoxide. Unconventional reservoir rock types are low permeability, coals, shale plays, and complex geological system. Perhaps, the most challenging type of unconventional reservoirs is those with unconventional rock types located in complex geological systems which is the subject of this study. Also, considering the fact that majority of the unconventional reservoirs require

some type of costly well stimulation and special recovery process to increase the well productivity and to be able to develop the field under economic limits, development of the intelligent reservoir characterization tools for unconventional resources is necessary.

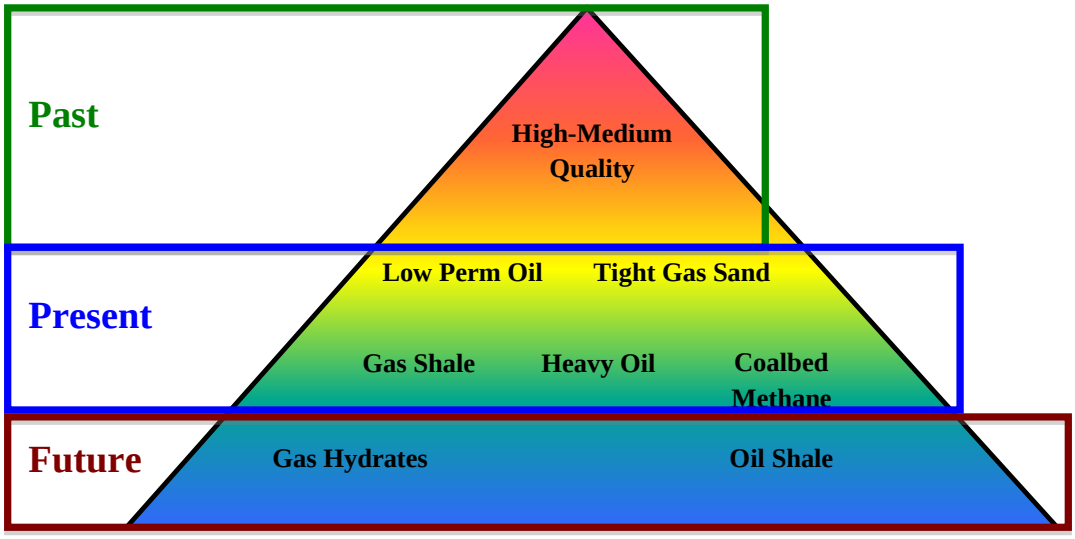

Figure 1.1: The resource triangle for oil and gas reservoirs (Holditch, 2006).

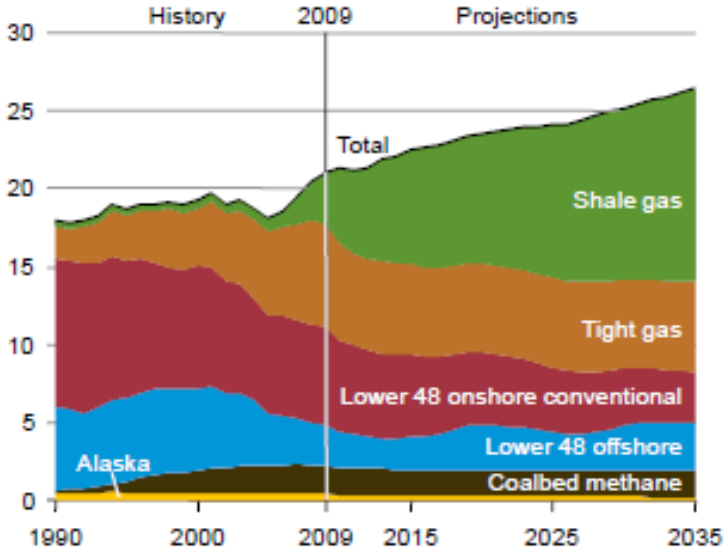

Figure 1.2: Total U.S. natural gas production in five cases, 1990-2035 (trillion cubic feet)(EIA, 2010).

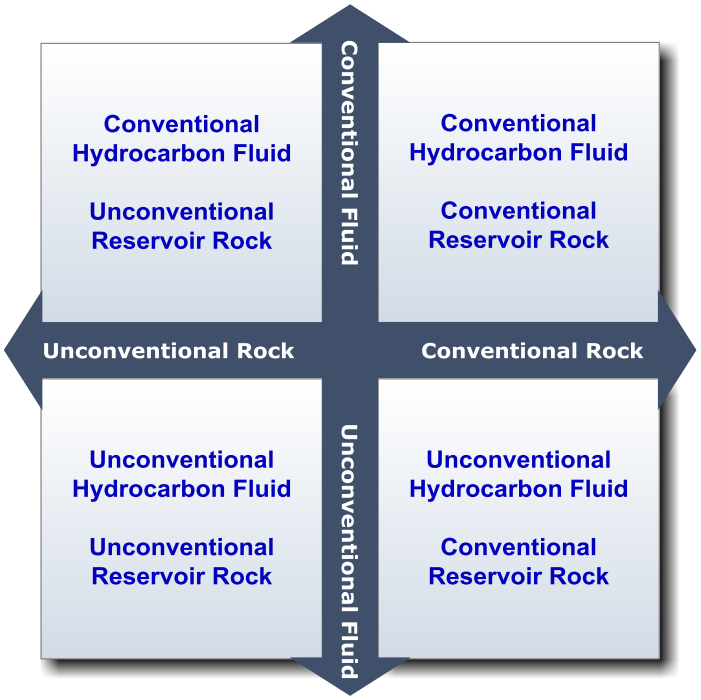

Figure 1.3: Classification of unconventional hydrocarbon reservoirs(Russum, 2010).

In order to maximize the value of a hydrocarbon asset, building a detailed reservoir model is necessary. The process of reservoir management is visualized in Figure 1.4. One of the key parts in this process is reservoir characterization and identifying important characteristics of the reservoir. Many decisions such as number and types of infill drilling wells, field development strategies, economic and risk evaluation, and forecasting future reservoir performance are made based on reservoir characterization studies. To characterize the reservoir accurately, integration of multi-disciplinary data such as seismic, well logs, production data, and completion data using an intelligent system is necessary. The final product is the reservoir model with a realistic tolerance for uncertainty (Tamhane et al., 2000). One class of solutions to the reservoir characterization problem is using soft computing techniques. Soft computing techniques have tolerance for imprecision and uncertainty and are efficient, low cost and robust (Nikravesh and Aminzadeh,

2001). The aforementioned properties of soft computing techniques can significantly assist reservoir characterization.

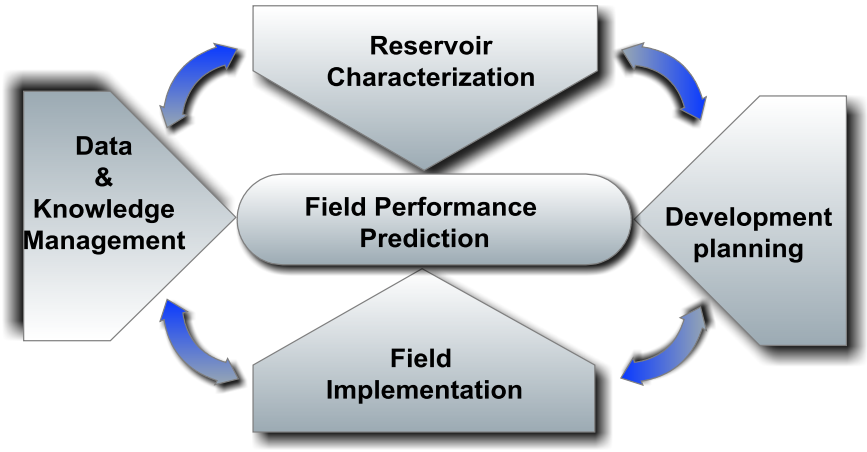

Figure 1.4: Schematic of reservoir management and field development cycle

Two important aspects of reservoir characterization include finding reservoir properties away from the wellbores and identifying the most productive zones of the reservoir both spatially and vertically. Well logs are obtained for the purpose of estimating recoverable hydrocarbon volumes, lithology identification, porosity estimation, and locating lithological boundaries. One of the most important reasons to perform well log analysis on a well is to estimate recoverable hydrocarbon volumes. Unfortunately, well logs can only estimate reservoir properties near wellbore region. Measurements of the reservoir properties across the entire reservoir are desirable to proper reservoir management and production optimization. Thus, remote geophysical measurements are required to find the reservoir properties between the wells (MacGregor et al., 2008). Seismic data are the most commonly used geophysical measurements for this purpose. In general, data from the well logs and seismic attributes are often difficult to analyze because of their complexity and lack of knowledge how to use the information content of these data

(Nikravesh and Hassibi, 2003). Accordingly, it is necessary to develop an intelligent system to assist reservoir characterization and perform the suggested tasks.

Another crucial aspect of reservoir characterization is addressing the identification of prolific zones along the cross section of the reservoir. Net pay is a key parameter in reservoir evaluation, completion and stimulation design. It identifies geologic sections that have sufficient reservoir quality and hydrocarbons to function as producing interval (Worthington, 2010). The most common method in the identification of the net pays is using geologic well logs and through the use of petrophysical cut offs applied to the well logs. This method is successfully used in conventional reservoirs; however in many unconventional reservoirs especially those with unconventional and complex reservoir rock, they are not successful and there exists the need for developing more sophisticated methods for such reservoirs.

Therefore, this research aims to develop intelligent reservoir characterization tools for unconventional reservoir structures and address following critical factors for developing unconventional resources:

1. Prediction of well performances
2. Estimation of ultimate recovery
3. Optimal development plans
4. Reservoir properties estimation away from the wellbores
5. Identification of prolific intervals of the reservoir

Intelligent reservoir characterization tool is a complex system, inetgrating different sources of information. However, the available data for such a system are from different kinds: qualitative, quantitative, and related to different types of measurements. Thus, one essential challenge is to account for available data (Schatzinger and Jordan, 1999). In this study well logs, production data, seismic data (2D and 3D), completion, and coordinate data are available. So intelligent tools are developed in such a way to take advantage of the afroementioned data.

The first objective of this research involves prediction of synthetic well logs. The importance of the synthetic well logs lies on the ability to estimate geological properties away from wellbore locations. In this study, two types of synthetic well logs are predicted:

I. Low-resolution well logs: consists of 50 log values for the entire gross thickness of the reservoir. This type of well logs are used for predicting well performances (oil, water and gas cumulative productions).

II. High-resolution well logs: consists of 350 log values for the entire gross thickness of the reservoir. This type of well logs are used to identify net pay and rank gross thickness of reservoir based on productivity.

The second objective involves identification of prolific intersections of the reservoir, i.e. payzone identification. This is particularly important in completion and fracturing optimization in which net pay thickness is of crucial relevance. Volumetric calculation of reserves is also another important outcome of net pay identification as discussed in Chapter 2.

Figure 1.5 presents a schematic of the proposed research workflow. In the first module using seismic data and coordinates information, two types of well logs are predicted namely low-resolution well logs "A_{LR}" and high-resolution well logs "A_{HR}". Then in module "B", in addition to seismic and coordinates data, predicted low-resolution well logs are used to estimate completion data. Using predicted well logs, completion data and seismic data, in module "C", oil, water and gas cumulative production profiles are predicted for two-year history of the well with the intervals of 3 month. Finally, using the networks developed in module "C", gross thickness of the reservoir is ranked based on the productivity at any given location (module "D"). Modules B and C are developed in the work by Y. Bansal (Bansal, 2011) and modules A and D are developed in this study. All modules are integrated within a graphical user interface.

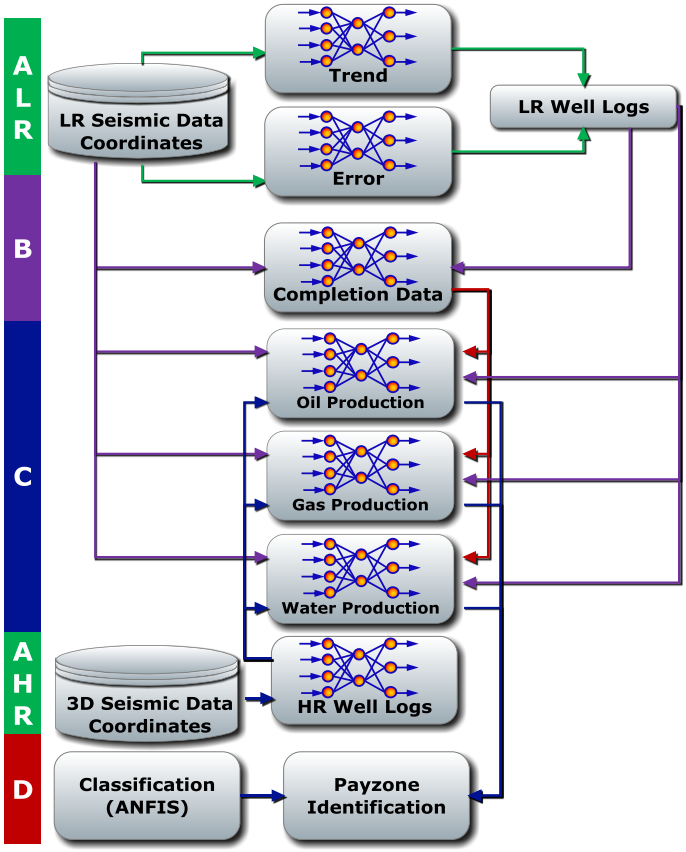

Figure 1.5: Schematic of the proposed research workflow

This thesis consists of seven chapters. Chapter 1 addresses the urgency of developing intelligent reservoir characterization tools for oil industry, and discusses various sources of information that needs to be integrated in the tool. Different modules of the research are explained. Workflow of the research and relationships between different components are described.

Chapter 2 involves a review of the literature on the research associated with the intelligent reservoir characterization. Background information about reservoir characterization techniques, soft computing methods, and artificial neural networks are provided in this chapter. Also, seismic and well log data are studied in more details.

Chapter 3 provides a general description of the problems to be solved and their impacts on the current industry solutions to mitigate these problems.

Chapter 4 presents the proposed methodologies for developing intelligent reservoir characterization tools. These methodologies are strongly influenced by the availability of different sources of information and tailored for particular data set.

Chapter 5 discusses the case study used to test the developed methodologies. Case study presented is an unconventional oil reservoir located in West Texas. Complex and discontinuous geology of this reservoir imposes several difficulties for deterministic modeling.

Chapter 6 illustrates the results of synthetic well log generation and payzone identification modules. Also, it involves another outcome of this research that is predicting well log values for the missing parts of the actual well logs.

Chapter 7 summarizes the work, the accomplishments, and major conclusions of this study. Recommendations for future research are given and possibility of the improvement of networks based on the availability of new pieces of information is explored.

Chapter 2

BACKGROUND AND LITERATURE REVIEW

Predicting geological properties such as porosity, permeability, water saturation, etc. are crucial in petroleum engineering. This is mainly because of their important effects in volumetric reserve calculations, wellbore completion and stimulation. One of the most commonly employed procedures worldwide is to use deterministic equations for calculating reserves. Equation (2-1) is a typical deterministic equation used for calculating original oil in place (Bassiouni et al., 1994; Helander, 1983):

$$OOIP = \frac{7758\, A\, h\, \phi\, (1 - S_w)}{B_{oi}} \tag{2-1}$$

Where:

$OOIP$: Stock tank original oil in place, in Bbls

A: Reservoir closure area, in acres

h: Average reservoir (net) thickness, in feet

ϕ: Average reservoir decimal porosity

S_w: Average reservoir decimal water saturation

B_{oi}: Initial oil formation volume factor

7758: Acre-ft to Bbls conversion factor

Areal extent of the reservoir is generally obtained from the seismic exploration analysis. Reservoir thickness, porosity, and water saturation are obtained from geophysical well log analysis. The scale and uncertainty of various sources of information such as core data, well log, and seismic data are presented in Figure 2.1. Core data are obtained by testing on the samples of formation rock. Data obtained from core analysis have high resolution however they suffer from

sampling bias and other problems such as damaged core plugs (Honarpour et al., 2003). Well log data are measured physical properties of rock at the well locations. Well log data have intermediate resolution and suffers from washouts, acquisition tool problems, and imprecision of the measurement system due to environmental conditions (Verga et al., 2002). The next important source of information is seismic data which is available over entire field. The uncertainty associated with seismic data is mainly related to the data acquisition tools and post-processing algorithms. In this study, well logs and seismic data are used extensively; therefore, in the next two chapters these sources of information are briefly discussed. Also, reservoir thickness (i.e. net pay) is discussed in more details.

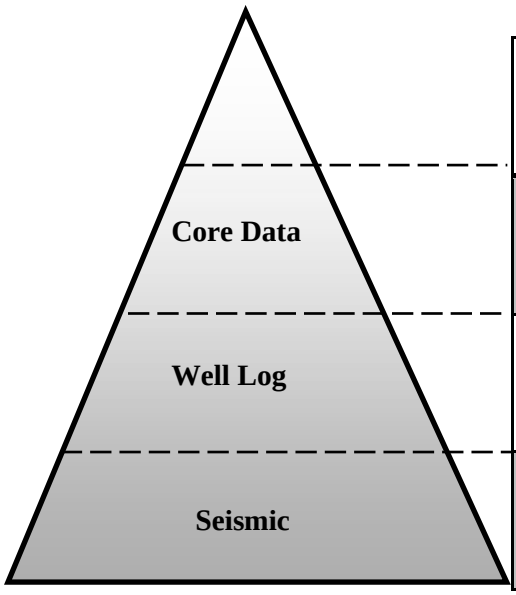

Scale	Uncertainty	Availability
$< 0.01\ m$	Sampling bias; Damaged plugs	Wellbore: Special cross section of wellbore
$0.1\ to\ 1\ m$	Washouts; tool problems	Wellbore: Mostly entire gross thickness of reservoir
$> 1\ m$	Acquisition and processing artifacts	Entire field: discreet points scattered over the entire field

Figure 2.1: Scale and uncertainty of reservoir characterization (Nikravesh and Hassibi, 2003)

Seismic Exploration

Petroleum reservoir exploration consists of wide variety of methods such as seismic, gravity, magnetic, etc. The goal of each method is to measure a parameter that relates to a physical property of rock (Gadallah, 1994). Geophysical survey methods are listed in Table 2-1.

Table 2-1: Geophysical surveying methods (Gadallah, 1994)

Method	Measured Parameter	Physical Properties Derived
Seismic	Travel time and reflected seismic waves	Density and elastic moduli which determine the propagation velocity of seismic data
Gravity	Variations in earth's gravitational field	Density
Magnetic	Variations in earth's geomagnetic field	Magnetic susceptibility and resonance
Electrical density	Earth's resistance	Electrical conductivity
Induced polarization	Frequency-dependent ground resistance	Electrical capacitance
Self-potential	Electrical potential	Electrical conductivity
Electromagnetic	Response to electromagnetic radiation	Electrical conductivity and inductance

While all methods can be used for reservoir exploration, seismic method is the most commonly used method, which can deliver extensive and comprehensive image of the reservoir.

In this method, energy source located on the surface of the earth (or submerged in the water in case of offshore exploration) generates low frequency sound waves. Then, the sound waves reflect toward surface because of changes in rock properties where receivers record the signals, travel time, etc. Depending on the locations of geophones (receivers) and energy sources, seismic profiles can be recorded in 2D or 3D. A 2D seismic is recorded using straight lines of receivers and energy sources crossing the surface of the earth. The data is gathered over a horizontal distance and compiled to create cross section of the earth (Berger and Anderson, 1981). Although 2D profiles are less expensive to obtain, they do not yield the correct image of subsurface when a complex subsurface structure exists. This is mainly because of acquisition geometry cannot distinguish reflections that originates from the outside of the vertical profile plane (Holstein, 2007). The limitations of 2D seismic imaging are overcome by the advent of 3D seismic method. In this method, data is recorded from the numerous closely spaced seismic lines providing a high spatially sampled measure of subsurface reflectivity (Glossary, 2010). 3D seismic data provides continues 3D sampling of the sub-surface (i.e. 3D volume)(Bacon et al., 2003; James, 2009). Schematics of the 2D and 3D seismic surveys are demonstrated in Figure 2.2.

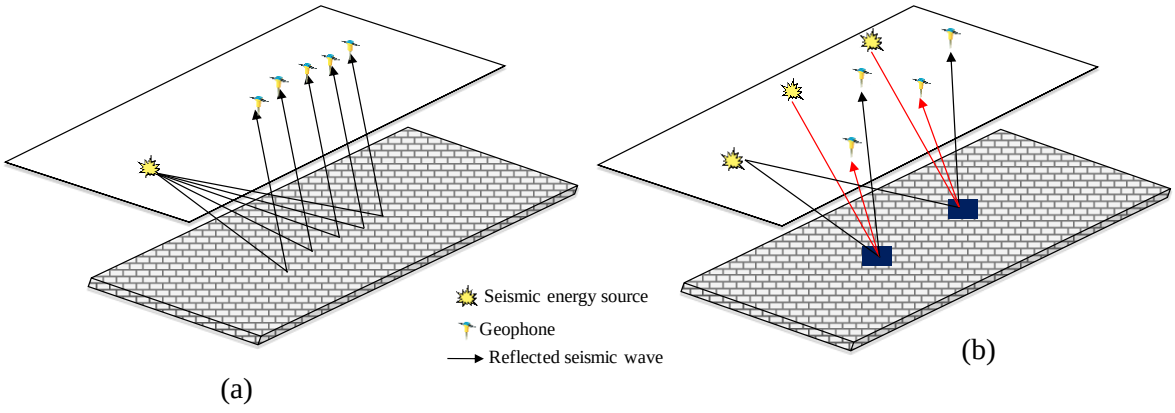

Figure 2.2: Schematic of 2D and 3D seismic surveys, (a): 2D seismic, (b): 3D seismic

The main source of information for seismic reservoir exploration is the seismic attributes. Seismic attributes are the information obtained from the seismic data either by direct measurement or by logical or experience-based reasoning (Taner et al., 1979). Attributes are derived based on important seismic characteristics such as time, amplitude, frequency, and attenuation. Seismic attributes are divided into two categories (Chen and Sidney, 1997):

- Horizon based: average properties are computed between two geologic boundaries.
- Sample based (or windowed attributes): use the sample values such as 2 or 4 ms intervals to produce a new output trace with the same number of samples as input.

The process of adding seismic traces to improve data quality and reduce noise is called seismic data stacking. Seismic attributes are then can be computed using pre and post stacking procedure. Pre-stack attributes have azimuth and offset information. Post-stack attributes tend to lose offset and azimuth information because of the stacking procedure. However, they are preferable because the pre-stack seismic data are comprised of huge amount of data and they are not practical for initial studies (Taner et al., 2005). Classification of the seismic attributes is presented in Figure 2.3.

Post-Stack		Pre-Stack
Horizon	**Window**	
Time Isochron Trend Residual Dip Azimuth Difference Edge Illumination Instantaneous Phase Cosine Phase Curvature Roughness	Coherence Continuity Semblance Covariance Peak-trough diff Dip Max Correlation Azimuth max corr Signal to noise ratio Parallel bed indicator Chaotic bed indicator Trace difference	Velocity

Post-Stack				Pre-Stack
Horizon	**Window**			
Reflection amplitude Composite amplitude Relative amplitude Reflection strength Amplitude ratio Amplitude over background	**Gross**	**Selection**	**Distribution**	AVO Intercept AVO gradient Intercept X gradient Far-near difference Fluid Factor
	Total absolute amp. Total energy Average absolute Average reflection strength RMS amplitude Average peak amplitude Variance of amplitude Percent grater than	Maximum amplitude Largest negative amplitude Maximum absolute amplitude Peak-through difference	Energy half-time Slope reflection strength Slope at half energy Ratio positive to negative	

Post-Stack			Pre-Stack
Horizon	**Window**		
Instantaneous freq. Response freq. Envelope-weighted inst. freq. Time serivative freq.	**Gross**	**Hybrid**	
	Reflection width Average inst. frequency RMS inst. frequency No. zero crossing Peak spectral freq. 1st dominant freq. 2nd dominant freq. 3rd dominant freq. Spectral bandwidth	Wave shape Loop area Arc length	

Post-Stack	Pre-Stack
Inst. Q factor Slope spectral freq. Slope inst. freq	

Figure 2.3: Seismic attributes classification (Brown, 2001)

Well Log Data

Petrophysical well logs are continuous measurements of physical parameters in the wellbore. The measured physical properties reflect characteristics of the formations at the location of well. Well log information contributes to the evaluation of lithology, porosity, saturation, and reservoir thickness. One of the earliest and most important quantities measured by well logs is electrical resistivity. Hydrocarbons and reservoir rocks are insulators, whereas connate waters are saline and good conductors. Archie (Archie, 1942) developed the basic relationship of electrical resistivity and formation properties, [Equation (2-2)]. He observed that in the fully water saturated rocks, the rock resistivity R_o is proportional to the resistivity of brine R_w and formation factor F. Formation factor is determined by the porosity and the pore structure properties such as cementation factor m and the lithology dependent constant a. Finally water saturation is determined from the ratio of rock resistivity to that of brine.

$$\begin{cases} R_o = F \times R_w \\ F = \dfrac{a}{\phi^m} \\ S_w^n = \dfrac{R_o}{R_w} \end{cases} \tag{2-2}$$

Archie's model was developed for a clean formation rocks and adjustments should be made in case of presence of clay, shale, and heterogeneity (Luthi, 2001). To date, well logs remain the most important source information for the purpose of formation evaluation. A complete list of quantities derived from the well logs is presented in Table 2-2.

Table 2-2: Comparison of different derived from well logs (Serra and Abbott, 1982; Tittman, 1986)

Primary Purpose	Tool/Technique
Lithology	Spontaneous Potential (SP) Gamma Ray (GR) Side Wall Cores (SWC) Photo-Electric Factor (PEF) Tri-Mineral, MID, & MN Plots
Porosity	Density (RHOB) Nuclear Magnetic Resonance (NMR) Neutron (NPHI) Acoustic (ΔT) Cross-Plots
Salinity/Water Resistivity	Spontaneous Polarization (SP) R_{wa} Analyses Hingle Plots Pickett Plots
Saturation	Resistivity (ES) Induction (IES, DIL) LateroLog (LL, LL3, DLL) Array Induction (AIT)
Flushed Zone Saturation	MicroSpherically Focused Log (MSFL) MicroLateroLog (MLL) Dielectric Constant (EPT, DPT) Nuclear Magnetic Resonance (MRL)
Permeability	Nuclear Magnetic Resonance (MRL) Formation Testers (FT, RFT, MDT)
Fluid Identification	Formation Testers Density/Neutron Overplot FID Plot S_w Tools
Structural/Stratigraphic Information	Dipmeter (HDT, SHDT) Borehole Televiewer (BHTV) Resistivity Microscaners (FMS/FMI) Nuclear Magnetic Imagers (NMI)
Borehole Imaging	Borehole Televiewer (BHTV) Resistivity Microscaners (FMS/FMI) Nuclear Magnetic Imagers (NMI)
Borehole Temperature	Temperature (TEMP)
Formation Pressure	Formation Testers (FT, RFT, MDT)
Borehole Shape	Caliper (CAL)

Net Pay

Net pay is a thickness of the reservoir containing significant volume of potentially exploitable hydrocarbons (Worthington, 2010). The term derives from the fact that it is capable of "paying" an income and also sometimes called pay zone (Glossary, 2010). The significance of net pay lies in the original hydrocarbon place, calculations of ultimate recovery factors, well test interpretations, stimulation and completion designs (Egbele et al., 2005). Net pay identification is the process of pinpointing the prolific intervals of the formation. Figure 2.4 shows relationships between net thicknesses and their terminologies.

The most common method to identify net pay is to select intervals based on their corresponding well log characteristics. This is achieved by the use of petrophysical cutoffs limiting values of formation parameters and removing the noncontributing intervals (Worthington and Cosentino, 2003). Snyder (Snyder, 1971) discusses the early methods to identify net pays using self-potential (SP), gamma ray (GR), porosity logs (NPHI) and core data. Cobb (Cobb and Marek, 1998) provides guidelines for selecting cut offs based on various reservoir properties. Although the early methods are to an extent effective, there exists the need to quantify the values of the cut offs. Worthington (Worthington and Cosentino, 2003) describes the primary method to discover net pay is to link a conventional core measurement to a refrence parameter that distinguishes between reservoir and non-reservoir rock. He proposes using the Leverett pore diameter expression as a referrence criteria for primary depletion. Others propose using different methods such as discriminnant analysis(Bouffin and Jensen, 2009), regression between log data and core paramaters (mainly permeability and porosity) (Egbele et al., 2005), and integrated use of seismic and well data (Azalgara and Floricich, 2001).

Although net pay identifcation is a complex procedure even for conventional reservoirs, it becomes increasingly complex for unconventional reservoirs. For example, in shale reservoirs,

the aforementioned method is not applicable because formation is mainly comprised of shales and relatively small porosity. Johnston (Johnston and Lee, 1992) provides guidelines for peaking the payzones in low permeability, multilayered gas reservoir using sensitivity analysis on the two-layered simplified reservoir model. Several studies attempt to identify payzones in terms of hydraulic flow units (HFU) (Abbaszadeh et al., 1996; D'Windt, 2007; Guo et al., 2010). A flow unit is identified as volume of the rock where pore throat properties of the porous media that govern hydraulic characteristics of the rock are consistently predictable and significantly different from those of other rocks (Abbaszadeh et al., 1996). Many authors have developed methods to characterize hydrualic flow units based on the injection and production flow rates (Ershaghi et al., 2008; Lee et al., 2011; Lee et al., 2009; Lin et al., 2010; Liu et al., 2009). These methods are developed for waterflooding processes and their main goal is to map the high permeability channel that affects water production rates. The HFU methods are more applicable for a field with wide range of permeability. For tight systems in which the permeability of the formation is low and high permeability channels are not present, the HFU method is not applicable since other factors such as well stimulation properties have more significant role in production predictions.

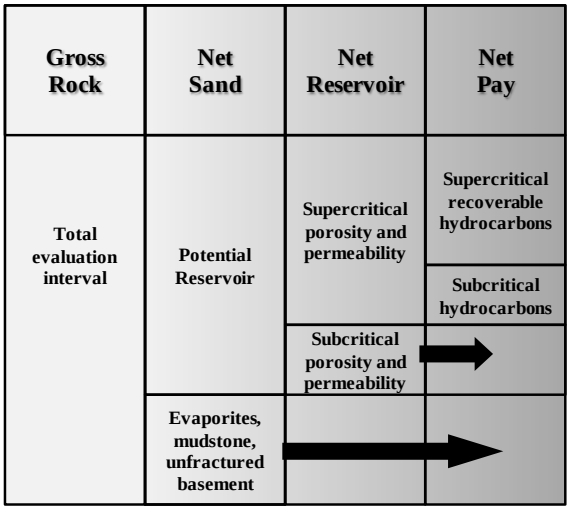

Figure 2.4 Interrelationships of net thicknesses (Worthington, 2010)

Soft Computing

Soft computing is the collection of techniques that uses the human mind as model aiming to formalize human cognitive processes (Cabrera et al., 2009). The main characteristics of this class of methods are their ability to handle uncertainty and imprecision. The objective of the soft computing methods is to produce low cost, analytic and complete solutions for complex systems in which traditional computational methods have not yielded such solutions (Zadeh, 1994). Soft computing techniques are comprised of fuzzy logic, neuro-computing, evolutionary and genetic computing, and probabilistic computing. Artificial neural networks are one of the main branches of soft computing. They have been used in numerous applications such as signal processing, image processing, control, etc.

In many aspects of reservoir engineering, artificial neural network have been used. Petrophysical properties estimation using artificial neural networks such as permeability estimation (Basbug and Karpyn, 2007; Elshafei and Hamada, 2009a; Malki et al., 1996; Mohaghegh et al., 1995; Shokir et al., 2006), hydrocarbon saturation estimation (Balch et al., 1999; Elshafei and Hamada, 2009b), and relative permeability predictions (Guler et al., 2003; Silpngarmlers et al., 2001) have been widely studied for different scenarios. Neural network applications in reservoir engineering also include PVT and fluid analysis (Elsharkawy, 1998; Hegeman et al., 2009; Panda et al., 1996), history matching (Ramgulam, 2006; Sampaio et al., 2009; Silva et al., 2006), and field development strategies (Ayala et al., 2007; Centilmen et al., 1999; Doraisamy et al., 2000; Gorucu et al., 2005). Since in this study artificial expert systems are used to perform reservoir characterization tasks, in the upcoming sections artificial neural networks and reservoir characterization techniques are described in more details.

Artificial Neural Networks (ANN)

Artificial neural networks were first introduced in late 1950s by McCulloch and Pitts (McCulloch and Pitts, 1943) and later with the invention of perceptrons by Hebb and Rosenblatt (Hebb, 1949; Hebb, 1961; Rosenblatt, 1957) . Minsky (Minsky and Seymour, 1969) showed the deficiencies of perceptron in representing linearly inseparable functions such as exclusive OR problem (XOR). However, for more than twenty years interests in artificial neural networks diminished before works by scholars such as Hopfield (Hopfield, 1982), (Kohonen, 1988), and (Hecht-Nielsen, 1990) reinvigorated the use of artificial neural networks. Since then, ANNs have been implemented to solve wide verity of problems such as:

- Face Recognition (Lawrence et al., 1997)
- Speech recognition (Sejnowski et al., 1990)
- Textual characters recognition (Le Cun et al., 1990)
- Control (Omatu et al., 1996)
- Stock market performance prediction (Zirilli, 1997)
- Economics and finance (Zhang and Hu, 1998)
- Robotics and system dynamics (Lewis, 1996)

Artificial neural networks offer a radically different approach in solving complicated problems by providing self-programming and self-learning tools. Comparisons of artificial neural networks and Von Neumann model of computation is given in Table 2-3. The Von Neumann computational design is a model for digital computers using central processing unit and separate storage structure. ANNs are massively parallel computing systems consisting of large number of processors. In comparison to Von Neumann design, artificial neural networks are self-learning,

self-programmable computational methods with the ability to handle unconstrained, poorly defined operating environment with a high fault tolerance.

Table 2-3: Comparisons of Von Neumann computers and artificial neural networks (Carpenter and Grossberg, 1991; Jain et al., 1996)

Properties	Von Neumann	ANN
Processors	Complex high speed (VLSI)	Artificial Neural Networks
Memory	Separate from processor	Integrated, Distributed content addressable
Computing	Sequential	Distributed parallel self-learning
Connections	Externally programmable	Dynamically self-learning
Fault tolerance	None without special processes	Significant
Operating environment	Well-defined, well constrained	Poorly defined, unconstrained
Programming	Rule based shell; complicated	Self-programming

Artificial neural networks are parallel computing algorithms that are designed to mimic the learning processes of human brain. Thus, in order to understand the artificial neural networks, it is recommended to study the structure of human brain. The fundamental processing unit of human brain is called neuron. Typically human brain contains more than 10 billion neurons. Each neuron has approximately 10,000 connections to other neurons (Müller et al., 1995). Incoming signals are collected by neuron receivers, *dendrites*, and the outgoing signal transmitted through signal transmitters called *axons*. The joint between the end of axon branch and other neurons is called *synapse*. Incoming signals from adjacent neurons carried by dendrites are processed in the

cell body part of the neuron called *soma*. Then the processed response value is sent out to other neurons using axons and synapses. The inputs to the neuron cause chemical reactions. When the chemicals approach to a certain threshold level, neuron discharges the expected response.

Figure 2.5 demonstrates the typical structure of a neuron in human brain. It should be noted that there are different types of neurons exist in human brain with large variations in neuron types and connections. These complexities are abstracted in brain theory to better understand the learning behavior of human brain (Arbib, 2003). Alternatively, mathematical representation of neuron is demonstrated in Figure 2.6. Inputs "$x(n)$" are fed to neuron with respective connection weight "$w(n)$". In addition to the inputs to each neuron, bias connections "$b(n)$" are also added to the neuron. Bias or threshold connections are equivalent to an intercept in a regression model. This helps the learning of the data and ultimately improves representation of the data by neural network. Each neuron contains a threshold function or activation function; responsible to control the amplitude of the neuron output and ultimately helps stabilizing the network. The typical ranges of activation functions are between 0 and 1 or -1 and 1, depending on the activation function type. Introduction of activation functions to the neural networks improve nonlinear mapping of complex problems. The mathematical equation of each neuron can be summarized by the following equation:

$$y = f\left(\sum_{i=1}^{n} x_i \cdot w_i + b\right) \tag{2-3}$$

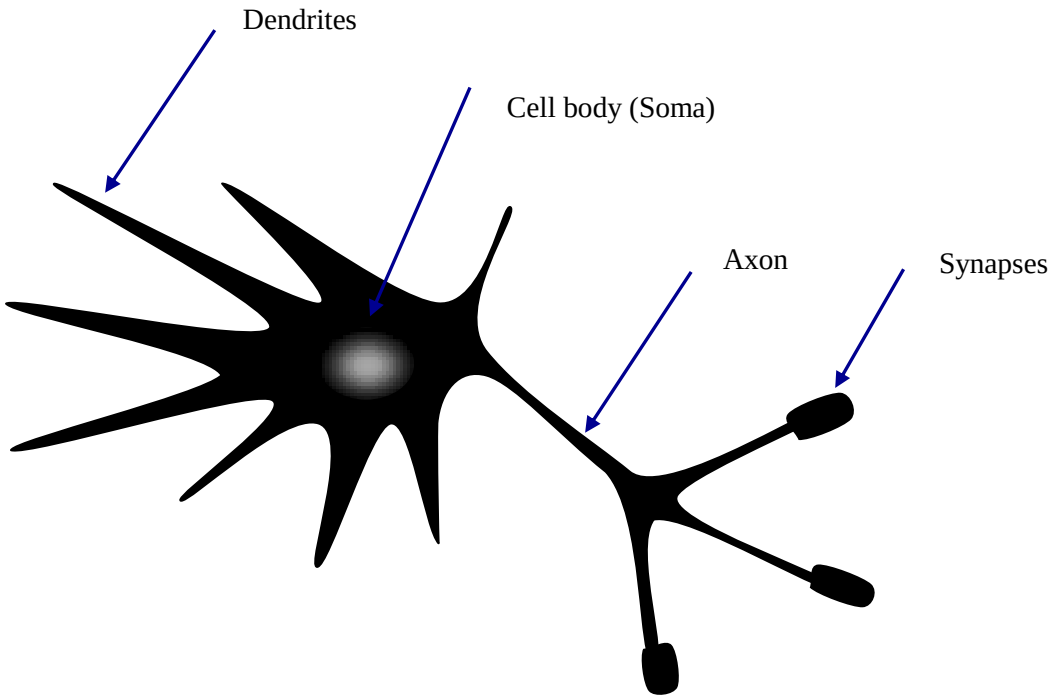

Figure 2.5: A schematic of basic neuron structure in human brain

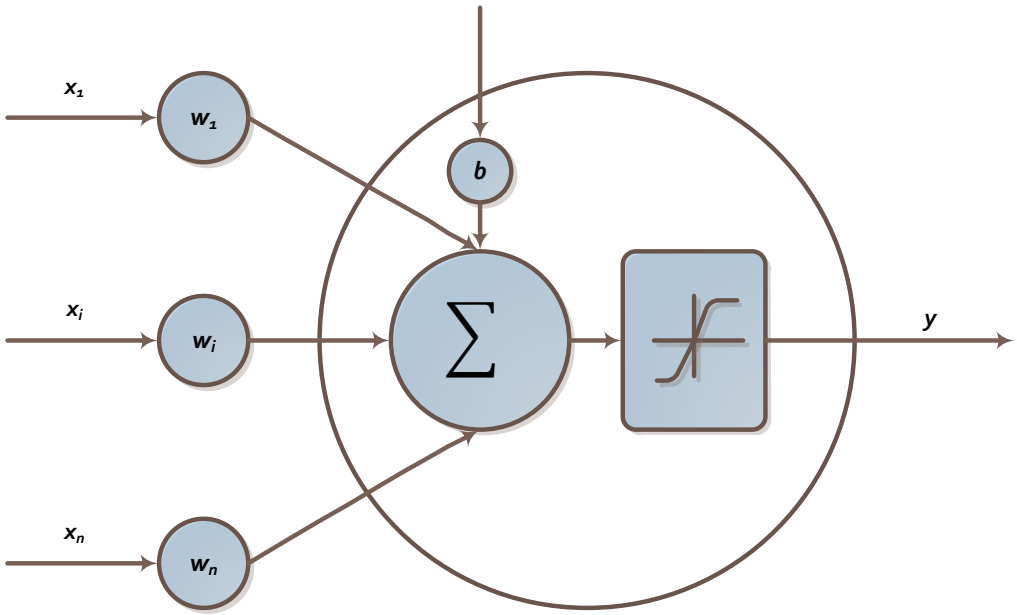

Figure 2.6: Mathematical representation of neuron; inputs denoted by "x" with weights "w" and biases "b", outputs denoted by "y"

Network Topology

Collection of multiple interconnected neurons is called neural networks. The topology of the neural network is governed by the way neurons are connected. Two main categories of network structure are: feed-forward networks and feedback networks. In feed-forward network structure information is processed in one direction only and there is no feedback or directed cycle or loop connections. On the other hand, feedback/recurrent networks can contain feedback or directed circle connections. These features can help neural networks to process sequences of inputs with internal memory of the network. Recurrent networks are mostly used to model dynamical systems (Narendra and Parthasarathy, 1990) and time series data (Giles et al., 2001).

Taxonomy of the neural network topologies is demonstrated in Figure 2.7. Perceptron is the simplest type of feed-forward neural network because it consists of a single-neuron with adjustable synaptic weights and threshold function. Perceptron is linear classifier and this makes its applicability of solving practical problems limited. However, it remains as a fast and reliable solution for simple problems. Also, analyzing the operations of perceptron provides fundamental understanding of more complex networks. Limitations of perceptron led to the invention of multilayer perceptron (MLP). MLPs are feed-forward neural networks with minimum of one hidden layer. Similar to perceptron, each processing unit has adjustable weights and nonlinear activation function. Adding nonlinear transfer functions to MLPs helps solving complex nonlinear problems. MLPs are the most popular neural network topology, used in huge number of applications. Their strength lies in robustness in modeling noisy data and ease of use. Another example of feed-forward networks is radial basis function (RBF) networks. RBF network consists of one hidden layer in which the activation of hidden layer is determined by radial basis functions. The mathematical equation of radial basis function is presented in Equation (2-4).

$$f(x) = \sum_{i=1}^{n} w_i \, \phi(\|x - x_i\|) \tag{2-4}$$

In Equation (2-4), n is the number of sampling points, x is the vector of input variables, x_i is the center of basis function ϕ, and $\|\cdot\|$ is l_p norm of vector $(x - x_i)$ (usually Euclidean distance is used) and w_i is the weight coefficients. RBF networks are capable of universal function approximation with only mild restriction on the form of the basis function (Ma et al., 2008).

The recurrent/feedback networks have wide variety of network topologies. Competitive network is one example of the recurrent neural networks comprising of two-layer network with inter-layer connections. Competitive networks' advantage lies in their ability of performing data clustering (Chartier et al., 2009). Self-Organizing Map (SOM) networks are used to classify complex data into the low-dimensional input space of data. SOM networks present a simplified relational view of a highly complex, high dimensional data. The mapping is simply done by comparing the neighborhood relationships and transforming it in the topological map. The main advantage of Hopfield network is an associative memory. In the Hopfield networks, each processing unit behaves as an elementary system in complex interaction with the rest of ensemble. They are classified as constant addressable memory systems with binary threshold units (Rojas, 1996). The adaptive resonance theory (ART) neural networks are developed based on the information process of human brain. The ART networks are defined algorithmically in terms of detailed differential equations intended as plausible models of biological neurons (Grossberg, 1987). Furthermore, the ART networks incorporate long-term and short-term memory to classify the data and gain more knowledge about data.

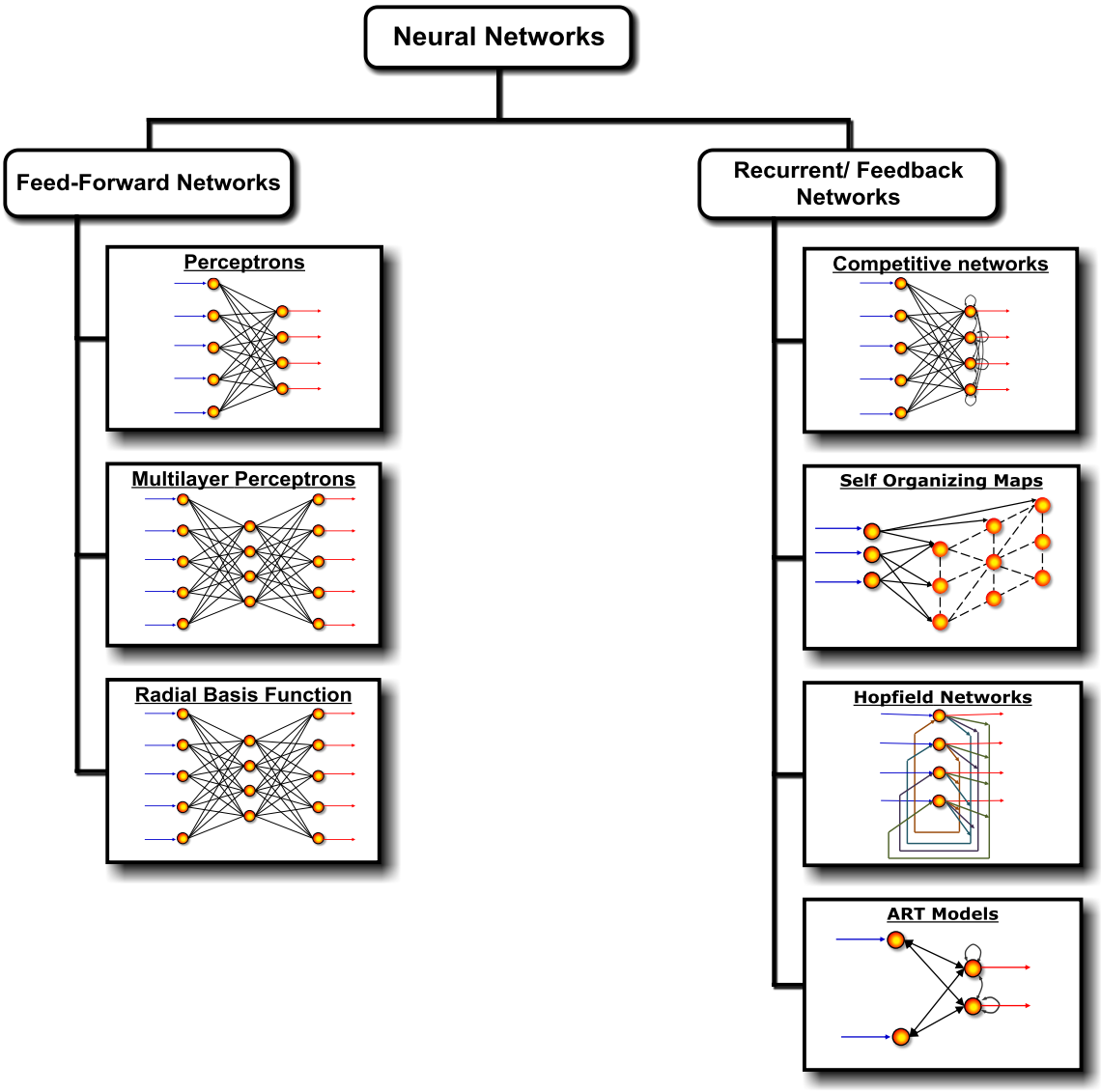

Figure 2.7: Classification of neural network topologies (Jain et al., 1996)

Learning Paradigms

One of the most important aspects of neural networks is the ability to learn complexities of the data. Learning is achieved by adjusting weight factors of neuron connections of neural network by using mathematical algorithms that depend on the network structure. Generally, there are three types of learning paradigms: supervised, unsupervised and hybrid learning. In supervised learning (often resembled as learning with a teacher), inputs and desired outputs of networks are supplied to the network in the learning stage. Then, by calculating the network error, the weights of neurons are adjusted in such a way to reduce the network error. Thus, the network learning is reduced to a minimization problem and any method such as gradient descent methods can be used to solve the problem. The aforementioned learning scheme is called error correction learning or corrective learning criteria. Another class of supervised learning is called reinforcement learning (RL). Reinforcement learning is often called learning with a critic because network learning is achieved by feedback from the given environment. Weights are reinforced for properly performed actions and punished for poorly performed actions (Simpson, 1989). The advantage of reinforcement learning is ability to learn the limited data sets (e.g. missing data).

Unsupervised learning is another type of learning paradigm in which the desired network outputs (i.e. training targets) are unavailable. To achieve learning, using unsupervised learning approach network discovers patterns, relationships or separating properties within the input data by the processes called self-organization. Unsupervised learning is mainly used to perform pattern recognition and identifying clusters (Hebb, 1949). Majority of unsupervised learning methods consists of maximum likelihood density estimation.

Hybrid learning paradigms are the combination of supervised and unsupervised learning criteria. The essence of hybrid learning is to accelerate learning process and achieve global minima. Hybrid learning is consists of network weights adjustment by error-correction and some

by automatic adjustment using patterns within the input data. Summary of learning algorithms is enlisted in Table 2-4. Since in this study backpropagation training algorithm is used, in next section backpropagation algorithm is further studied.

Table 2-4: List of famous learning paradigms algorithms (Jain et al., 1996)

Paradigm	Criteria	Architecture	Algorithm
Supervised	Error-Correction	Perceptrons & MLP	Perceptron learning, backpropagation
	Boltzman	Recurrent	Boltzman
	Hebbian	Multilayer, Feed-forward	Linear discriminant analysis
	Competitive	Competitive	Learning vector quantization
Unsupervised	Error-Correction	Multilayer, Feed-forward	Sammon's projection
	Hebbian	Feed-forward, Competitive	PCA
	Hebbian	Hopfield	Associative memory
	Competitive	Competitive	Learning vector quantization
		SOM	Kohonen's SOM
Hybrid	Error-Correction	ART, RBF	ART1, ART2, RBF learning

Activation Functions

Activation functions for the hidden layers of multilayer neural networks are necessary to introduce nonlinearity into the network. Without activation functions networks are unable to map nonlinear functions such as mapping the exclusive OR problem (XOR) using perceptrons. There are many activation functions proposed such as threshold function, symmetric saturating linear transfer function, etc.; however some learning algorithms such as backpropagation algorithm require the activation function to be differentiable. One of the most popular activation functions is the sigmoid function. The mathematical equation of sigmoid function is represented in Equation (2-5) and plotted in Figure 2.8.

$$f(x) = \frac{1}{1 + \mathrm{e}^{-c \cdot x}} \tag{2-5}$$

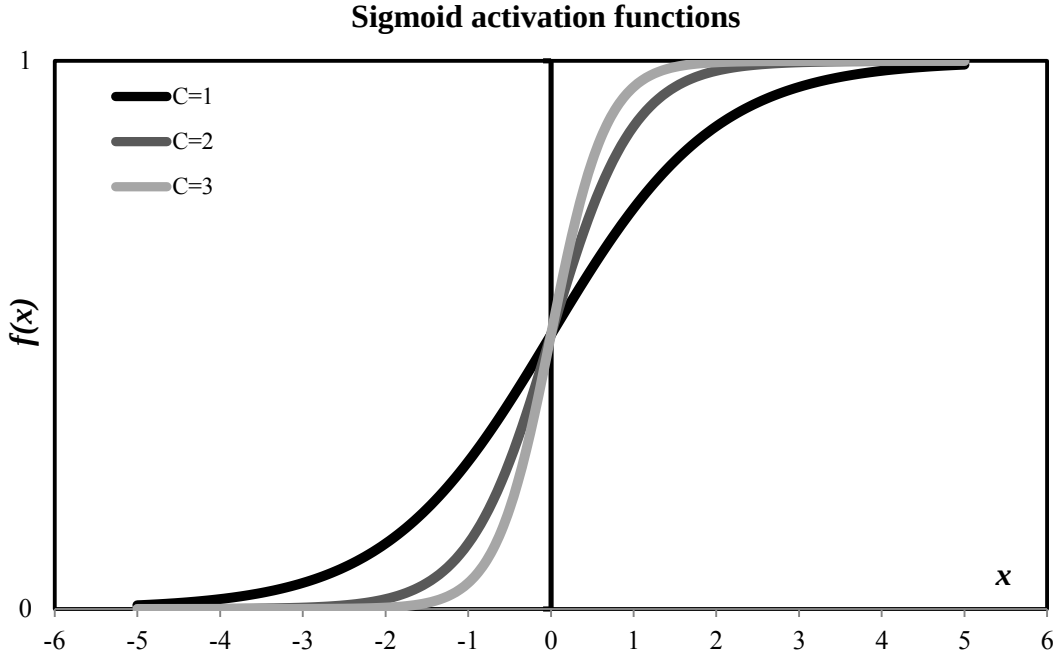

Figure 2.8: Sigmoid activation functions

Backpropagation

Backpropagation is error-correction learning type used to train multilayer neural networks. The goal of the backpropagation is to minimize the error between the output of the neural network and the actual desired output values.

The backpropagation process is explained in the following steps:

(1) Initially, connection weights are randomly populated and the output of the network is calculated.

(2) Then, mean squared error of network is calculated using Equation (2-6):

$$E = \frac{1}{2}\sum(y_i - d_i)^2 \tag{2-6}$$

where y_i are the network outputs and d_i are the actual desired values.

(3) Sensitivity of the error function with respect to each input is calculated using:

$$\varepsilon O_i = \frac{\partial E_i}{\partial y} = y_i - d_i \tag{2-7}$$

(4) Sensitivity of the error function with respect to input parameters are then calculated:

$$\varepsilon x_i = \frac{\partial E}{\partial x} = \varepsilon O_i \frac{\partial y}{\partial x} \tag{2-8}$$

In Equation (2-8), considering the term $\frac{\partial y}{\partial x}$ it is evident that transfer functions should be differentiable since the output of the network "y" is determined by the activation function. Using sigmoid activation function, Equation (2-8) then becomes:

$$\varepsilon x_i = \frac{\partial E}{\partial x} = \varepsilon O_i y_i (1 - y_i) \tag{2-9}$$

(5) The next step is to calculate the sensitivity of error function with respect to connection weights using:

$$\varepsilon w_{ij} = \frac{\partial E}{\partial w_{ij}} = \varepsilon x_i \cdot y_i \tag{2-10}$$

(6) Weights are then updated by:

$$W_{ij}^{t+1} = W_{ij}^{t} + \lambda \cdot \varepsilon w_{ij} \cdot y_i \tag{2-11}$$

where λ is called learning rate

(7) Repeat the process until the minimization is converged.

Backpropagation process is visualized in Figure 2.9. The problem of minimizing the error function can be solved with many mathematical algorithms such as gradient descent method. After the network is successfully trained, by presenting new data set to the network, network compares the patterns within the data and those in training data sets to produce outputs. This process is called neural network testing or prediction.

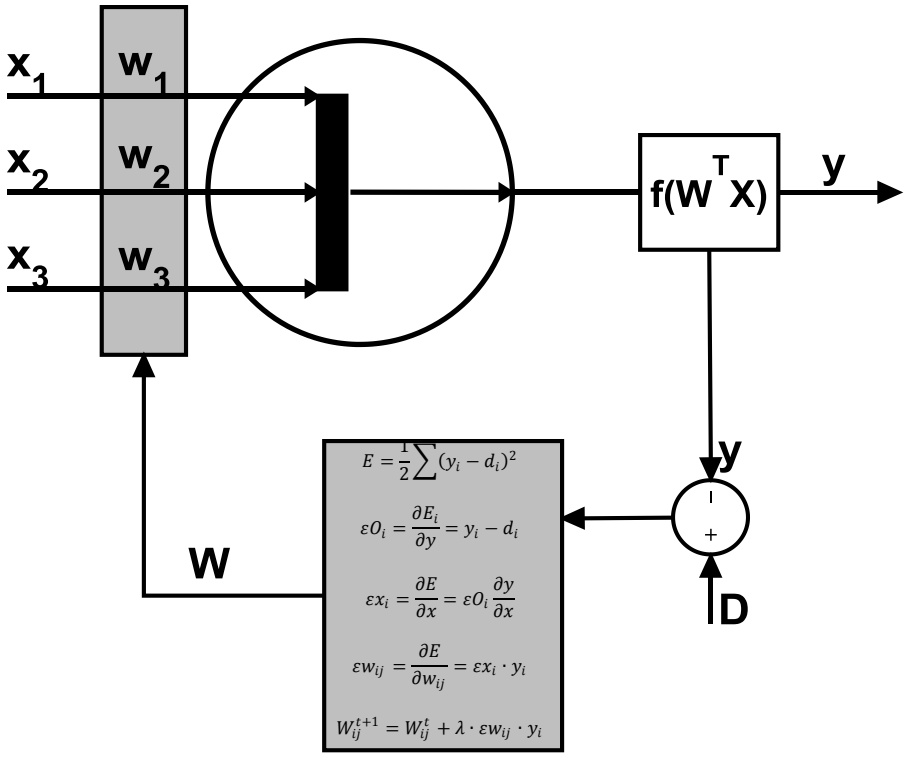

Figure 2.9: Artificial neural network training using backpropagation learning

Reservoir Characterization

The challenge in understanding and predicting reservoir behavior is in describing the reservoir geology realistically and modeling the reservoir behavior accurately and efficiently (Lake et al., 1991). However, this process can become complicated because oilfield data such as seismic, well logs, core data, etc. provide limited view of the reservoir. Therefore, the problem of identifying reservoir properties from the field data, so called reservoir characterization, boils down to an inverse problem in which given the field data, properties of the reservoir are to be estimated. Deterministic data derived from the actual measurement on reservoir properties at certain locations can come from different scales and sources. However, uncertainties are associated with the data because of the resolving power of the tool used and the inability of many tools to measure desired properties directly. Different approaches are made to characterize reservoir based on the available field data. Approaches based on the seismic data perhaps have the greatest potential to provide reliable information on reservoir property variations in the inter-well region (Schatzinger and Jordan, 1999).

Seismic reservoir characterization aims providing reservoir description using seismic information. Properties such as porosity, permeability, lithology, fluid type, etc. can be obtained using seismic reservoir characterization methods. Applications of 3D seismic data in reservoir characterization and reservoir management are shown in Figure 2.10. Since well logs measure the rock properties at well locations, it is desired to correlate seismic to well log data in order to obtain reservoir properties across the entire reservoir. Therefore, in next section the process of predicting synthetic well logs is discussed.

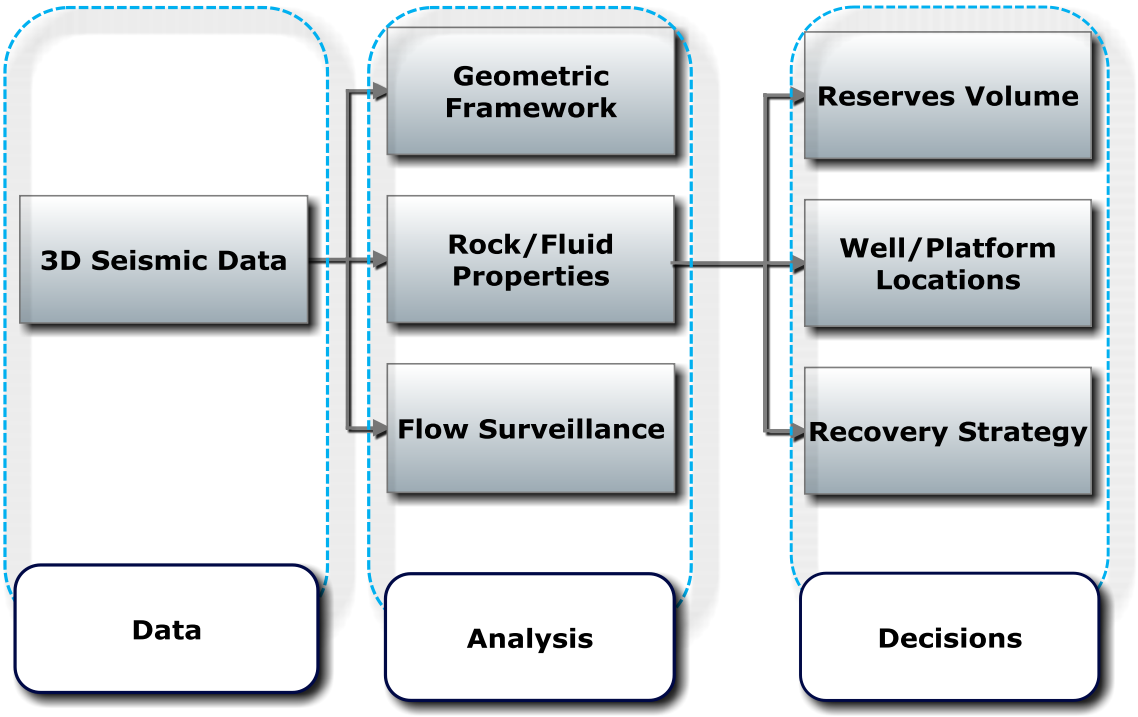

Figure 2.10: Applications of 3D seismic data to reservoir characterization and management (Sheriff and Brown, 1992)

Synthetic Well Logs

The process of transforming seismic data into essential rock properties such as porosity, lithology, and fluid types is called seismic inversion process. Apart from seismic data, which is the main source of inversion process, well logs and cores are typically the most critical part of the inversion process. The inverse modeling of the well logs has been widely studied by numerous authors (Anguiano-Rojas et al., 2003; Artun et al., 2005; Cooke and Schneider, 1983; Oldenburg et al., 1983; Yao and Journel, 2000). Pre-stack or post-stack attributes are both used for well log prediction. Mainly core data is used as the key source of information for calibration of the predictions.

The methods used to predict well logs from seismic data can be classified into deterministic, stochastic, geostatistical and soft computing techniques. Deterministic methods take advantage of the rock physics and known relationships between the seismic reflections and well log responses. The limitation of such methods is the uncertainty and imprecision of the seismic data. Also, relationships between the seismic data and well logs are functions of the geology and in complex geological settings such relationships are hard to identify. Geostatistical methods are used to interpolate and/or extrapolate spatially distributed properties such as well logs, core data, etc. However, the main assumption behind the geostatistical methods is that the distribution of the model parameters can be known a priori (e.g., Kriging methods assume stationary stochastic processes with constant mean). Probabilistic and stochastic methods are also used to address the uncertainty quantification of the inversion process. However, mainly they require a priori information about the problem setting. Prior distribution in many cases is derived either from theoretical considerations or field observations (Gouveia and Scales, 1998).

Soft computing methods can handle large number of unknowns and allow for fault tolerance impression. However, they require relatively large amount of data for analysis. Neural networks are the main soft computing method used in the seismic inversion. Nonlinear pattern recognition aspect of neural networks made them preferable choice over geostatistical methods. In comparison to the probabilistic methods, neural networks do not require prior information about the data; however, they require large data sets to train the networks.

Different methods have been used in incorporating seismic data and well logs into the artificial expert systems depending on the available data. Artun (Artun et al., 2005) used vertical seismic profiles (VSP) as intermediate step between the well logs and surface seismic data. They used synthetic seismic model to develop the general correlation between the seismic, VSP and well logs. Then, they incorporated estimated correlations into the real field well log predictions. Soto (Soto B and Holditch, 1999) developed intelligent reservoir characterization using core data,

well logs, and seismic information. They used 3D seismic data, horizon depths, and location of the wells to predict gamma ray logs. Only the information of limited number of wells (8 wells) is used for training and testing their developed networks. However, they achieved the predictions with more than 86% correlation coefficient. Barhen (Barhen et al., 1999) used the so-called DeepNet neural networks for well log predictions. DeepNet is modified feed-forward neural network with additional layer (a.k.a virtual input layer) between input layer and hidden layers. They predicted sampled well logs from five seismic variables with good accuracy.

In another study, three component 3D seismic data is used to predict well logs (Todorov et al., 1998). Seismic attributes are selected based on the smallest RMS error between the known log and the predicted logs using multi-regression analysis. Then, neural networks are used to predict well logs using the selected seismic data. Bhatt (Bhatt, 2002) developed multiple neural networks based on one data set. Based on the performance of the networks (those with minimum bias and variance on the validation data sets) 9 networks are selected to predict porosity well logs. The predictions are made using the outputs of 9 networks with ensemble averaging and optimum linear combination (OLC) method.

Chapter 3

PROBLEM STATEMENT

Identifying the reservoir properties with an accurate predictive capability is at the heart of reservoir management. Geological descriptions are estimated due to the lack of information underground. To develop a reliable predictive reservoir property model, the static, dynamic, and measured data required to be integrated in the model. Static data may include information from conventional wire-line logs, core data, and seismic data. On the other hand, dynamic data may include information from well tests, tracer tests, and flow rate data. Therefore, the challenge is to combine different sources of information in order to understand reservoir properties. Simple mathematical models may become inaccurate because several assumptions are made to simplify the problem, while complex models may become inaccurate if additional equations involving approximate description of phenomena are included (Nikravesh and Aminzadeh, 2001). The reservoir characterization problem is further intensified in unconventional reservoirs because of complex geology, insufficient of technologies to develop these types of reservoirs and existence of hydraulic fractures in the wellbore.

Two challenging aspects of reservoir characterization are finding the reservoir properties away from the wellbores and identifying reservoir net pays. In this study, the first problem is addressed by predicting well log data from seismic data. Then well log data are predicted for entire reservoir using the trained neural networks. In the next stage, payzone identification problem is addressed. The main challenge in identifying pay zones is the lack of production versus depth data. Therefore, training of the new neural networks to predict pay zones is not directly possible. Additional considerations should be made to devise new approaches to solve net pay identification problems.

This study aims targeting the aforementioned challenging reservoir characterization problems using artificial expert systems. Neural network methods offer alternative solutions to the reservoir characterization problem. They are nonlinear pattern recognition tools applied to complex, multi-dimensional data. However, in order to take advantage of capabilities of neural networks, data selection, screening, and sampling are required.

Incorporating different types of data into the neural networks is another challenging aspect of this work. Data screening involves selecting different data types to feed neural networks. Then ate the next stage, selected data is processed in order to be used in networks. In this research data processing method is developed for particular data set comprising of well logs, seismic data, completion/stimulation data, and production data. This process is illustrated in Figure 3.1.

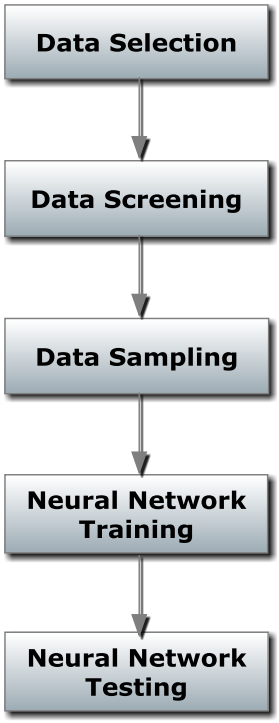

Figure 3.1: Neural network training procedure

Chapter 4

METHODOLOGY

As described earlier, this research aims predicting the reservoir properties away from the wellbore and identifies pay zones. The process is divided into three steps:

I. Data preparation

II. Neural network training

III. Prediction

Data preparation stage involves selection, screening, and sampling of oilfield data. Generally, oilfield data involves information such as: production, petrophysics, drilling, geophysics, and completion/stimulation. The first stage of data processing is to select data types for neural network training. This stage involves elimination of irrelevant data types and coming up with a list of data types to be used in further stages of data processing. It is beneficial to incorporate knowledge of people who have great knowledge about data such as geologist, petroleum engineers, completion engineer, etc. For example, in order to decide which completion parameter is more relevant in predicting data, completion engineer can help identifying most important parameters.

In the second stage, data is screened based on seismic data to create consistent data based. This is primarily important because neural networks require consistent data base. Seismic data is primary input data used in many neural networks to predict lithological properties. Therefore, in order to use seismic data, wells found within the seismic boundaries should be used. As a result, those wells located outside seismic domain are eliminated from the database. Screening the well logs involves elimination of:

- Irrelevant well logs (e.g. drilling collar locator log as network input and porosity log as networks output)

- Well logs with limited availability both in large number of wells

The final stage of data processing is to sample data and if necessary pre-process the data (e.g. averaging, denoising, removing outliers). Sampling is very important because it helps to reduce the complexities of the data and provide a unified data set for training and testing the networks. Well log data are generally lengthy measurements recorded at every few inches of formation. To sample well logs, first top and bottom depth of formation is determined at every location. Then, formation thickness is divided into several equal length segments. At each segment, weighted average value of the logs is calculated as a representative log value of the corresponding segment. Clearly, by increasing number of sampled log segments, sampling resolution increases and by decreasing it sampling resolution decreases. 3D seismic data sampling is performed by selecting seismic attributes locating at the same depth as the well log data. To perform seismic data sampling, time to depth conversion is required since seismic data is recorded on time scale and well logs are recorded on depth scale. In this study, time to depth conversion charts is available. As a result, seismic responses at the same depth can be correlated to the well log responses. Since production rates are often noisy and contain outliers, cumulative production data is selected for neural network analysis. Depending on the frequency and availability, production data is selected over finite intervals (e.g. three month intervals). Completion and stimulation data screenings greatly depends on the nature of the data. For example, corresponding hydraulic fracturing data of different stages can be lumped together to form a massive single-stage fracture data.

Once the data is collected and sampled, neural networks can be trained and tested to predict reservoir properties. In order to estimate reservoir properties, well logs should be predicted. Using averaged seismic data (low-resolution seismic attributes) low-resolution well logs are predicted. Analyzing the trained networks revealed the inability of networks to capture sharp transitions of the log features. By incorporating the error adjustment networks, the log

predictions are improved. The predicted well logs are comprised of 50 values at every seismic location. The significance of low-resolution well logs is their ability to approximate reservoir properties. Thus, they are used to predict cumulative productions (oil, water, and gas) of the wells. However, the disadvantage of low-resolution logs is their lack of details and their inability to capture sharp changes in well logs. Therefore, problems such as pay zone identification in which well log details are required should not use low-resolution well logs. To alleviate this issue, high-resolution well logs are predicted using 3D seismic attributes. Formation is divided into several seismic horizons in which separate different rock layers in depositional environments characterized by different reflection properties. Therefore, for each seismic interval that confined by two seismic horizons, one neural network per each log is trained to capture details of the well log. Combining the outputs of different networks results the high-resolution well log.

Having the petrophysical prediction tools, it is possible to predict production data at every location in which seismic data is available. Production prediction tools attempt to establish the relationship between the averaged seismic attributes, low-resolution well logs, completion, and production data. Three networks are trained to predict oil, water, and gas productions. Outputs of each of the networks are four numbers; production data sampled every three-month for the entire two year production history.

Completion data is only available in the well locations. However, in order to predict production rates way from the wells an auxiliary network is required. This network is trained to predict the completion parameters based on the current practices employed on the field. Inputs of the completion network are seismic and log data. It is important to note that the completion network does not attempt to optimize the completion parameters.

The final stage of reservoir characterization is to identify prolific intervals of the reservoir. As described in the previous chapter, lack of production data versus depth is the primary challenge in pay zone identification. In the first approach, production prediction

networks are used. Corresponding 3D seismic data and high-resolution well logs of each seismic interval is fed to the networks to predict productions. The most prolific segments are identified by ranking of gross thickness of reservoir. In the second approach, attempts have been made to construct the production logs. This achieved by sliding the moving window over the gross thickness of the reservoir and resampling well log and seismic data. The size of moving window is fixed and depending to the thickness of the formation several production values are predicted.

Production logs are important because they can be further studied in order to determine their relationship versus different lithologies. Fuzzy logic is used to classify production logs versus different lithology logs obtained from mud logging analysis. The outcome of such analysis can potentially results in identification of prolific lithology.

Chapter 5

CASE STUDY: WOLFCAMP RESERVOIR

This research is focused on the characterization of the ATM region of the Wolfcamp field. The Wolfcamp is a tight-rock play covering 5700 square miles in the Delaware basin. The locations of Wolfcamp field and Delaware basin can be seen in Figure 5.1. Because of the down-dip position, Wolfcamp reservoir was not explored until 1960s and later on the expansion of the play was unsuccessful because of complex structural pattern of the reservoir (Montgomery, 1996). 3-D seismic surveys and advances in technology helped more successful development of this field. Currently, the field is operated by the Wolfcamp Joint Venture between Chevron, Henry Petroleum and Summit Petroleum.

The Wolfcamp Formation is subdivided into seven units based on regionally mapped shale markers. These horizons were mapped throughout the area utilizing 3D seismic data and well logs. The lithology of the Wolfcamp formation consists of carbonates, black shales and siltstones. However, the geological system is greatly dominated by shales and limestones. Limestones represent shelf to proximal basin deposits while shales represent a more basinal setting. Limestones in the Wolfcamp Formation can be categorized into four facies groups: lithoclastic facies, grain-supported facies, matrix-supported facies, and boundstone facies. Shales within the basin are predominantly black, suggesting a biogenic origin (Flamm, 2008; Merriam, 1999).

The formation contains pockets of oil distributed along the entire field. The Wolfcamp play produces oil with API gravity 40-43. The gross thickness of formation is 600 to 1500 feet. The formation has very low permeability (average permeability: 0.013 mD) and relatively low porosity (less than 11%). ATM section of the Wolfcamp field has 341 wells that have been used in this study. Production in Wolfcamp field is achieved by hydraulic fracturing of the wells and

producing the oil until the economic limits has reached. Re-fracturing of the subsequent intervals is performed to increase the production from the wells.

Because of complex nature of the Wolfcamp formation, pattern-drilling strategy is employed to drill new wells in the field. Moreover, pay zones are identified by the regions with gamma ray less than 75 API. Thus, considering the complexity of the formation and current strategies used to drill new wells, development of the new intelligent characterization tools is necessary.

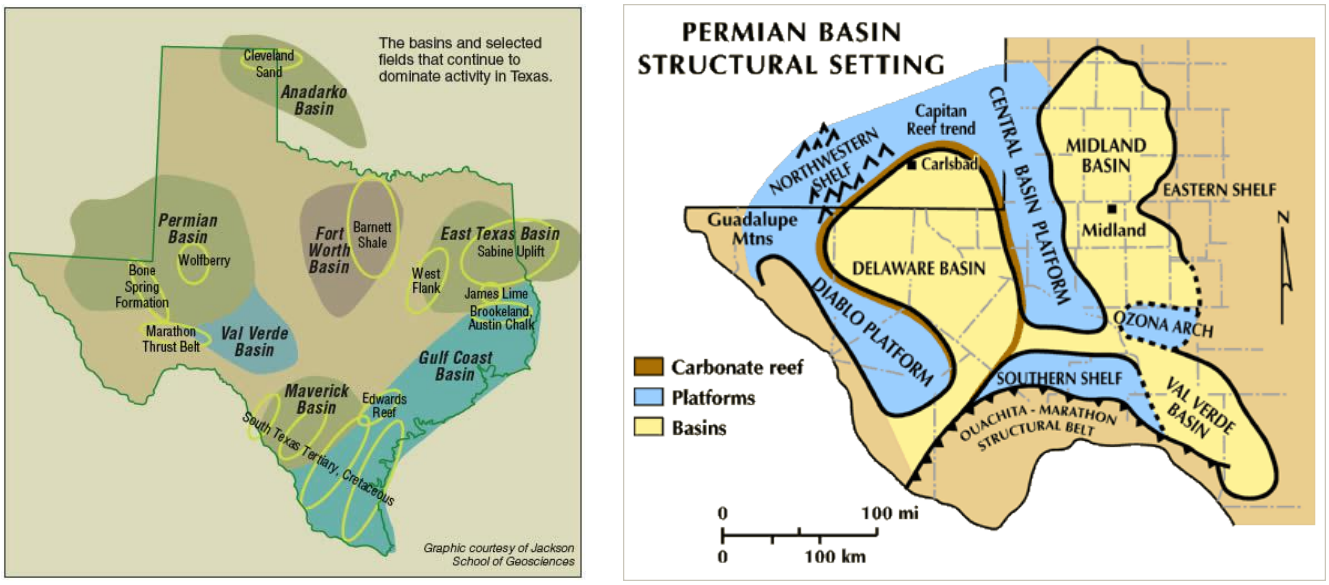

Figure 5.1: ***Left:*** **Wolfcamp play location in Texas (Brown, 2008)** ***Right:*** **Delaware basin location (Dutton et al., 2000)**

Data Availability

As described earlier, in order to take advantage of capabilities of neural networks, a complete and consistent database is required. Various types of data are supplied to this research by the Chevron Corporation. Geophysical data includes low-resolution seismic attributes calculated over each seismic interval (seismic interval is located between two subsequent horizons) and 3D seismic attributes. The 3D seismic attributes are recorded in the ASCII files with the SEG-Y format. The data is sampled over 2 millisecond window in time domain. Figure 5.2 demonstrates the plot of RMS amplitude versus time. List of seismic attributes used in this is presented in Table 5-1. Seismic data availability is limited to ATM region of the Wolfcamp field. The ATM region is comprised of 341 stimulated wells (hydraulically fractured). Well information consists of well logs, production data, artificial lift, completion, and stimulation data.

More than 1000 well log files were received in the form of LAS format. Screening the log files revealed that all of the wells in ATM region possess well logs. However, availability of specific log types varies in each well. Two types of production data are available: allocated monthly production rates, and daily well test rates. Since allocated production data is calculated from the combined flowrates of all wells in the field (back allocated based on well test information), the characteristic of data is masked and may not be useful for neural network training. On the other hand, daily well test data reveal more details of reservoir characteristics and used for network training.

Completion data is comprised of wellbore tubular information, perforation, artificial lift, and well information such as API name, coordinates, and well elevation. Stimulation data includes hydraulic fracturing information such as proppant volume, slurry rate, packer set depths, and pressure information of each fracture stages. Each well has minimum of five stages of hydraulic fracturing jobs. List of available data for this research is given in Figure 5.3.

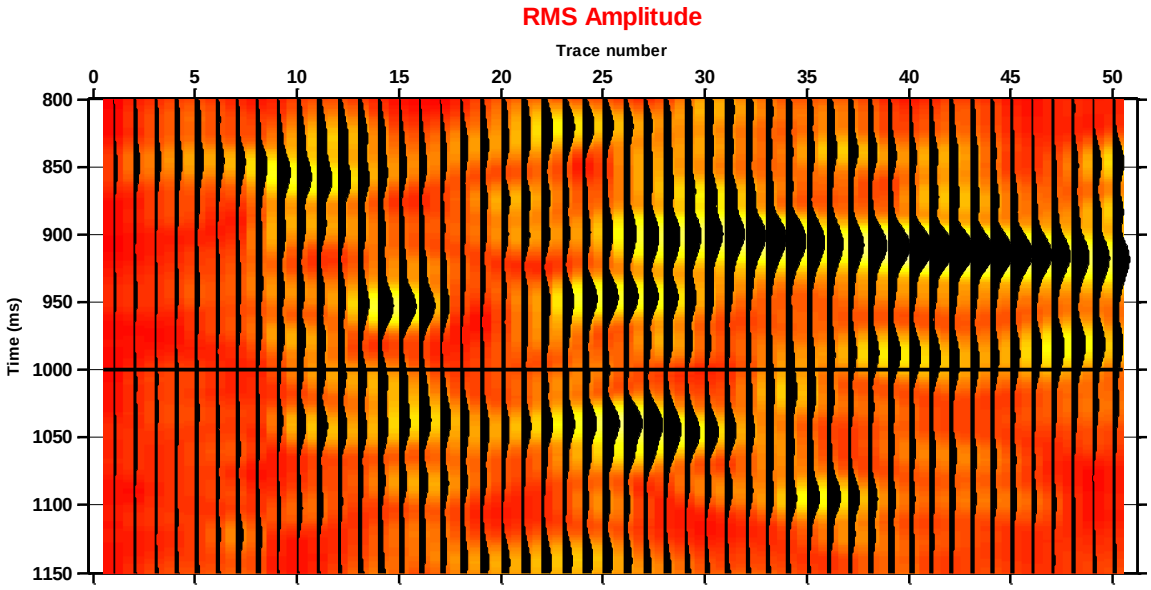

Figure 5.2: Sample of available 3D seismic attributes (RMS amplitude)

Available Oilfield Data		
Type	**Data**	**Format**
Geophysics	**Seismic (3D attributes)**	• **SEG-Y** • **ASCII**
Petrophysics	**Well Logs**	**LAS**
Production	**Oil, water, gas (daily)**	**Access Database**
Completion	**Tubing, casing, perforation etc.**	**Access Database**
Stimulation	**Hydraulic fractures information**	**Access Database**

Figure 5.3: List of available data and their respective formats

Table 5-1: List of seismic attributes used in this study

No.	Attribute	No.	Attribute	No.	Attribute
1	RMS Amplitude (sliding time window 50 ms)	11	Amplitude Change (average over 100 ms)	21	Amplitude Change (average over 200 ms)
2	Amplitude Acceleration	12	Energy Half-Time (average over 100 ms)	22	RMS Amplitude (100 ms sliding window)
3	Dominant Frequency (average over 100 ms)	13	Energy Half-Time (average over 50 ms)	23	Cosine of Phase
4	Instantaneous Frequency (average over 100 ms)	14	Thin Bed Indicator (50 ms window length)	24	Bandwidth (average over 100 ms window)
5	Reflection Strength	15	Differentiation	25	Instantaneous Q Factor (average over 100 ms window)
6	Quadrature Trace	16	Integration	26	Dominant Frequency (average over 50 ms window)
7	Thin Bed Indicator (window length 100 ms)	17	RMS Amplitude (25 ms sliding window)	27	Arc Length (50 ms sliding window)
8	Bandwidth (average in a 200 ms window)	18	Reflection Curvature	28	Arc Length (100 ms sliding window)
9	Response Frequency	19	Absolute Amplitude	29	Amplitude Variance (3 traces, 3 lines, 5 samples)
10	Instantaneous Q Factor (average over 200 ms window)	20	Amplitude Change (average over 50 ms)	30	Amplitude Variance (7 traces, 7 lines, 5 samples)

Synthetic Well Log Prediction

Synthetic well logs have been developed as a tool for reducing costs or whenever logging proves to be insufficient and/or difficult to obtain (Rolon, 2004). Furthermore, correlating well logs against production data can potentially help engineers to handpick the locations of infill drilling wells and ultimately increase the recovery from the reservoir. To develop the synthetic well logs, we propose using artificial neural networks in conjunction with conventional wireline well logs. The development strategy of the synthetic well logs prediction neural networks is demonstrated in Figure 5.4. Since two types of seismic data, coarse resolution seismic data (averaged attributes over 10 intervals) and high-resolution seismic data (time-volume seismic data sampled every 2 milliseconds) are available, we generated two families of synthetic well logs. The first is called low resolution well logs in which 50 average well log values are predicted for the entire well depth. The other family of well logs is called high-resolution well log predictions, using time-volume seismic data for each seismic interval, 50 average well log values are to be predicted (total of 350 values for seven seismic intervals).

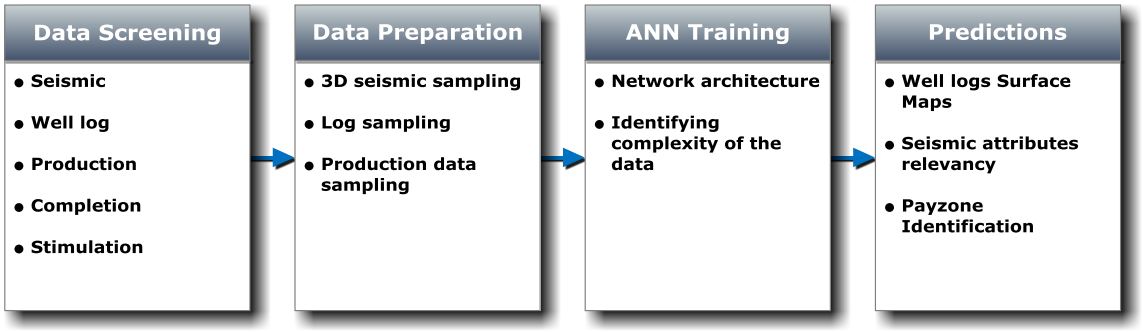

Figure 5.4: Reservoir characterization development algorithm

Data Screening

Data screening involves scanning the database based on consistency of the data sets and on their respective relevancies for predicting synthetic well logs. The first step of data screening involves scanning based on the well locations corresponding to seismic survey area. After screening based on seismic data, number of wells reduced from 651 to 221 wells. The next step in data screening is screening based on well log availability.

The well log availability for the existing wells in the ATM region is presented in Table 5-2. As it can be seen from Table 5-2, more than 90% of the wells have normalized gamma ray (GKUT_NRM), neutron porosity (PHIN), and raw gamma ray (GR) well logs. These well logs in conjunction with long space neutron count rate (LONG) and short space neutron count rate (SHORT) were selected for neural network developments. The rest of the well logs were ignored because of two reasons. First, some of the well logs such as WCJV_PAY, PAY_FLAG, PERFFLAG, etc. are the pay identifiers used by Chevron and in order not to bias the network outcomes; they have been omitted from the neural network training data sets. Second, some well logs have low availability and they have been omitted (e.g. LPOR, CNPOR, etc.). After well screening based on well logs, 144 wells are passed to the final stage of data screening. In the final stage of data screening, wells with two years of production history are selected. A total of 87 wells are selected for neural network developments. Figure 5.5 shows the complete well screening procedure.

Table 5-2: Well log availability for ATM region

Logs	Description	Availability (%)
'GKUT_NRM'	Normalized GR log	96
'PHIN'	Neutron Porosity	95
'GR'	Gamma Ray	93
'WCJV_PAY'	Current Pay Flag	93
'PERFFLAG'	Perforation Flag Curve	59
'CCL'	Collar Locator	53
'PAY_FLAG'	PAY FLAG	49
'SHORT'	Short Spaced Neutron Count Rate	48
'RAT_CALC'	Calculated Ratio Curve	46
'LONG'	Long Spaced Neutron Count Rate	43
'CNSSC'	CN Short Space Counts	43
'CNLSC'	CN Long Space Counts	43
'LPOR'	Limestone Porosity	42
'PAY_FLAG_GR'	Discriminator curve for PHIN	37
'CNPOR'	CN Selected Porosity	33

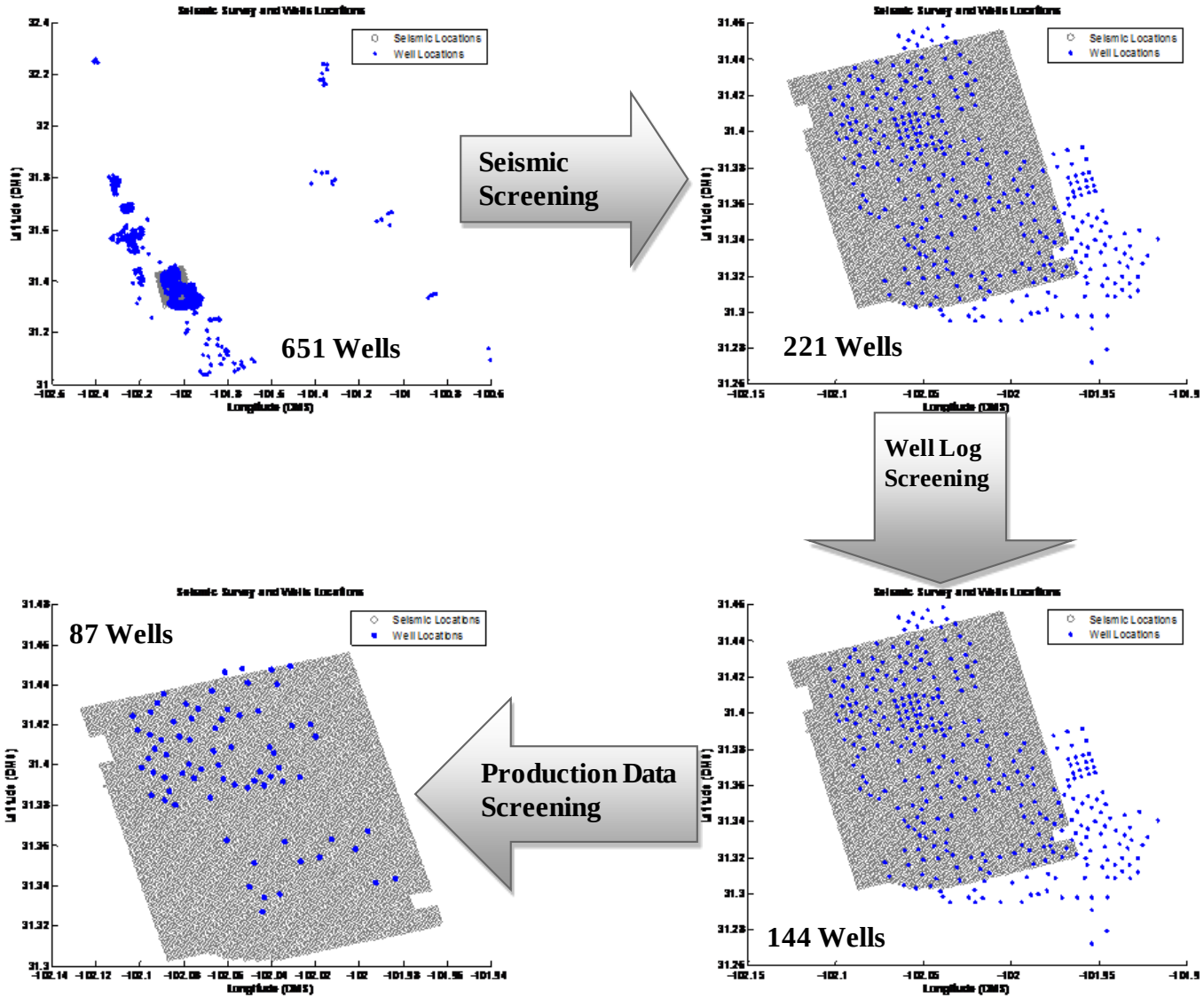

Figure 5.5: Schematic of well screening procedure

Data Preparation

Seismic data locations do not exactly match the well locations and surface interpolation technique was used to find seismic attributes at well locations. At any given well location, the four closest points were identified based on their coordinates. Then, utilizing an inverse distance interpolation, seismic attributes for well locations were obtained. The same procedure was also applied to find the respective seismic horizon depths at any given location. The depths of shallowest seismic layer (top depth) and the deepest seismic interval (bottom depth) were used to calibrate the well logs in the next step. Moreover, top and bottom seismic depths were checked against the perforation interval depths for consistency purposes. For example, if the bottom seismic depth were shallower than the maximum perforation interval depth, bottom depth would be adjusted to the maximum perforation interval depth. For the high-resolution well log prediction approach, the same methodology is applied. However, seismic data within each seismic interval is further subdivided into 10 sub-intervals and the respective seismic data is calculated based on root mean square average technique. This results into a matrix of 7 (intervals) by 30 (attributes) by 10 (sub-layer) for each location. A comparison of the time-volume seismic data and sampled seismic data is illustrated in Figure 5.6.

Once the top and bottom depths are obtained, well logs are scaled to the respective seismic depths (the rest of the well log data is ignored) and average well log responses of the corresponding well are calculated. For the case of low-resolution well log generations, the entire thickness of the well log (bottom seismic depth minus top seismic depth) was divided into 50 intervals and the average well log responses for each interval was calculated. The sample averaged well logs are demonstrated in Figure 5.7. The same methodology is also applied in preparation of high resolution well log generation data sets, however instead of dividing the entire

well log thickness into 50 intervals; each seismic interval is divided into 50 intervals. So, since seven seismic intervals are identified from the seismic data, the total number of logs data points for each well is increased to 350 points. Figure 5.8 demonstrates the comparison between sampled well logs and actual well logs in high-resolution approach. Comparing the two figures, it is evident that high-resolution approach captures the overall well log signatures more effectively.

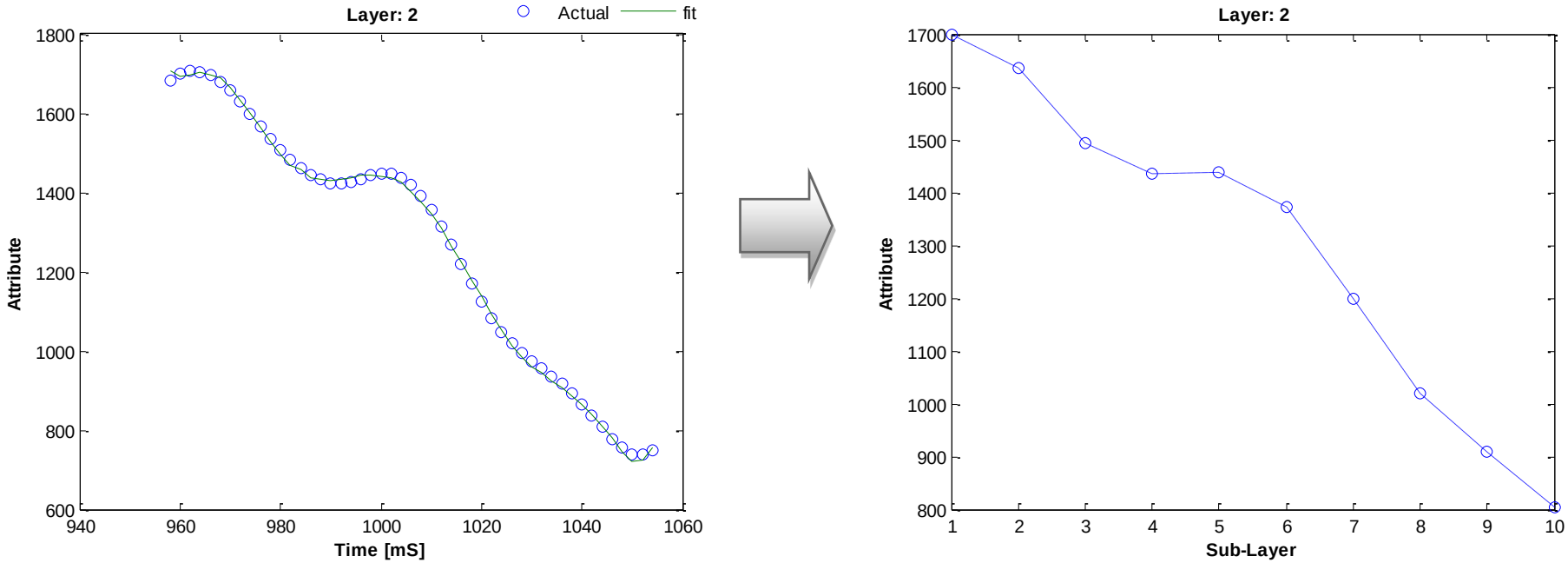

Figure 5.6: Comparison of the time-volume seismic data and sampled seismic data

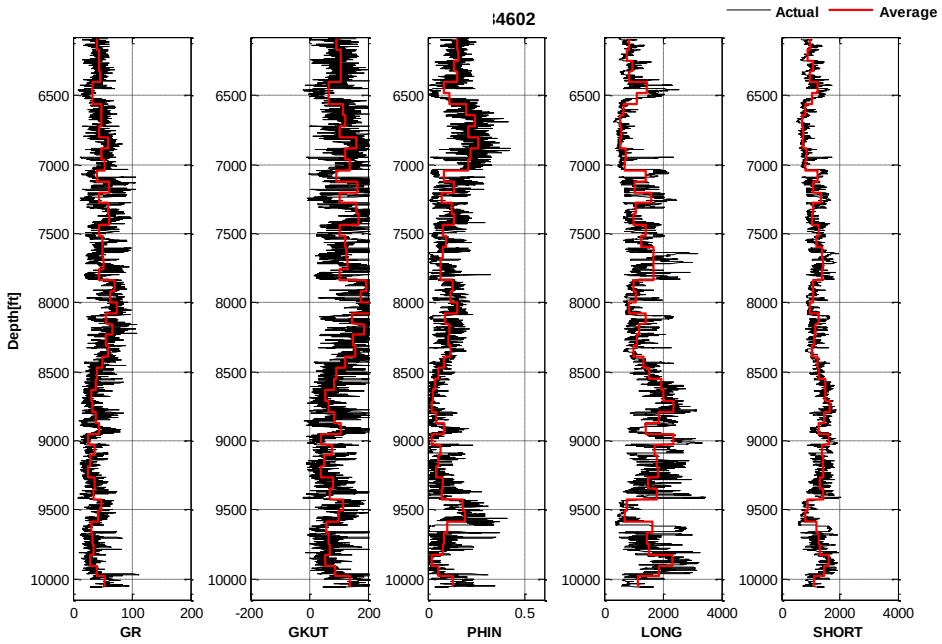

Figure 5.7: Sample low-resolution well log response comparing to actual well logs

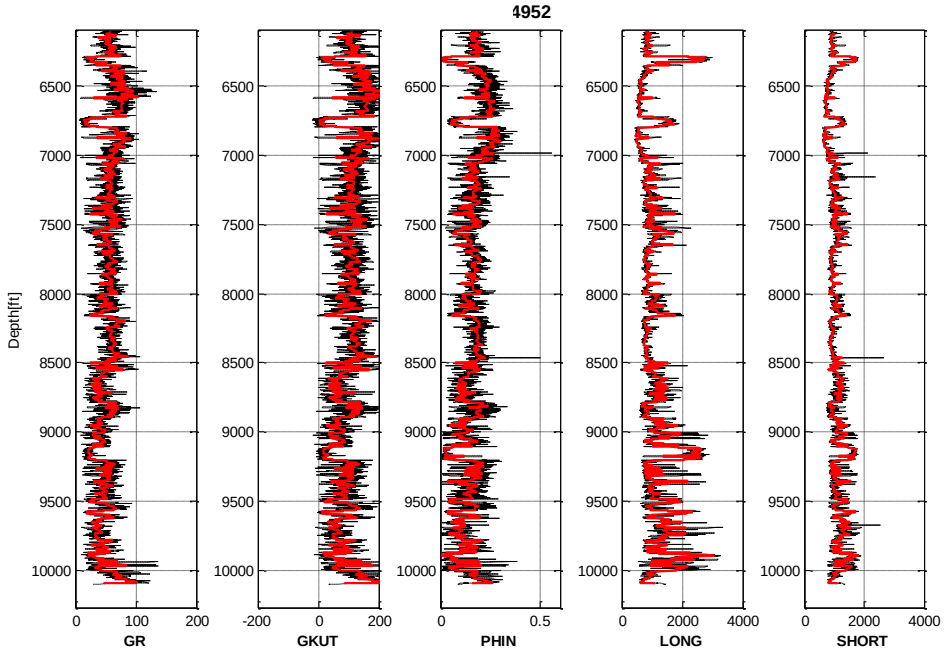

Figure 5.8: Sample high-resolution well log response as compared to actual well logs

Neural network Development Strategies

A. Low-resolution well log generation

Initially seismic attributes (low resolution seismic data) and well coordinates were used to predict the well logs. However, after analyzing the prediction performance of neural networks, it became clear that networks were able to only predict the overall trend but failed to predict sharp variations of well logs. To confirm this hypothesis, 10 numerical experiments were designed in which 77 wells were used for training, 5 wells for validation and 5 well for testing. In each experiment, one specific well (overlap well) remained in the testing set while the other four shuffled with training wells randomly. The results of this overlapping exercise can be seen in Figure 5.9. The results confirm that regardless of network structure and training/testing data sets, the networks are unable to capture the entire behavior of the well logs including well log overall trend and well log sharp jumps and variations. Also by analyzing Figure 5.9, it is clear that the maximum errors are related to the sharp jumps of the well logs (e.g. interval 30 of well A and intervals 12 and 40 of well B). The error values of 10 different experiments create a band (black curves in Figure 5.9) implying that the predicted well log values with different network structures and testing data sets are approximately the same.

These comparisons demonstrated the inability of the neural networks to completely characterize well logs using low-resolution seismic data. At this point, the use of two types of neural networks for predicting low-resolution well log data was attempted. The first family of networks, the so-called trend networks, requires seismic data (300 values) and coordinates data (5 values) as input and predicts the overall trend of well logs (50 values). A total of five networks were used to predict the well log trends (one network for each well log). The trend networks generally have three hidden layers. The hidden layers transfer functions[1] are all ‘logsig’, while output layer transfer function is ‘tansig’. Once the trend of the

[1] Definitions of transfer functions are given in Appendix B

well log is obtained, prediction errors can then be calculated from the actual well logs. Then, a second family of networks, error-adjustment networks, was used to adjust the predictions of trend networks. The inputs of error adjustment networks are seismic attributes (300 values) and the outputs are predicted error values (50 values) calculated from the outputs of trend networks. Five networks were then used to estimate the prediction error of each well log. Error adjustment networks have three hidden layers with the transfer functions of 'tansig', 'softmax', 'radbas', and 'stalins' (output layer). Once prediction error is estimated, well log trends are adjusted accordingly. Figure 5.10 summarizes the workflow of low-resolution well log predictions. Total of 10 neural networks are used to predict well logs including 5 trend networks and 5 error adjustments networks. The details of each network are documented in the results section.

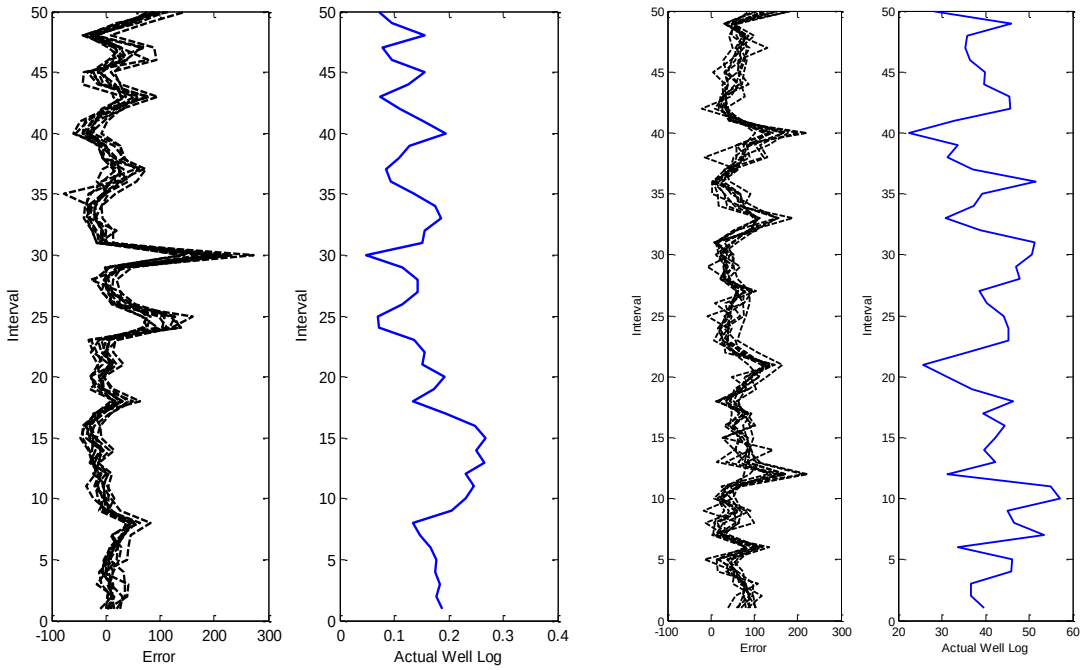

Figure 5.9: Typical results of overlap exercises for two wells

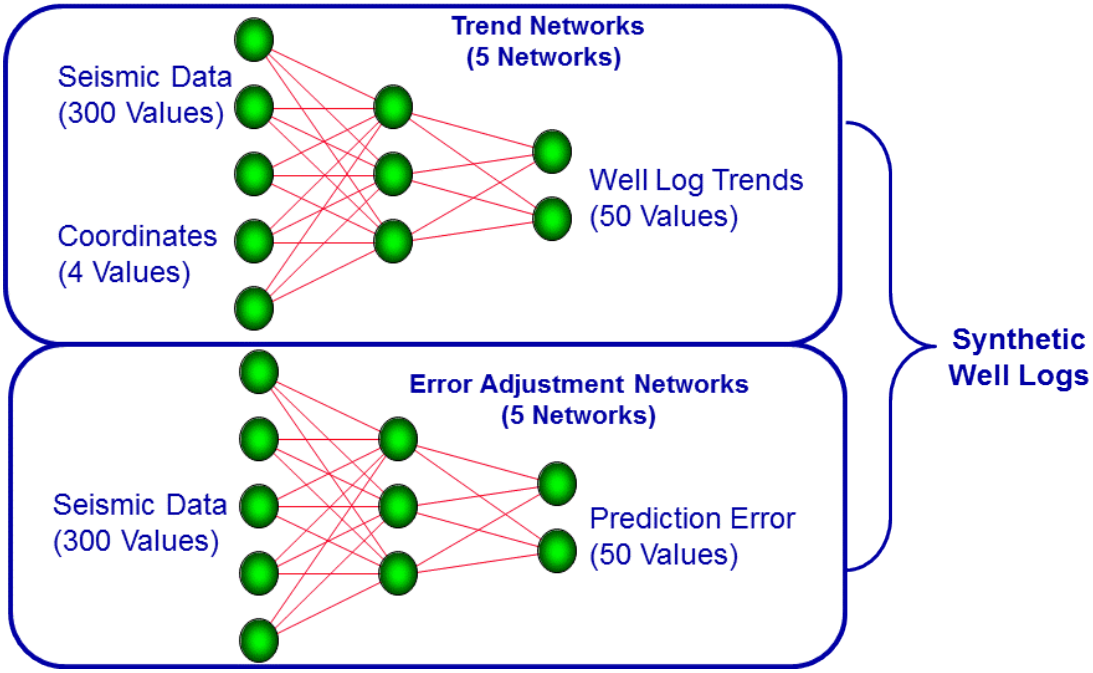

Figure 5.10: Schematic of low-resolution well log generation neural networks

B. High-resolution well log generation

The initial approach of training the high-resolution well logs was using raw time-volume seismic data (30 attributes × 401 values =12030 values) to train the well logs (350 values). However, the networks required large number of neurons and hidden layers with time consuming neural network training (more than 6 hours). Moreover, the network training and testing performances were very poor with an average 80% testing error. The second approach was training 7 neural networks (one network per seismic interval) for each well log (totally 35 neural networks). The inputs of the neural networks are sampled time-volume seismic data (10 sub-layer × 30 attributes) and outputs are well logs (50 values) for each seismic interval per well log. High-resolution well log networks have two hidden layers with "tansig" transfer functions both in hidden layers and output layers. The training performances with this approach were much better than the previous approach. Moreover, simplifying the network structure helped increasing the

performance of the networks and reducing the network error. Also, in comparison to the low resolution well log prediction networks, no error adjustment networks were required and networks were able to capture the structure of well logs. Schematic of the high-resolution well log generations are demonstrated in Figure 5.11.

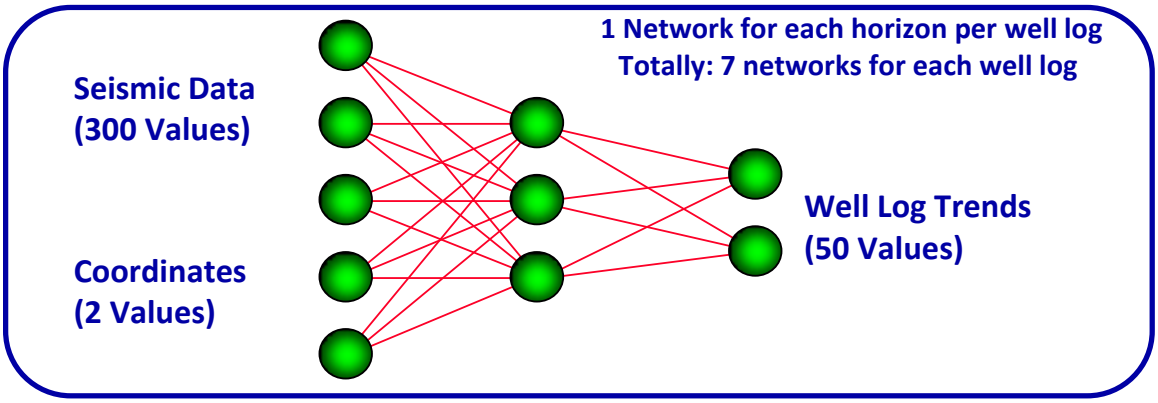

Figure 5.11: Schematic of high-resolution well log generation neural networks

Payzone Identification

Net pay is a key parameter in reservoir characterization and in many other contexts such as reserves evaluations, identification of intervals for perforation and stimulation, and prediction of permeability from well tests (Jensen and Menke, 2006). The main challenge in payzone identification is the lack of field data to train neural networks and validate prediction results. Also, existence of hydraulic fractures at the well locations adds more complexity to the problem. In this analysis, we propose to use the neural networks developed in the earlier section to predict oil, gas, and water performances in payzone identification. These networks are expert systems that integrate seismic data, well logs, and completion data to predict the production characteristics of the wells. Using a sliding window along the well depth, it is possible to predict the production of the well from different zones. Schematic of payzone identification methodology is presented in Figure 5.12. Gross pay thickness is divided into multiple segments (e.g. four

segments are demonstrated in Figure 5.12) and the representative sampled well logs are fed to neural networks to predict production profiles. The outcome of payzone identification is the ranking of different pay intervals with respect to oil, gas and water productions.

Three approaches were tested in this study to identify pay zones. In the first approach, the gross pay thickness (identified by the depth of shallowest and deepest seismic horizons) is divided into four intervals of equal thickness. Within each interval, well logs are sampled into 50 values and fed to the neural network along with the completion data (same completion data for all four intervals) and seismic data and the respective production profiles are calculated. This approach is called coarse resolution approach since entire gross thickness is divided into four large intervals. In the second approach, the size of sliding window is reduced to 50 feet. In this approach, actual well logs are used instead of average well logs. Actual well logs are sampled every one-foot and predictions (oil, water, and gas) are made at every 50 feet interval. This approach is called high-resolution approach because in this approach details of actual well logs are exposed to neural networks. One advantage of high-resolution approach is by using the classification methods it is possible to obtain new trends and correlations between production data and well logs. This can potentially help engineers and geologists to gain more understanding about the relationships between common wireline well logs and production profiles in Wolfcamp/ATM region. This method however, cannot be used throughout the entire seismic survey area because actual well logs are required and they are available only at the locations of the wells. Accordingly, it is proposed a third method to be used for the entire seismic survey area in which production profiles are predicted for each seismic interval using the sampled well logs (50 values) and seismic data (300 values). In this method, at the location of the wells for each interval sampled well logs are used. However, in other locations a new well is yet to be drilled, the predicted well logs by high-resolution well log prediction approach are used as input for the neural network. The results of this approach are seven production profiles for each phase (oil, water, and gas).

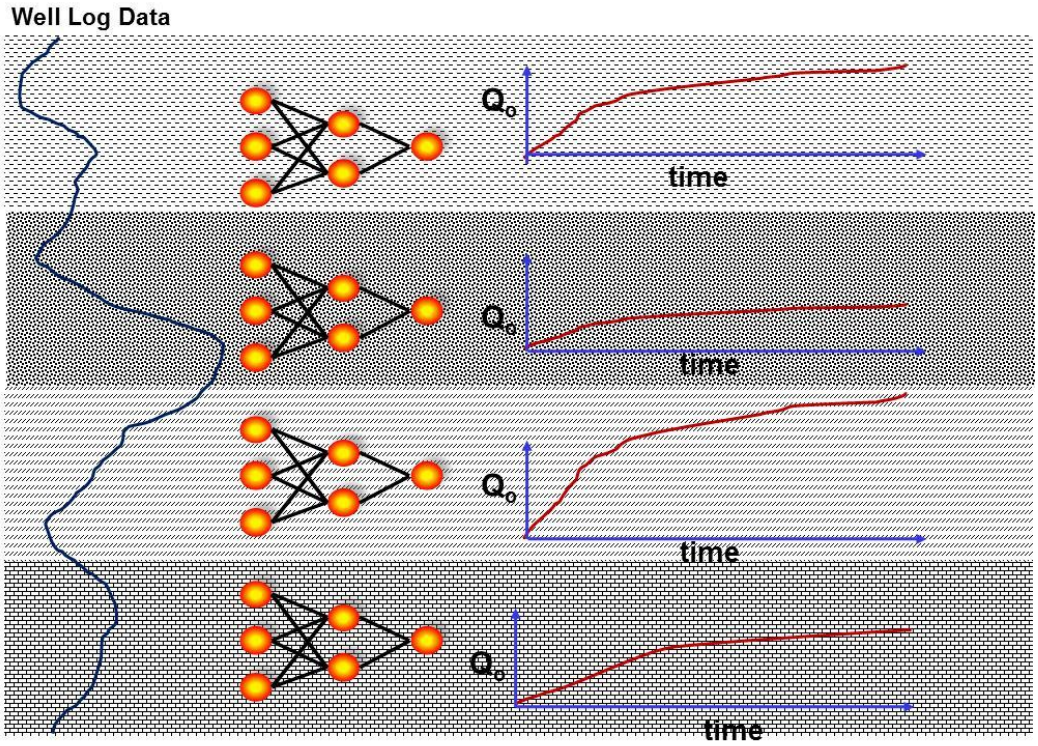

Figure 5.12: Schematic of payzone identification methodology

Chapter 6

RESULTS AND DISCUSSIONS

This study aims at solving the reservoir characterization problem for an unconventional reservoir system. The first module of the research involves prediction of well logs in the inter-well regions. As discussed in Chapters 4 and 5, the well logs are predicted using the seismic data. In the first section of this chapter, the results of synthetic well log generation tools are presented. In the second part of this chapter, pay zone identification results are discussed.

Synthetic Well Log Generation Tools

A. Low-resolution well log generation

The first sets of results are related to the low-resolution well logs. A total of 87 wells used in training (77 wells), testing (5 wells) and validation (5 wells) data sets. The wells in each data set are selected randomly. Figures 6.1 to 6.10 show the result of low-resolution well log predictions for a testing well A1 (randomly selected for testing), in the testing data set. Raw gamma ray (GR) prediction results are shown in Figure 6.1. As it can be seen, the trend network captured overall trend of the well log with a correlation coefficient of 0.374. Using the error adjustment network, the correlation coefficient improved to 0.896. It is evident that error adjustment network helped in improving the predictions and capture the behavior of the well logs. The GR trend network has four hidden layers with 15, 25, 14, and 23 neurons, respectively. The hidden layers transfer functions are all ‘logsig’ while the output layer transfer function is ‘tansig’. The GR error adjustment network has three hidden layers with 25, 40, and 30 neurons with transfer functions of ‘tansig’, ‘softmax’, ‘radbas’, and ‘stalins’ (output layer), respectively. Figure 6.2 demonstrates the correlation coefficient (between prediction well logs and actual well logs) histograms of

the prediction before and after error adjustments. It is clear that the use of error adjustment network shifted correlation coefficients more toward one and thus improved the overall quality of the predictions. None of the trend prediction correlation coefficients are higher than 0.8 while with error adjustment, more than 70 well logs have correlation coefficients more than 0.8.

Normalized gamma ray (GKUT) predictions are demonstrated in Figure 6.3 and Figure 6.4. The trend correlation coefficient for the testing well is 0.366 and it is improved by using error adjustment to 0.916. The histograms of correlation coefficients demonstrate significant improvement by using the error adjustment networks. Only two wells have correlation coefficients less than 0.5 while more than half of the predicted trends have correlation coefficients less than 0.5. Neutron porosity (PHIN) results are demonstrated in Figure 6.5 and Figure 6.6. As it can be seen from Figure 6.5, after corrections, the correlation coefficient is improved from 0.55 to 0.929. With this significant improvement, details of the well logs are captured accurately (for example, note intervals 35, 40, and 46). Analyzing the trend well logs histogram reveals most of the prediction correlation coefficients are within 0.5 and 0.8. Trend predictions of neutron porosity well logs have overall better correlation coefficients than raw gamma ray and normalized gamma ray well logs. By using error adjustment networks, correlation coefficients of most of the well logs are improved. The next sets of results are related to the long space neutron count rate (LONG) and short space neutron count rate (SHORT). As it can be seen from the results of both well logs (Figure 6.7 to Figure 6.10), the predicted well logs are in good agreement with the actual well logs. Also, in case of SHORT well logs, minimum correlation coefficient after error adjustment is 0.7. The LONG well log predictions also have high correlation coefficients; only one well has correlation coefficient less than 0.7.

One of the main advantages of neural networks is their power to perform pattern recognition and to be able to find correlations within a given data set. This can be done by analyzing input weights of neural networks in the form of relevancy plots and locating the input parameters with highest impact on the neural network outputs. Relevancy of each input parameter is defined by the individual neuron weight

of input parameter divided by summation of weights for all input parameters. The relevancies of input parameters are demonstrated in Figure 6.11. As it can be seen, "cosine of phase" has the highest impact among thirty seismic attributes. Other important attributes are amplitude change (averaged over 100 and 200 ms) and instantaneous Q factor (averaged over 100 and 200 ms) and thin bed indicator. On the other hand, differentiation, integration, reflection strength, amplitude acceleration and absolute amplitude have the least impact on the well log predictions. The definitions of all 30 seismic attributes used in this study are given in Appendix B.

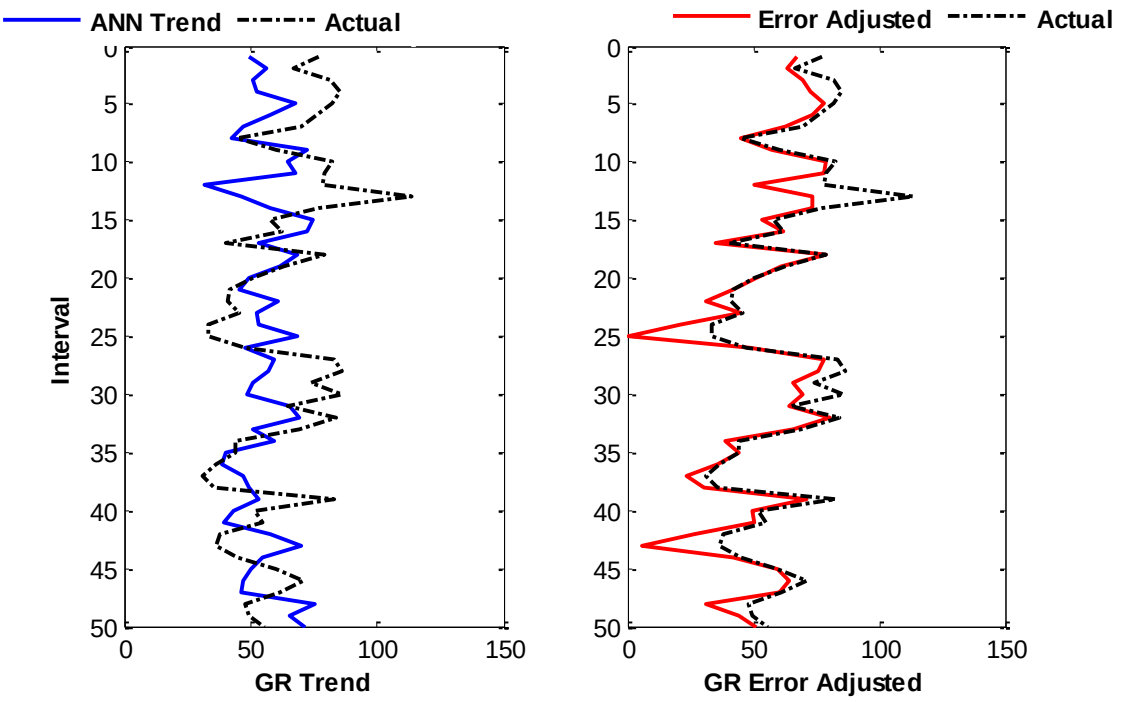

Figure 6.1: Low resolution well log generation: GR; Trend well log correlation coefficient: 0.374; Error adjusted well log correlation coefficient: 0.896

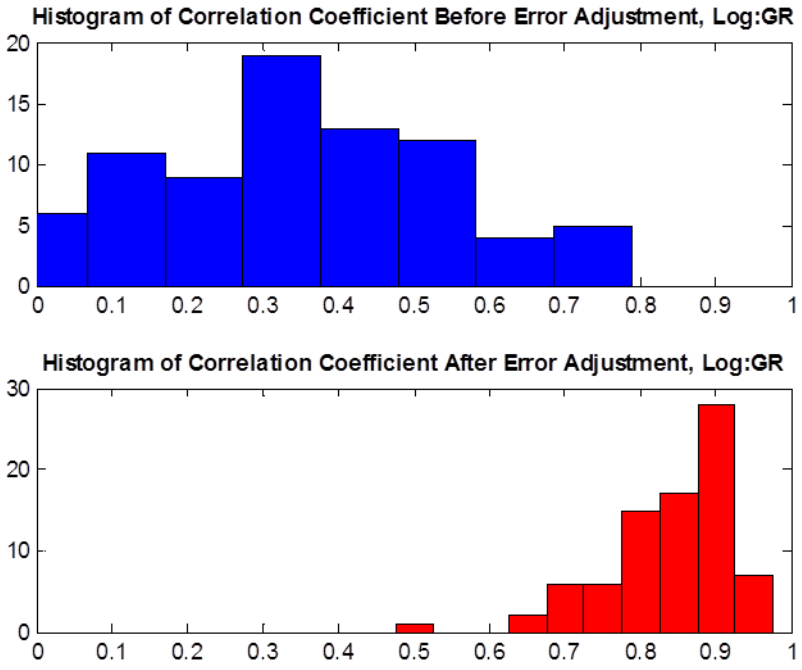

Figure 6.2: Low resolution well log generation: GR; Correlation coefficients of predictions

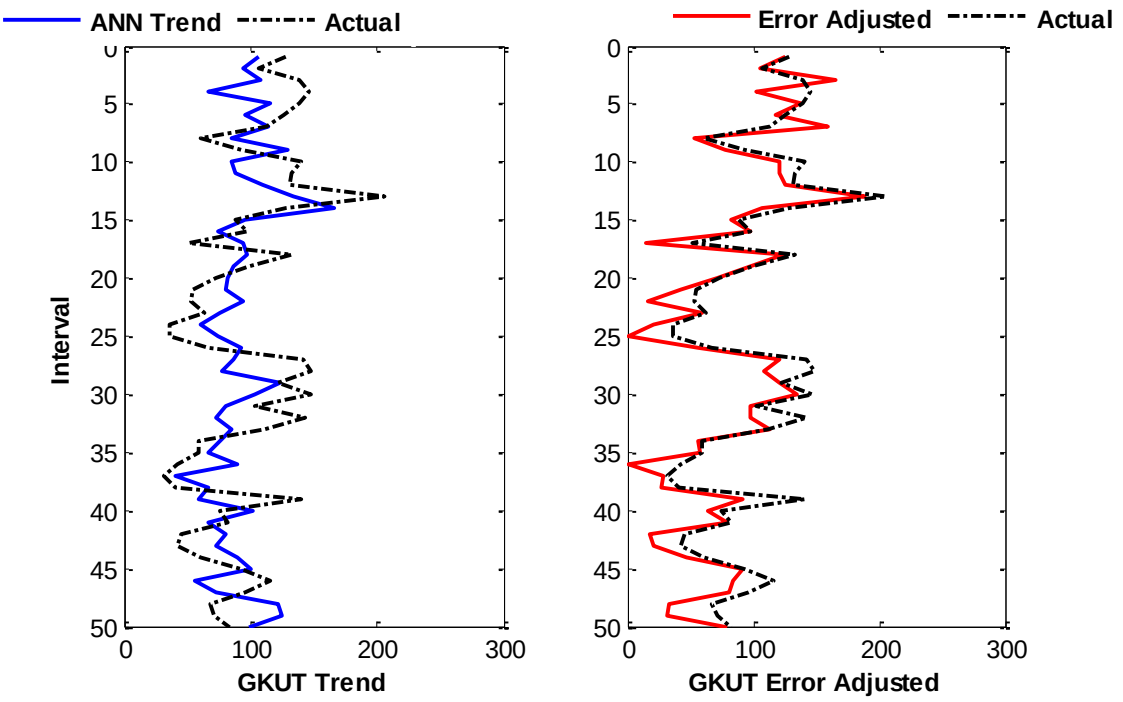

Figure 6.3: Low resolution well log generation: GKUT; Trend well log correlation coefficient: 0.366; Error adjusted well log correlation coefficient: 0.916

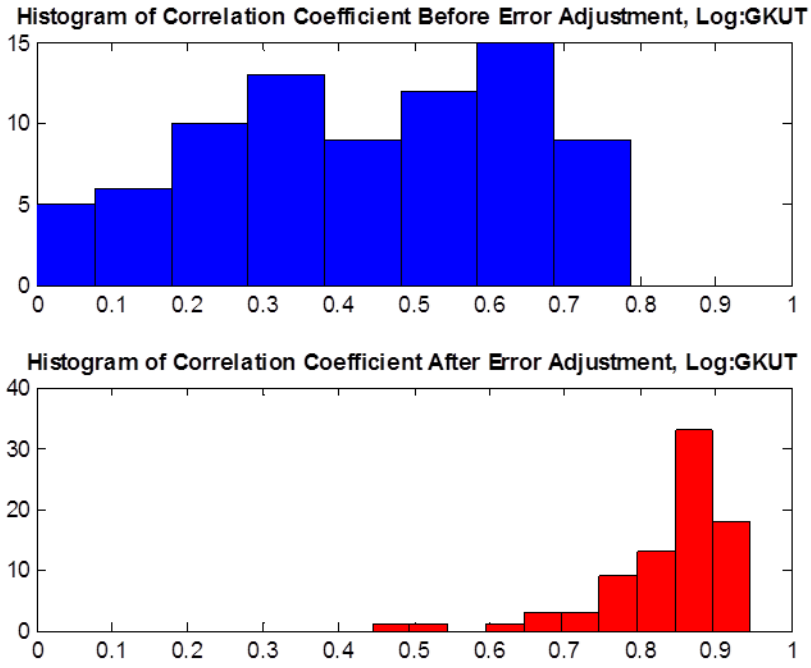

Figure 6.4: Low resolution well log generation: GKUT; Correlation coefficients of predictions

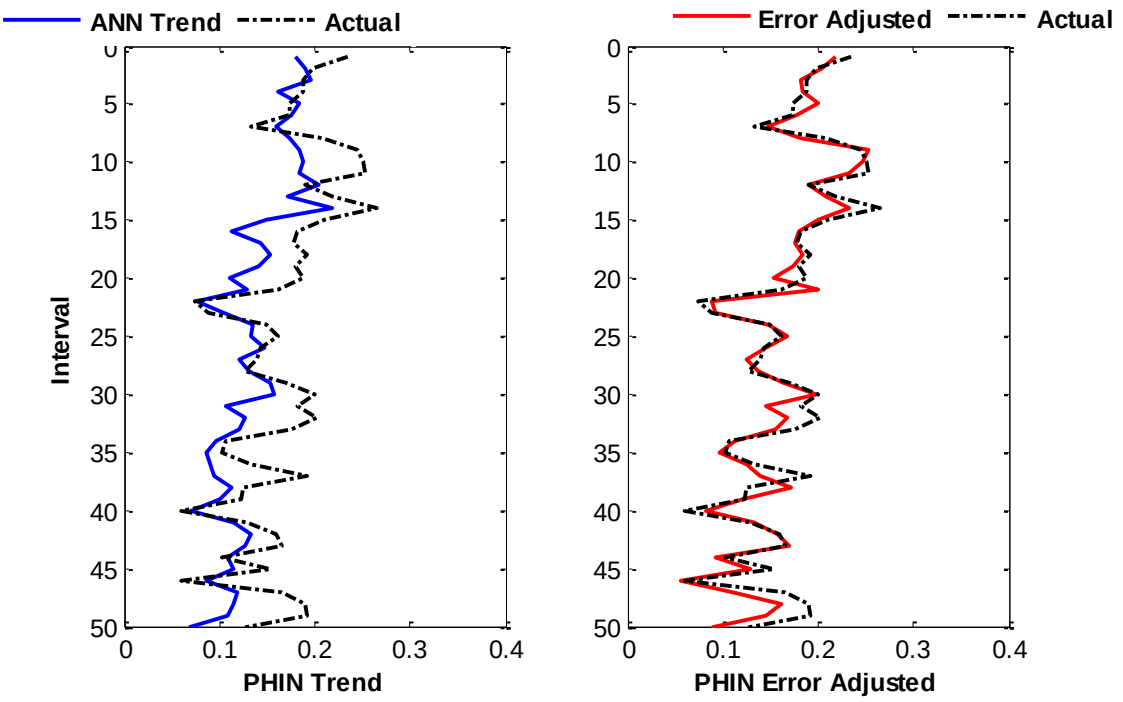

Figure 6.5: Low resolution well log generation: PHIN; Trend well log correlation coefficient: 0.550; Error adjusted well log correlation coefficient: 0.929

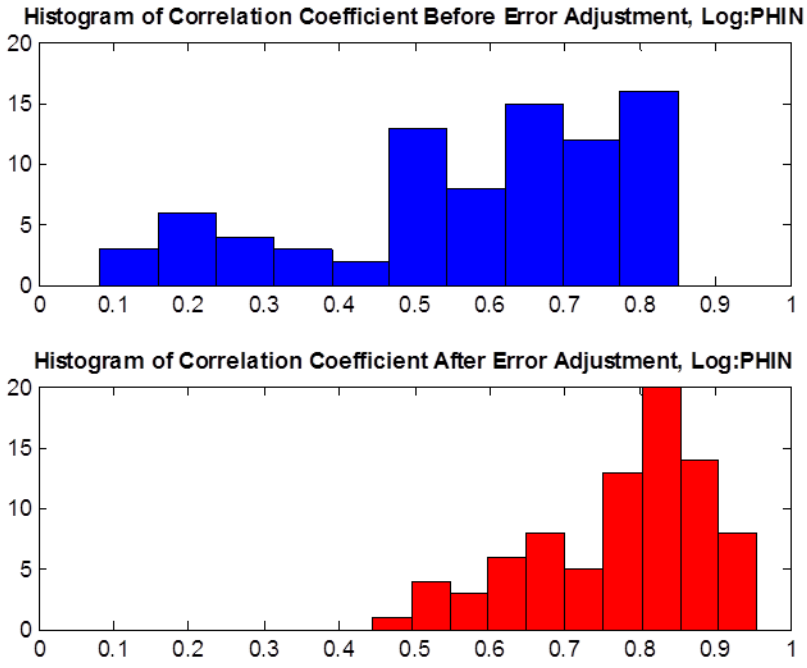

Figure 6.6: Low resolution well log generation: PHIN; Correlation coefficients of predictions

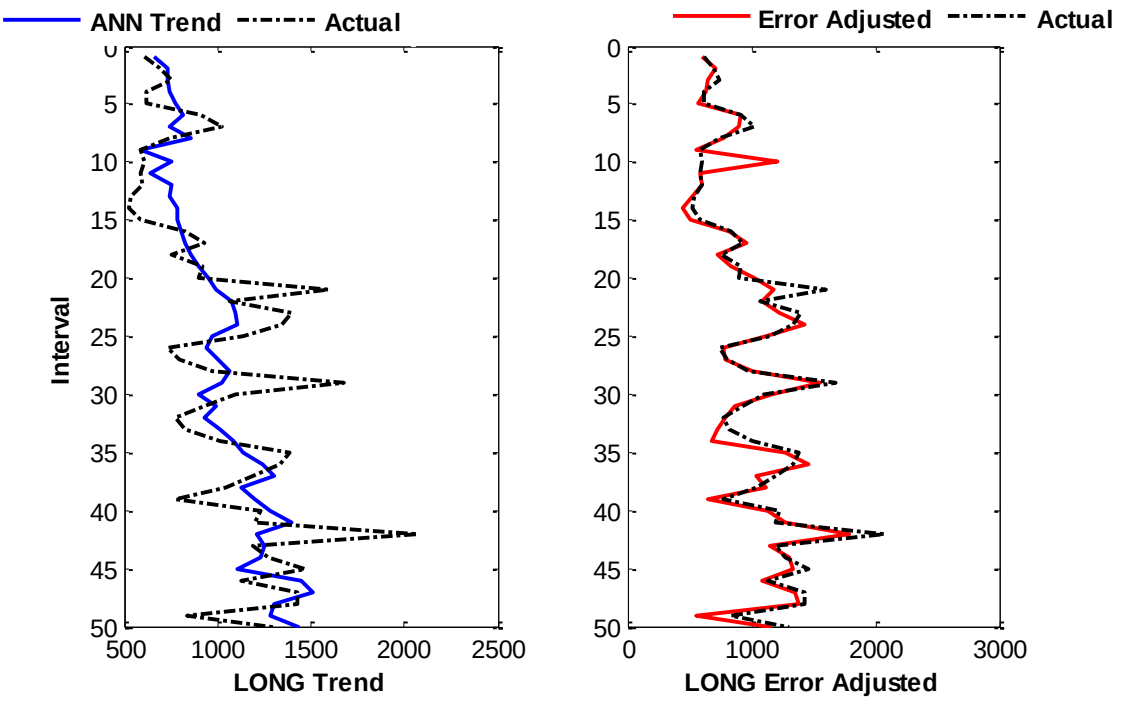

Figure 6.7: Low resolution well log generation: LONG; Trend well log correlation coefficient: 0.685; Error adjusted well log correlation coefficient: 0.908

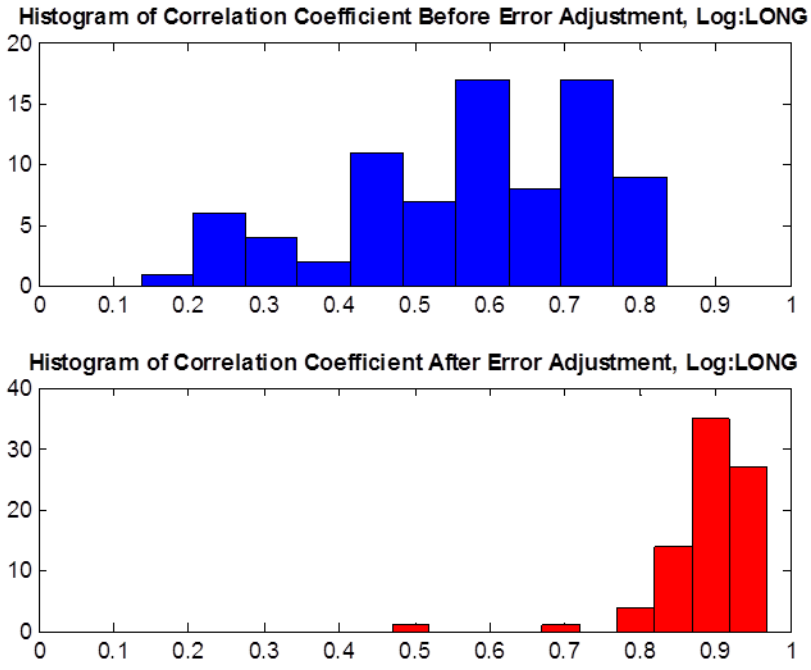

Figure 6.8: Low resolution well log generation: LONG; Correlation coefficients of predictions

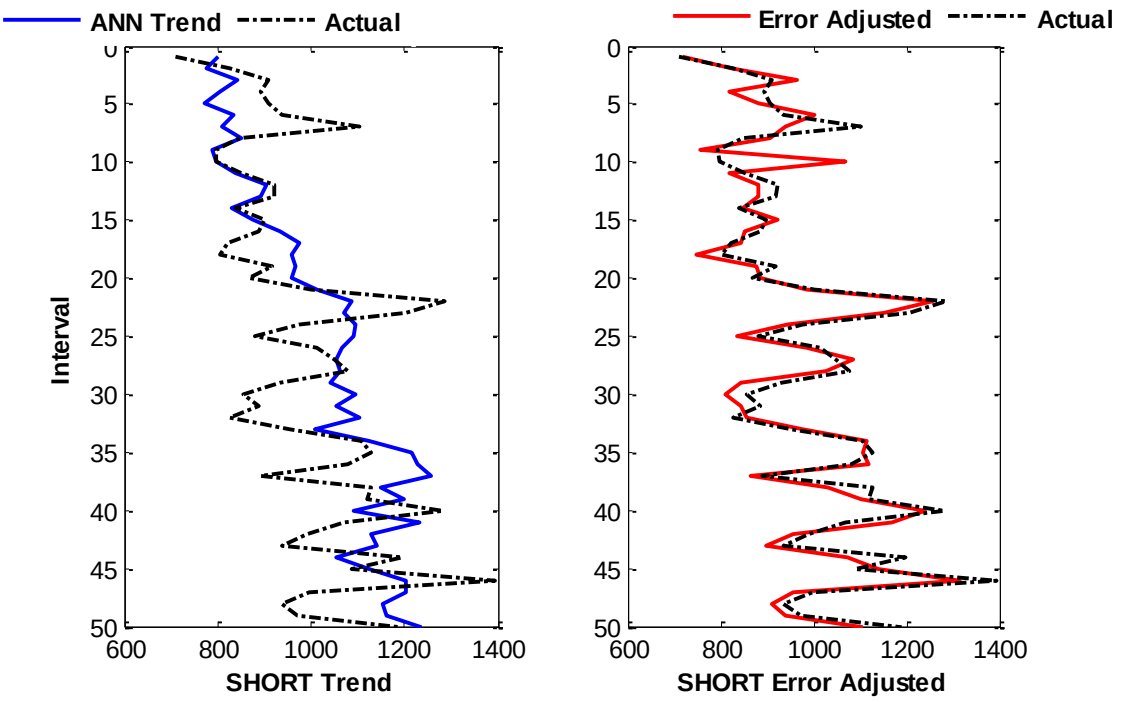

Figure 6.9: Low resolution well log generation: SHORT; Trend well log correlation coefficient: 0.577; Error adjusted well log correlation coefficient: 0.898

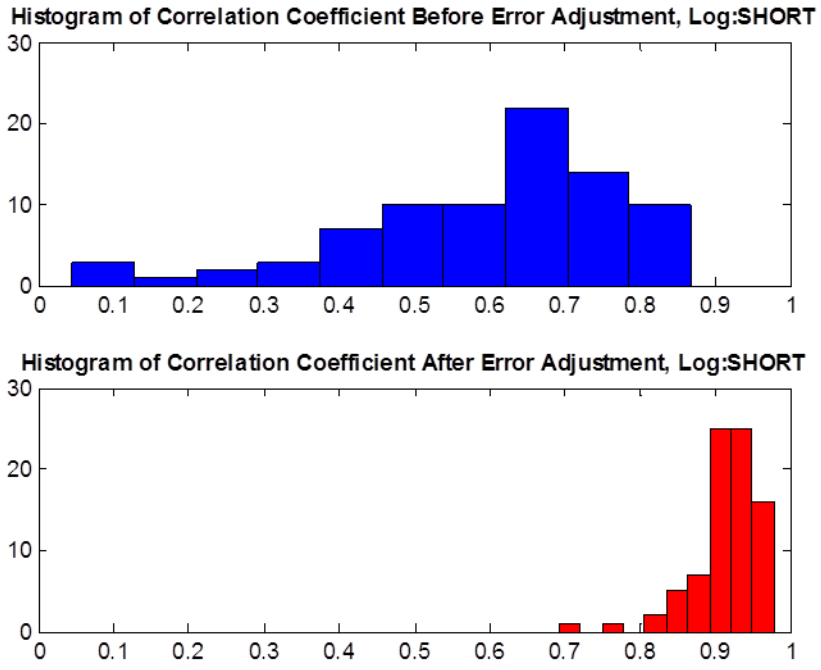

Figure 6.10: Low resolution well log generation: SHORT; Correlation coefficients of predictions

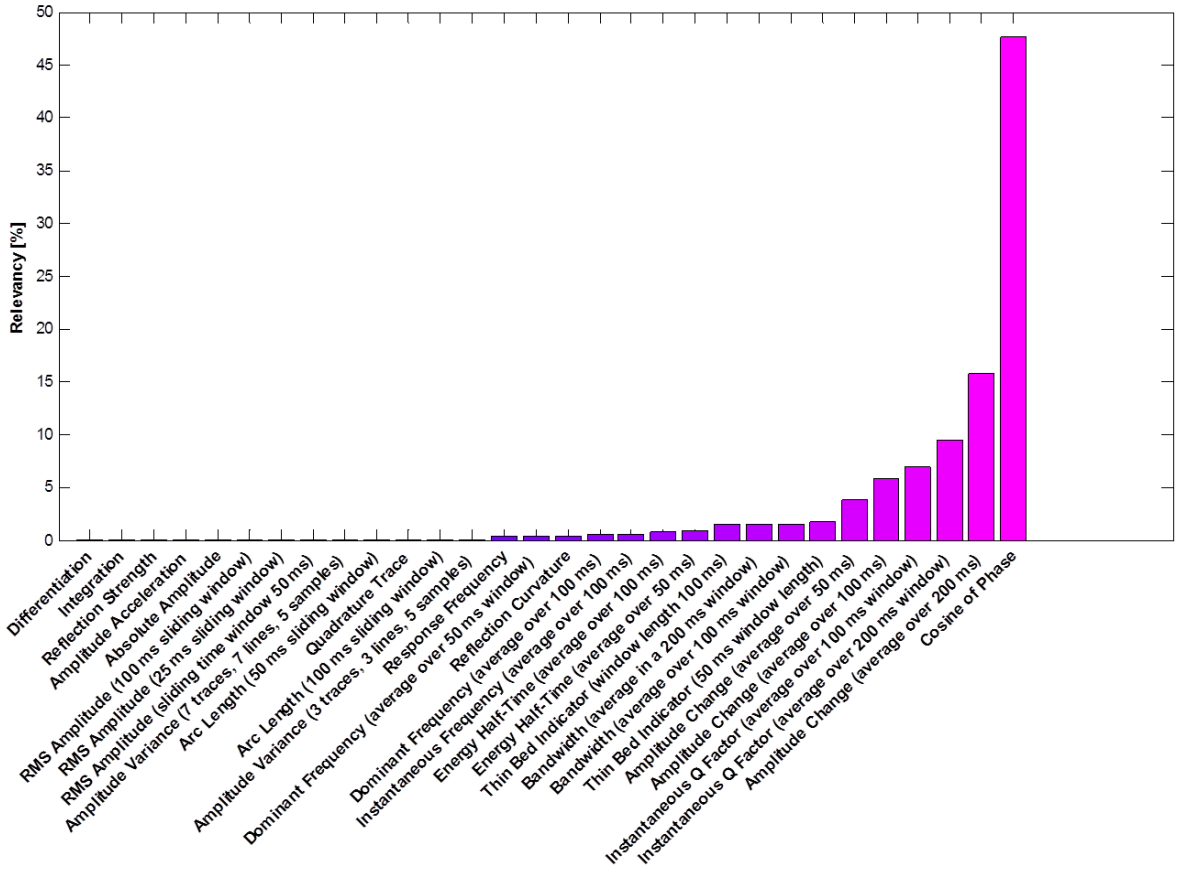

Figure 6.11: Relevancy of seismic attributes in low resolution well log prediction

B. High-resolution well log generation

High-resolution well logs were predicted using time-volume seismic data. For each seismic layer, five neural networks were trained to predict the five well logs. A total of 35 neural networks were trained to predict high-resolution well logs. Initially, 87 wells were used for high resolution well log generations. However, some particular wells resulted in high prediction errors. Analysis of these wells demonstrated that unrealistic flat well log profiles were the cause of high prediction error. Therefore, to improve the performance of the network, flat well log profiles were omitted from the neural network data sets. As a result, total number of wells in training the expert system was reduced. However, the performance of the network did not change significantly, suggesting that the omitted wells were not helping in training the network. The same heuristic procedure was adopted to train the expert system with reduced number of wells. The performance of the network did not change significantly. Therefore, it became clear that more wells should be added to training data sets. The new well log pool for high-resolution well log prediction consists of 230 GR, 231 GKUT, 231 PHIN, 146 LONG, and 175 SHORT logs. 80% of the wells were used for training, 10% for validation and 10% for testing. Wells were selected randomly for each datasets.

The inputs of the high-resolution prediction networks were the sampled time-volume seismic data (300 values) and coordinates (2 values), and the outputs are sampled well logs (50 values). The results of the high-resolution well log networks are demonstrated in Figure 6.12 to Figure 6.16. The first sets of results were related to predictions of raw gamma ray logs (GR). The GR networks are two hidden layer cascade neural networks with 120 and 60 neurons, respectively. Results of GR networks are illustrated in Figure 6.12. More than 70% (160 wells) of the well logs show good correlation with actual well logs (correlation coefficient higher than 0.8). 5 wells consistently have low correlation coefficients and at this point in time this may be attributed to the seismic data and well log data quality. Normalized gamma ray networks are cascade networks with three different networks structures: 120 and 60 neurons (intervals 1 and 2), 110 and 60 neurons (intervals 3 and 4), 90 and 60 neurons (intervals 5 to 7). Normalized gamma

ray predictions also have high correlation coefficients. Prediction correlation coefficients for intervals 1 to 4 are higher than intervals 5 to 6 (refer to Figure 6.13).

Neutron porosity logs (PHIN) results are demonstrated in Figure 6.14. As it can be seen, results are not as good as gamma ray predictions. This may be attributed to the scale of the well logs. Neutron porosity log scale varies between 0 and 1 however; gamma ray logs scale is between 0 and 500 API (maximum observed in the field). Small variations in the neutron porosity logs can reduce the correlation coefficients significantly. Prediction results of long space neutron count rate and short space neutron count rate well logs are presented in Figures 6.15 and 6.16. LONG well log networks are cascade networks with 120 and 60 neurons. Similarly, SHORT networks are also cascade networks with 100 and 40 neurons, respectively. Once the networks are successfully trained and tested, it is possible to predict well logs for entire seismic survey area. The typical well log predictions are demonstrated in Figures 6.17 and 6.18. These well logs will be used in payzone identification when production profiles are predicted for each seismic interval using the high-resolution well logs.

Table 6-1 summarizes the networks structures of all high-resolution well log generation networks. All 35 networks have ‘tansig” transfer functions in hidden layers and ‘satlins” transfer functions on the output layer. Individual predictions of each network are presented in Appendix D. Because of large number of wells in testing pools for predicting high-resolution well logs (more than 10 wells), only five wells are randomly selected for demonstration. Figure 6.19 demonstrates the predicted well logs for two locations overlay on the different seismic attributes. Around 900 to 1000 milliseconds, amplitude seismic data have higher values and predicted well logs demonstrate sharp jumps. This relationship is less visible with instantaneous frequency at the intervals 1250 to 1400 milliseconds.

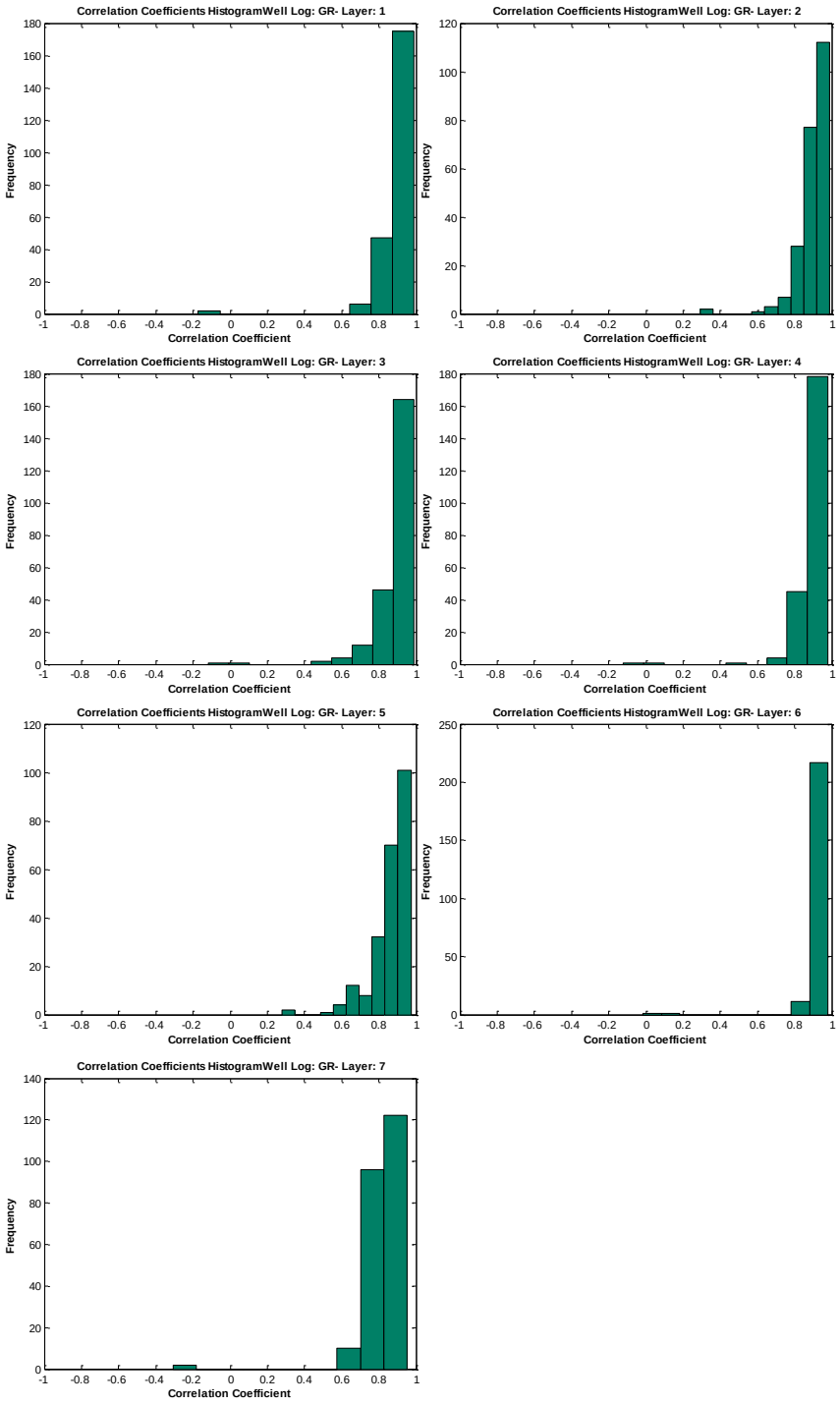

Figure 6.12: High-resolution well log predictions: GR correlation coefficients

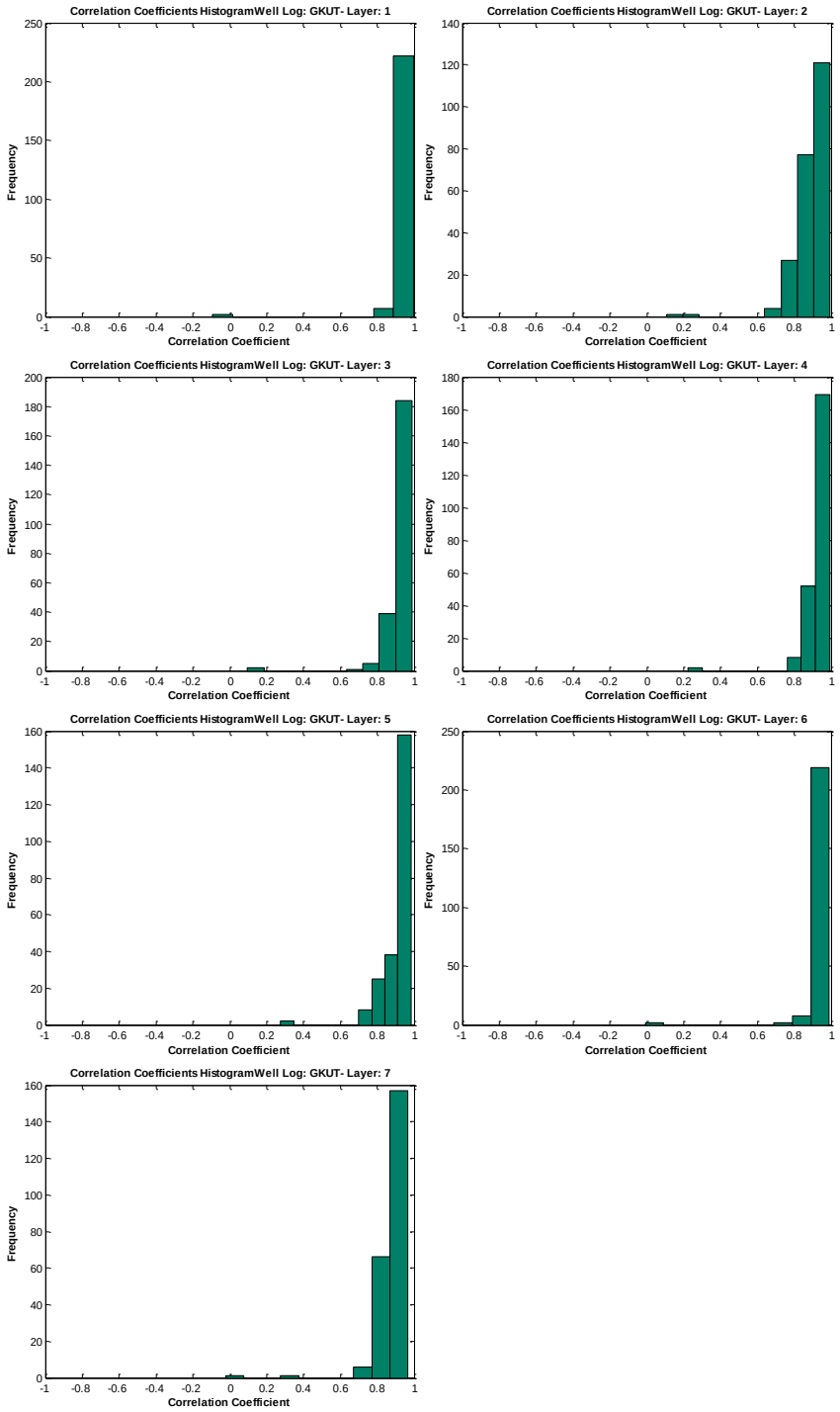

Figure 6.13: High-resolution well log predictions: GKUT correlation coefficients

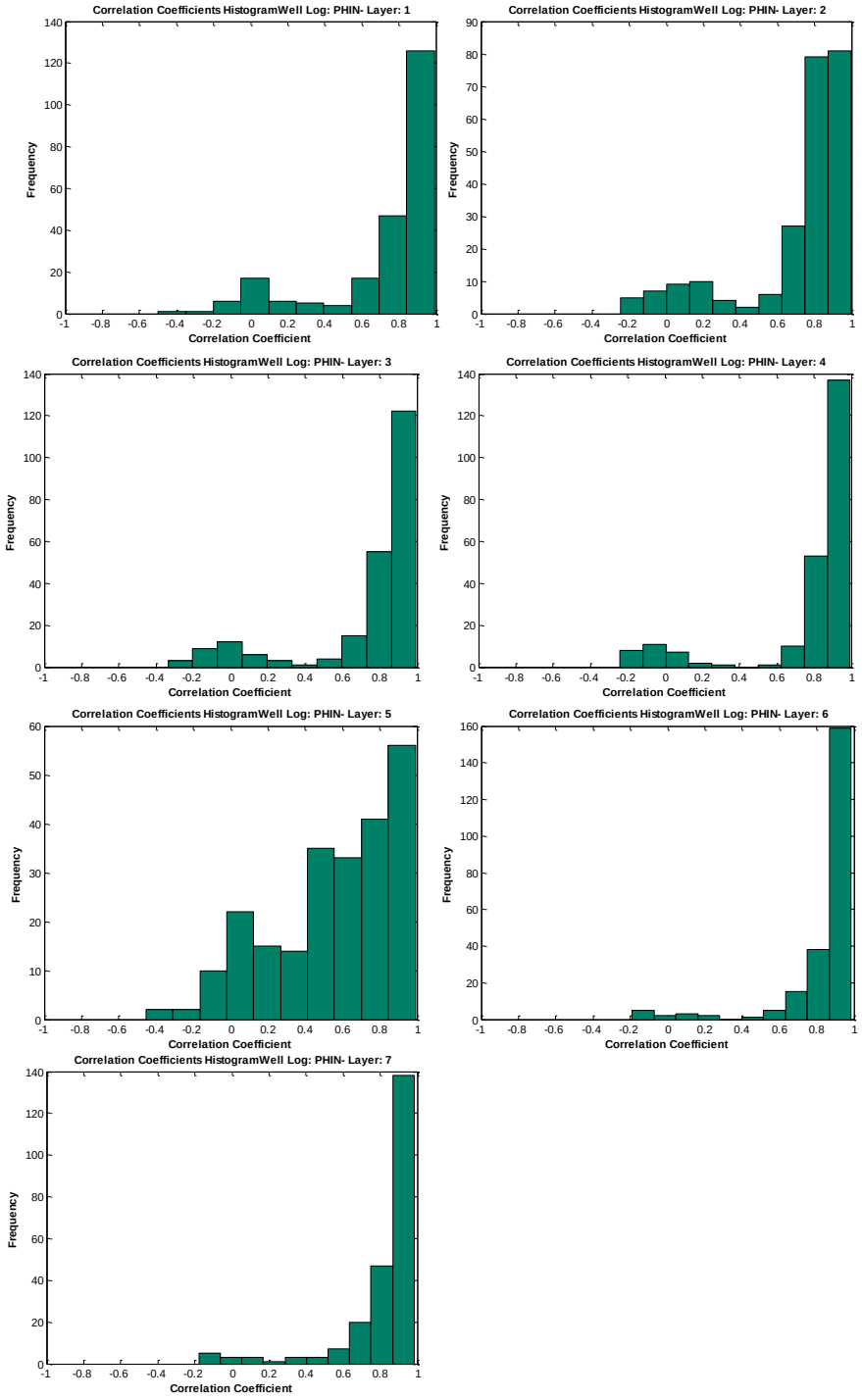

Figure 6.14: High-resolution well log predictions: PHIN correlation coefficients

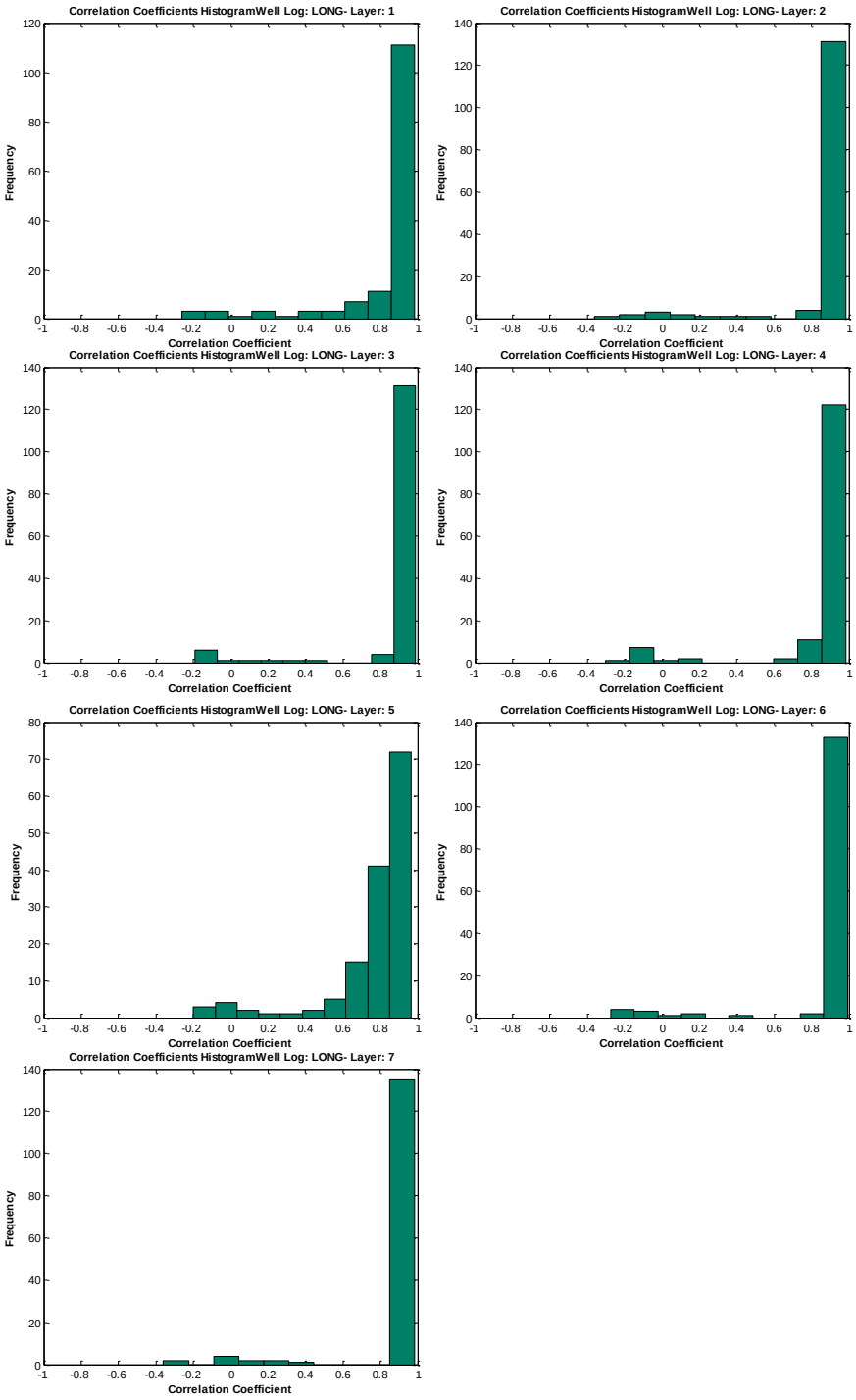

Figure 6.15: High-resolution well log predictions: LONG correlation coefficients

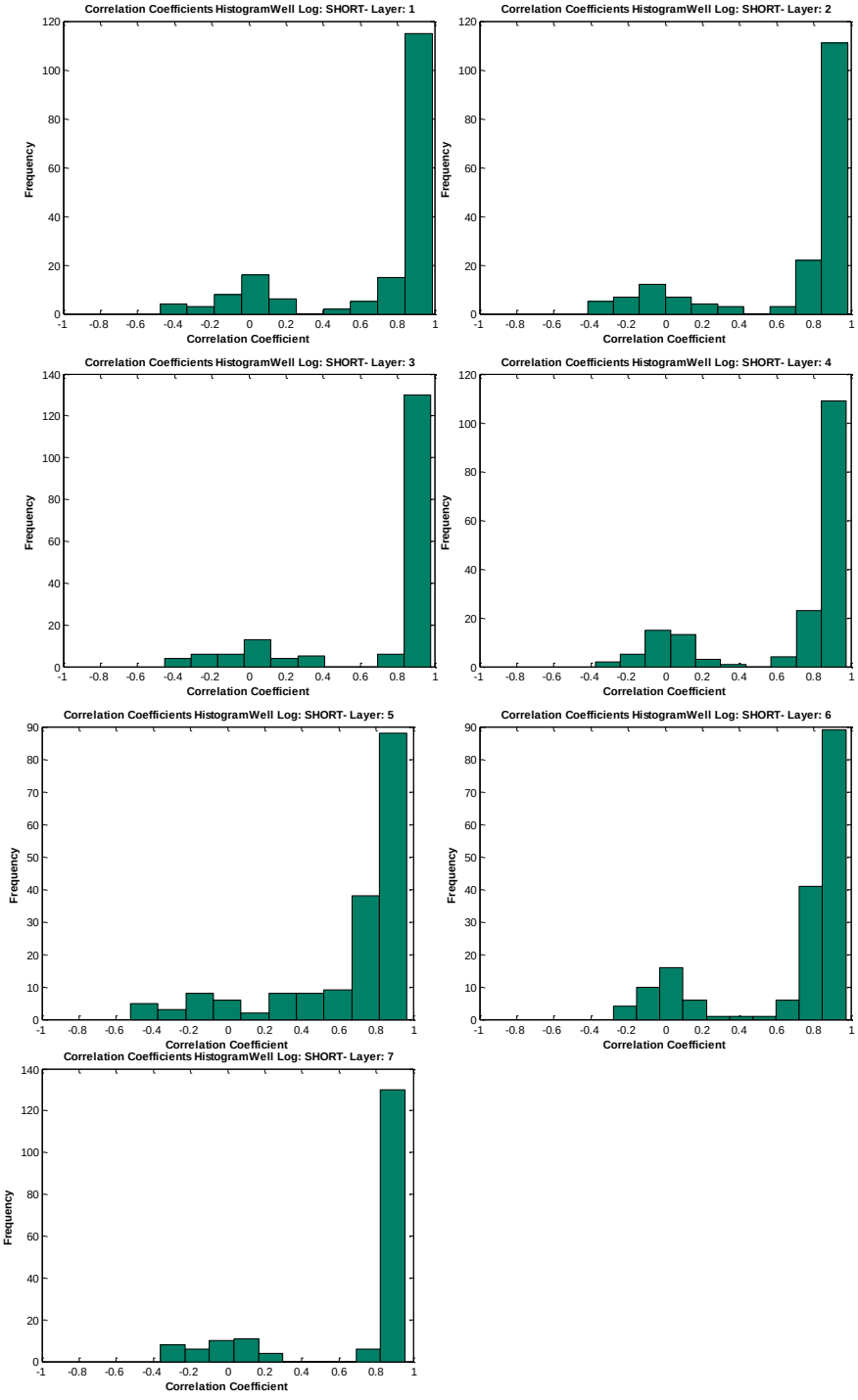

Figure 6.16: High-resolution well log predictions: SHORT correlation coefficients

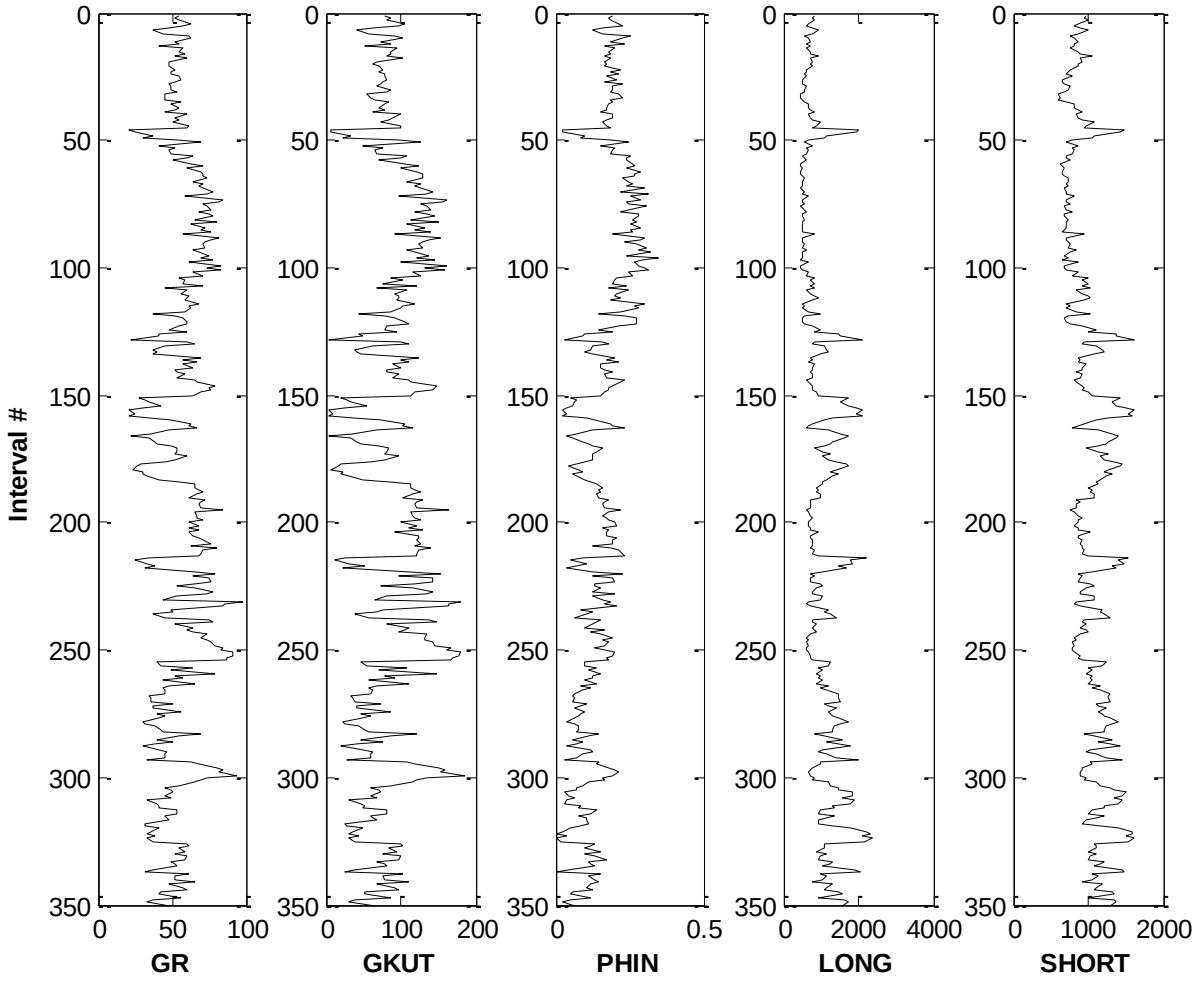

Figure 6.17: Predicted high resolution well logs: testing well A1

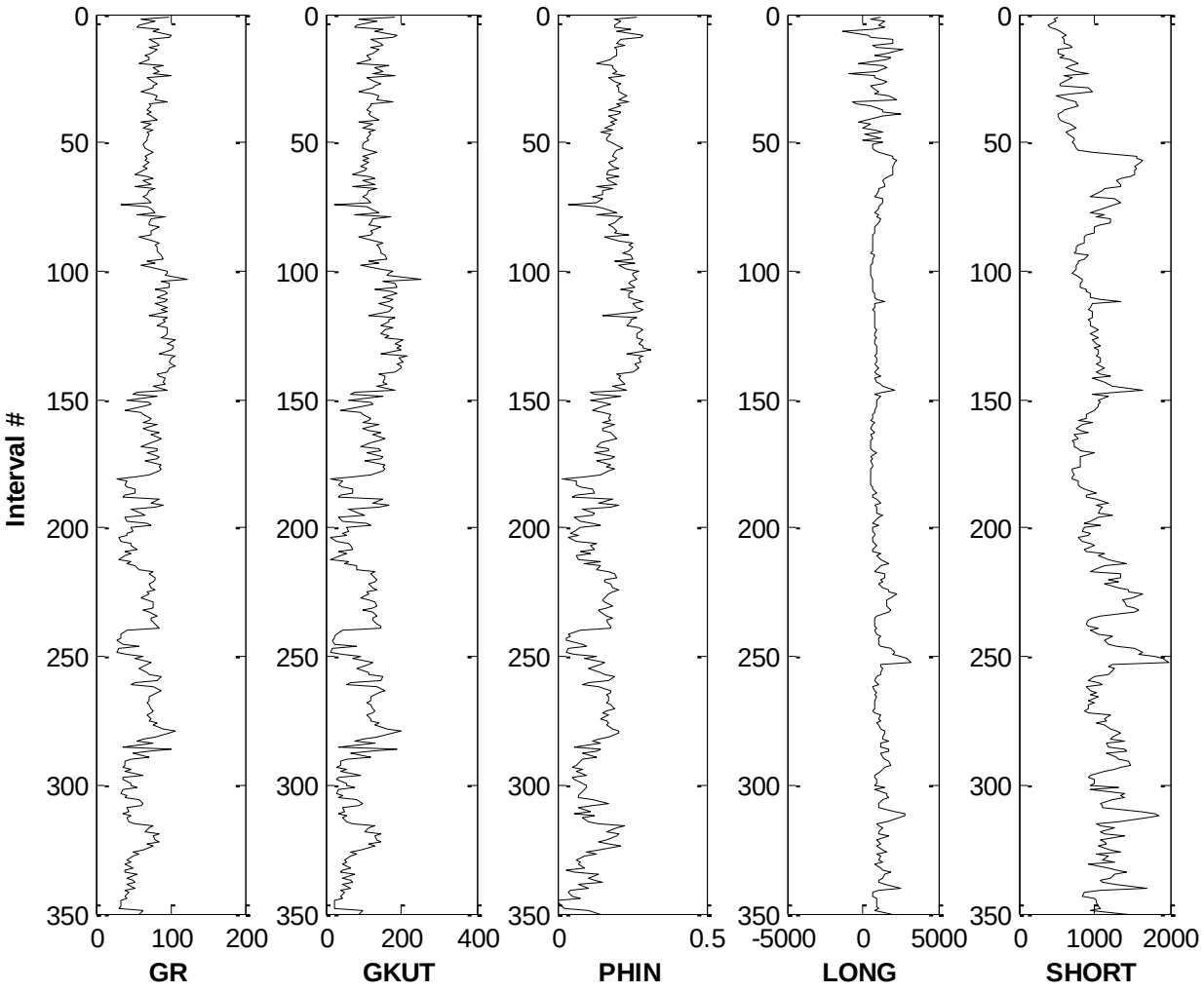

Figure 6.18: Predicted high resolution well logs: testing well A2

Table 6-1: High-resolution well log networks: number of neurons

	GR	GKUT	PHIN	LONG	SHORT
Interval 1	120, 60	120, 60	110,60	120, 60	100,40
Interval 2	120, 60	120, 60	110,60	120, 60	100,40
Interval 3	120, 60	110,60	110,60	120, 60	100,40
Interval 4	120, 60	110,60	110,60	120, 60	100,40
Interval 5	120, 60	90,60	130,80	120, 60	100,40
Interval 6	120, 60	90,60	130,80	120, 60	100,40
Interval 7	120, 60	90,60	130,80	120, 60	100,40

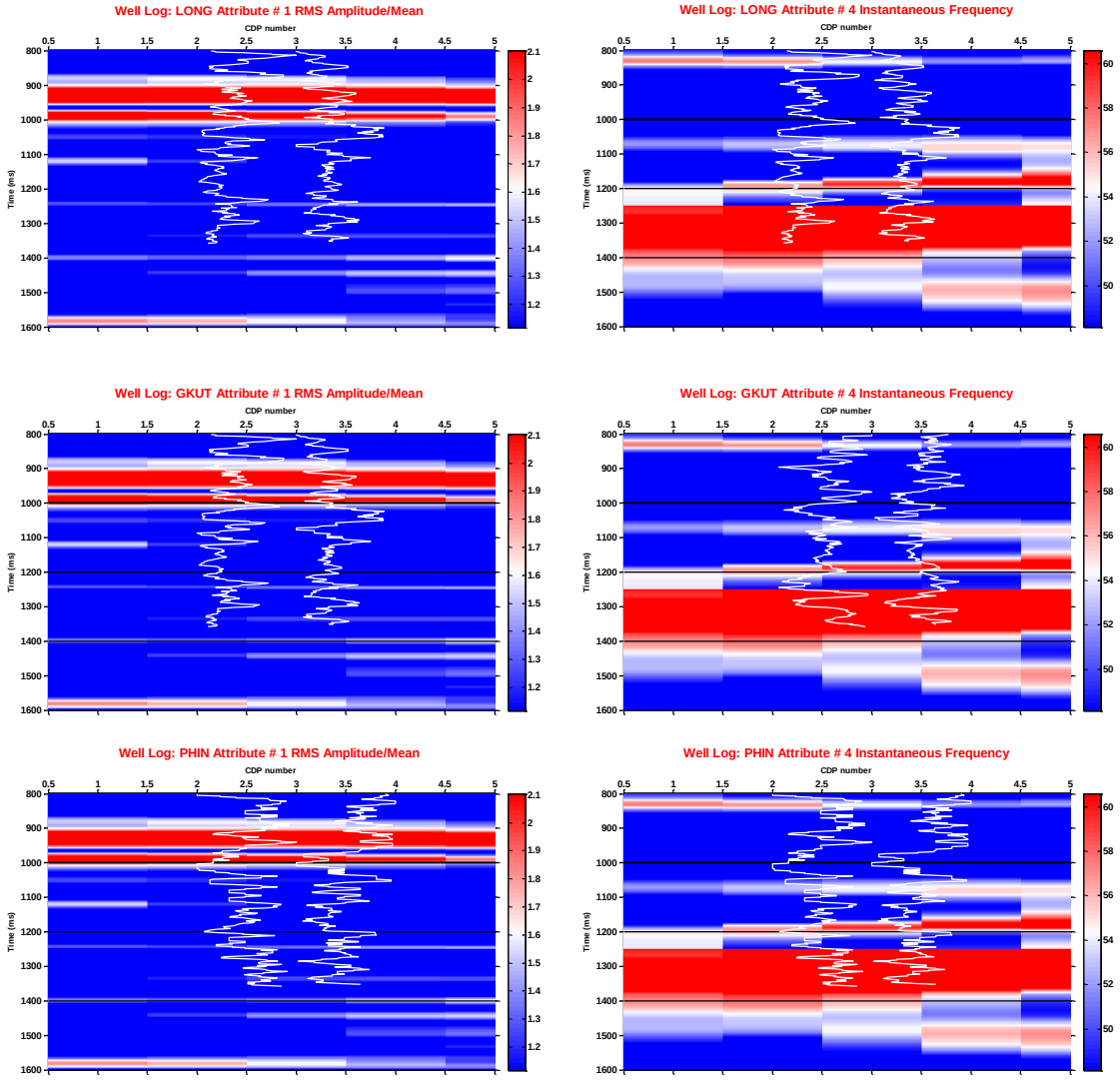

Figure 6.19: Sample predicted well logs and seismic attributes

Well log repair

Many well logs require editing and correcting for further analysis. The main reasons can be attributed to (Walls et al., 2004):

- Wellbore washouts
- Mud filtrate invasion
- Gaps and missing data

Typical approach to resolve the aforementioned problems is to use combination of theoretical, empirical and heuristic methods. Missing data in the well log suites are usually denoted with null value (-999.2500). The most common practice to find the well log values at the null locations is to use interpolation techniques. Interpolation is good only for the small sections of the well logs and in case of large segments it is not accurate since well logs are nonlinear curves. One of the outcomes of this study is to use developed neural networks to predict well log responses for the missing segments. Figure 6.20 demonstrates the well log predictions for the null segments for two wells. Null segment for the first well is located from 1250 to 1305 milliseconds. It is evident that interpolation technique cannot match the predictions of neural network because network predictions are made based on the discovered pattern within the seismic data. The null segment of second well is starting from 1100 to 1190 milliseconds. Analyzing the trend of the predictions with the rest of the well log segments, it is evident that predictions more or less follow the general trend of the well logs. However, for the second well, in some parts (e.g., at time 1180 of the second well) predicted well logs demonstrate very low value. This can be fixed by using the user specified threshold values (e.g. PHIN logs thresholds are 0 and 1).

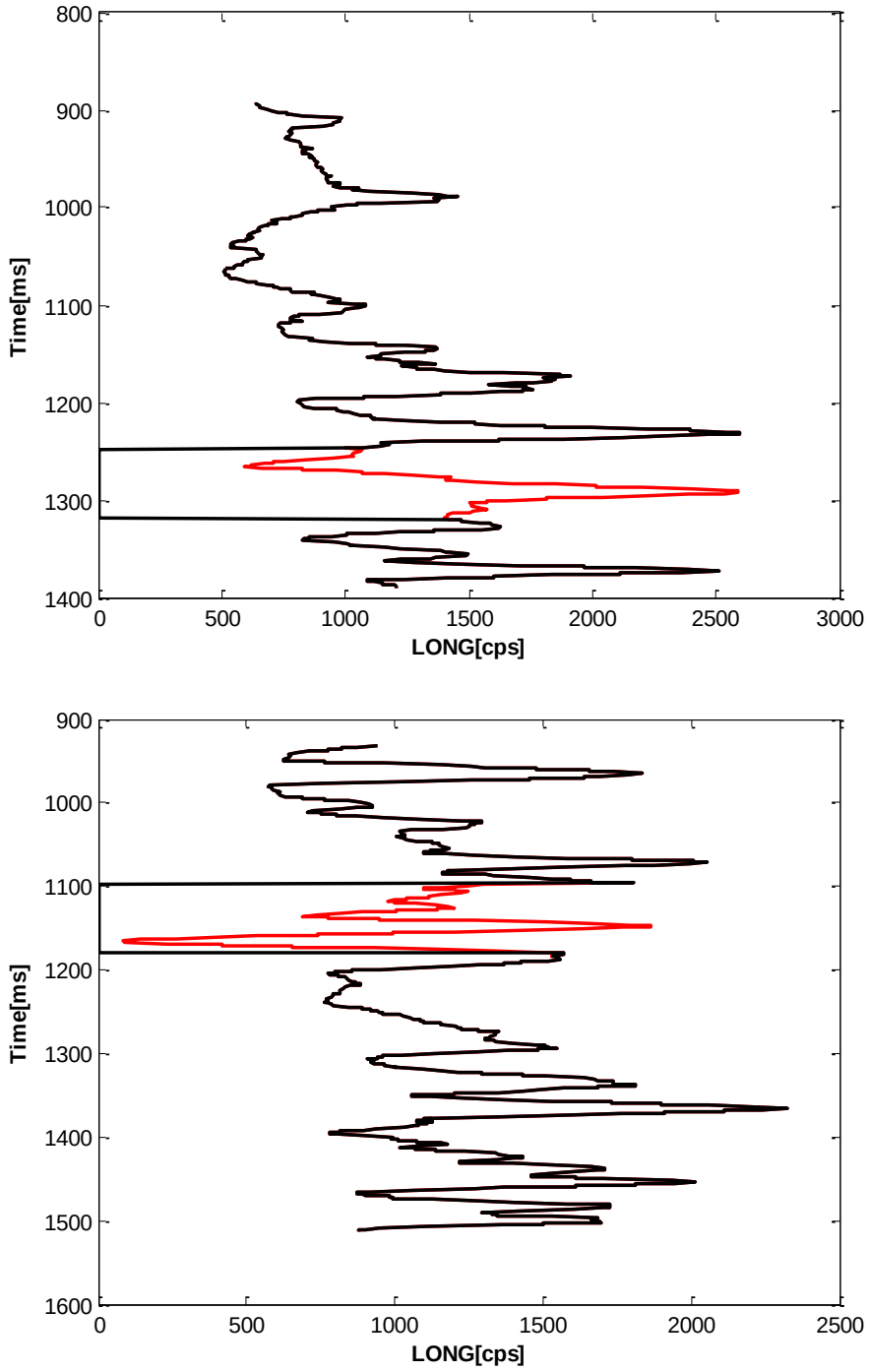

Figure 6.20: Well log predictions for the null segments (predictions are demonstrated in red color); Top: null segments starting from1250 to 1305 milliseconds, Bottom: null segments starting from1100 to 1190 milliseconds

Payzone Identification

In this section, the results of payzone identification methodologies are discussed. Figure 6.21 displays typical results of the coarse resolution payzone identification approach. Comparing all three cases, the deepest layer (layer 4) is consistently found to be among the top oil producing intervals and similarly, layer 1 is observed to be among the lower producing intervals. The summation of oil production from different intervals is approximately the same as the actual total well production in case A (best case). For the cases B and C, total oil productions from four intervals are different than the actual values. Most of the predicted oil production profiles are in good agreement with actual oil production of the wells (57 wells out of 87 wells).

Figure 6.22 to Figure 6.24 demonstrate the results of the high-resolution approach. In the high-resolution approach, actual well logs were used and every 50-feet interval predictions were made by testing the oil performance neural network. The best-case results are shown in Figure 6.22. The top figure demonstrates 24-month cumulative oil production along the depth of the well versus common well logs and mineralogy logs. As it can be seen, a high oil production zone is located 7000 to 7200 feet deep and low producing zones predicted to be located at 8500 feet deep. The summation of oil productions from different zones is in good agreement with the actual production values of the well. Typical results are demonstrated in Figure 6.23 and worst-case result is shown in Figure 6.24. In general, most of the predictions can be classified as average accuracy predictions (62 wells out of 87 wells).

The advantage of high-resolution approach over low-resolution approach is clear by analyzing productions and well logs along the well depth new relationships and correlations can be understood. In this study, two types of classifications have been made based on wireline well logs and mineralogy logs obtained from mud logging. In this study, Neuro-fuzzy classification (ANFIS) method was used to develop fuzzy relationships. ANFIS method is like a fuzzy inference system with this different that here

by using a backpropagation tries to minimize the error. Advantage of incorporating neural network in fuzzy inference system is neural network learning algorithm which helps finding optimal solution.

First step of using ANFIS in this study is to extract initial guesses for fuzzy rules using multidimensional regression analysis of input/output data. These initial fuzzy rules are used as initial guess for the ANFIS classifier. In the next step, fuzzy rules are trained in such a way to reduce the error between fuzzy output and actual targets. Outputs of regression analysis are demonstrated in Figure 6.25. According to regression analysis, LONG well log is the key factor in classifying oil production data. Figure 6.26 displays the fuzzy surfaces of oil production data versus LONG and GR. As it can be seen, production declines rapidly around LONG values of 1000 cps. High oil production was correlated to the gamma ray log values of higher than 80 API. Mineralogy based classification results are demonstrated in Figure 6.27 to Figure 6.31. The fuzzy surfaces are demonstrated in Figure 6.28. Pick of oil production is related to the shaly segments of the formation with more than 50% shale. In Figure 6.29 and Figure 6.30 the cross-section of the fuzzy surface of mineralogy logs are presented. At zero percent limestone segments of the formation, high oil production zones are correlated to 40% to 70% shale. Similarly, at zero percent shale intervals, high oil production zones are correlated to the formations with limestone less than 20%. Since formations typically consist of multiple minerals, it is necessary to expand the classifications to all minerals present in the formation. We propose using ternary classification of the minerals. The three groups of the minerals are limestone, shale, and other mineral (combination of 15 minerals such as chalk, bentonite, chert, etc.). Using the ternary classification, two regions of high producing oil are identified from Figure 6.31 with 50% and 85% limestone.

The third approach of the payzone identification is to predict the oil production profiles for each seismic interval. In the ATM region of the Wolfcamp field, seven seismic intervals were identified. In this approach for each seismic interval, production profiles were predicted using well logs (high resolution well logs), seismic data (sampled time-volume seismic data) and completion data. Production predictions are presented in the form of production potentials. Production potentials describe the potential of each

interval to produce oil, gas and water. For example, for a given location in the ATM region, total oil, gas and water productions are predicted using information of all seven intervals (results are given in Figure 6.32). Then, by analyzing production potentials (results are given in Figure 6.33 to Figure 6.35) it is possible to rank gross thickness of the reservoir. Analysis of oil production potential of all seven intervals reveals that for the selected location, interval 6 outperforms other intervals. Interval 6 is also among the top gas and low water producers. Thus, Interval 6 at this location is a good candidate for completion. Intervals 1, 4, and 5 are observed to be among the top water producing intervals.

It is necessary to dig dipper in the payzone identification and one possible way might lie in understanding of the predicted production logs. Essential information for predicting the production logs are well logs. Trained networks establish relationships between well logs and production data. Therefore, attempts are made in this section to expose the hidden relationships in the trained network and increase understanding of the pay identification. Production logs are predicted at the seismic locations scatter over the entire field (schematic is illustrated in Figure 6.36). Histogram of the predicted production values are demonstrated in Figure 6.37. As it can be seen, histogram demonstrates the log normal type behavior with two distinct classes: low and high production points. Well log data of each corresponding class is compared on the histogram of well logs and the results are presented in Figure 6.38. Histogram of well logs (blue lines) is obtained using the entire well logs of the field. As it can be seen, the lowest production points are corresponding to gamma ray of more than 60 while highest production zones corresponds to gamma ray of less than 60. This result may be contradictory to the previous results, especially those obtained using fuzzy classification method (refer to Figure 6.28). It should be noted that fuzzy classification results are obtained considering the entire production logs while the earlier approach is based on then point by point correspondence. A typical well can have a high production zone while the rest of the zones are average or low producers.

Parallel to the earlier argument, mud logs of the wells are analyzed. Figure 6.40 demonstrates the mud logs results of two typical wells along with the gamma ray log. It is evident that most of the

intervals are dominated by the shales and clean sand intervals are non-existent. This trend can be seen in all the wells with mud logs (25 wells). Therefore, it can be concluded the amount of shale percentages in each intervals plays the crucial rule in the production data. This leads to the connection with the fuzzy classification results in which it is determined that 40 to 60 shale percentages result higher oil production values.

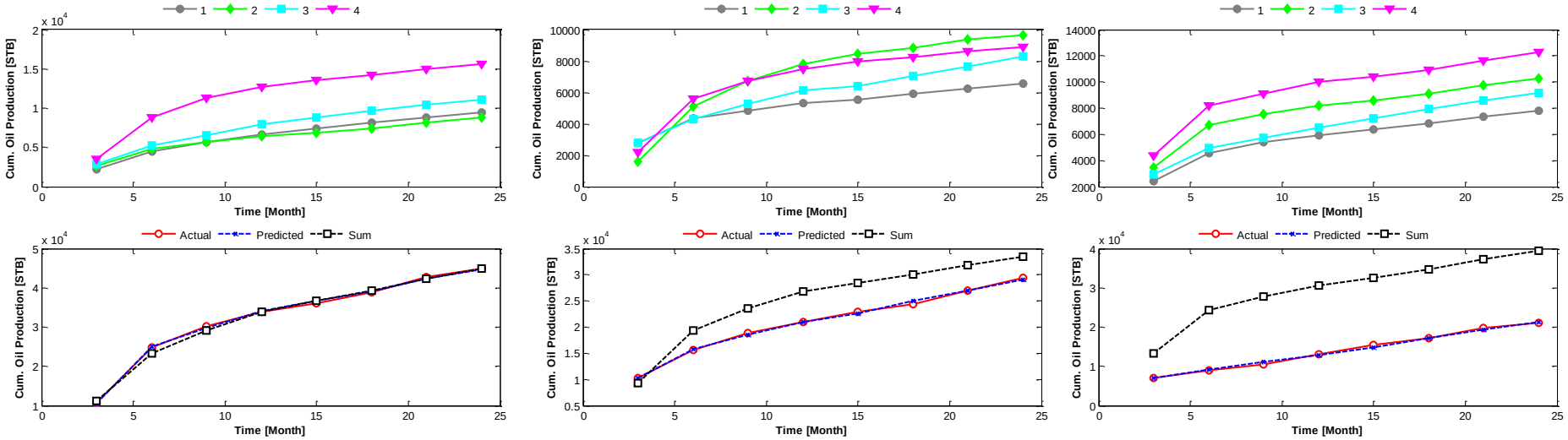

(a) (b) (c)

Figure 6.21: Typical results of coarse resolution approach: a) best result, b) average result, c) worst result

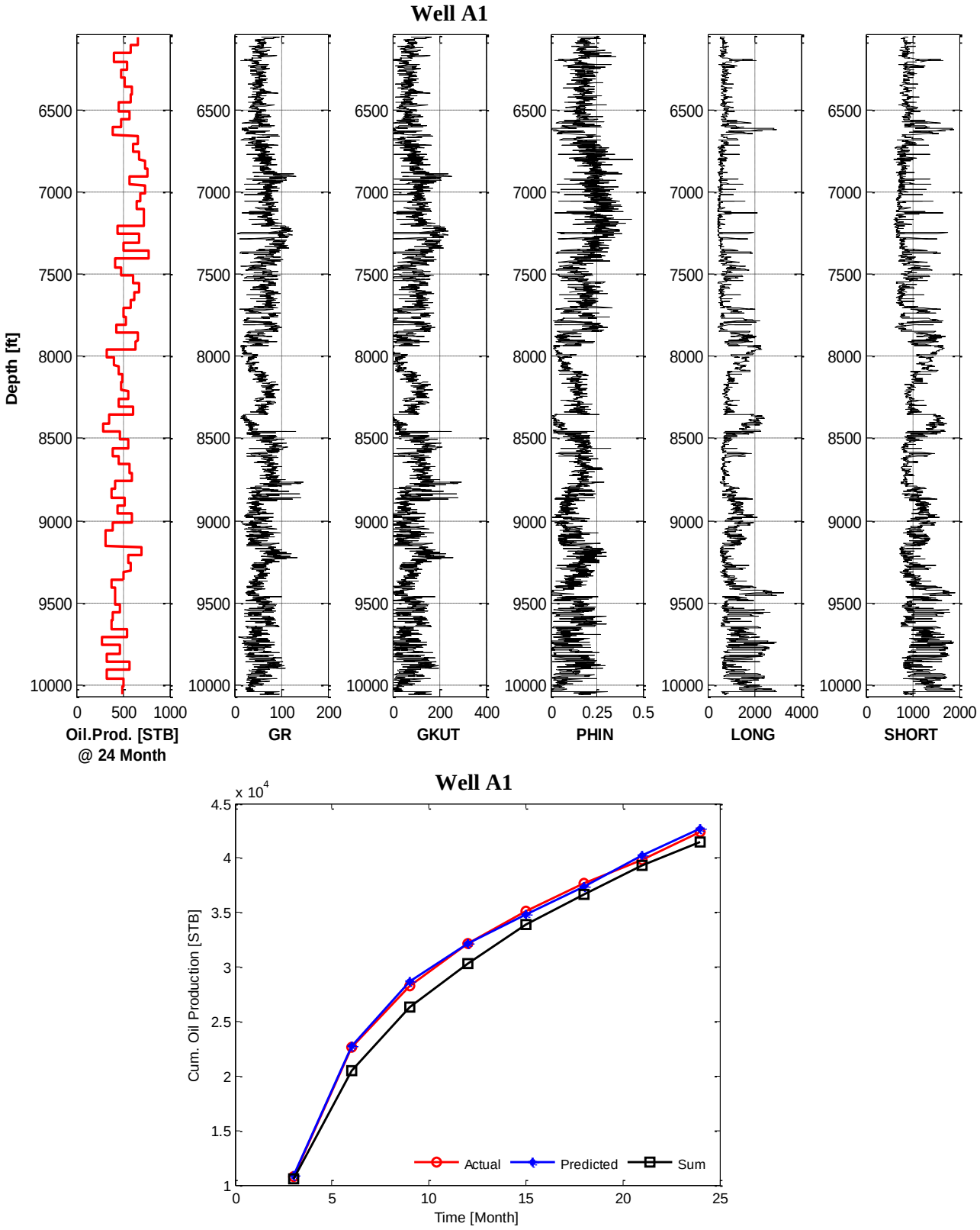

Figure 6.22: Typical results of high resolution approach, top figure: production versus depth versus well logs, bottom figure: total cumulative production profiles; best result

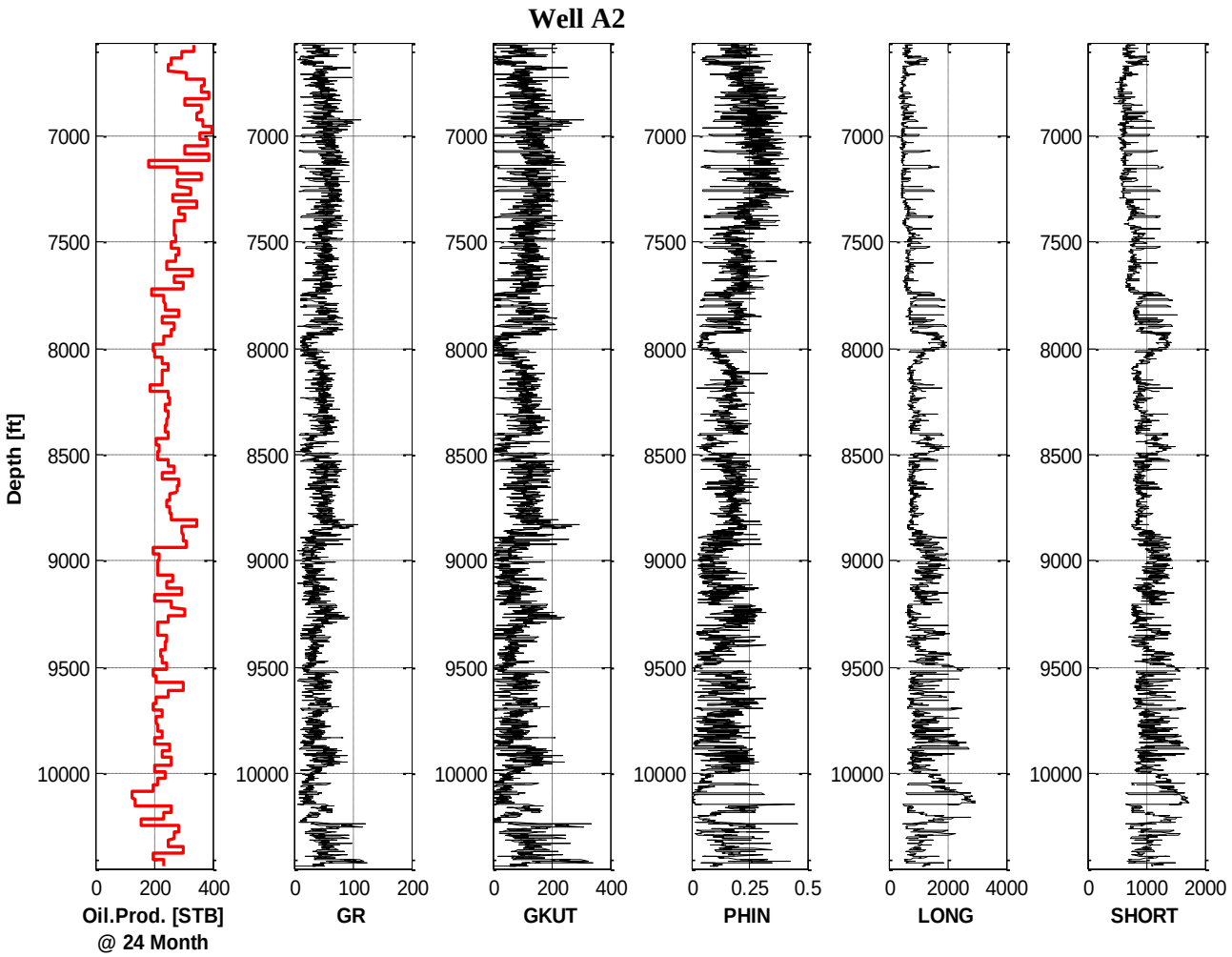

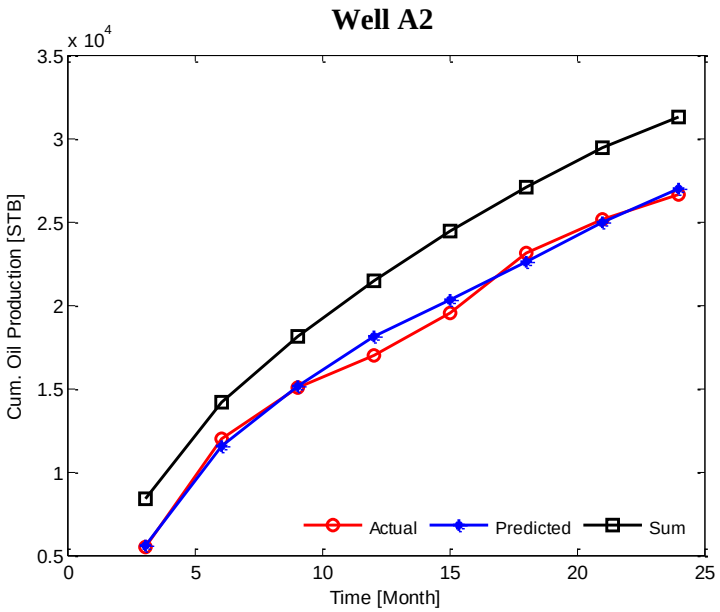

Figure 6.23: Typical results of high resolution approach, top figure: production versus depth versus well logs, bottom figure: total cumulative production profiles; average result

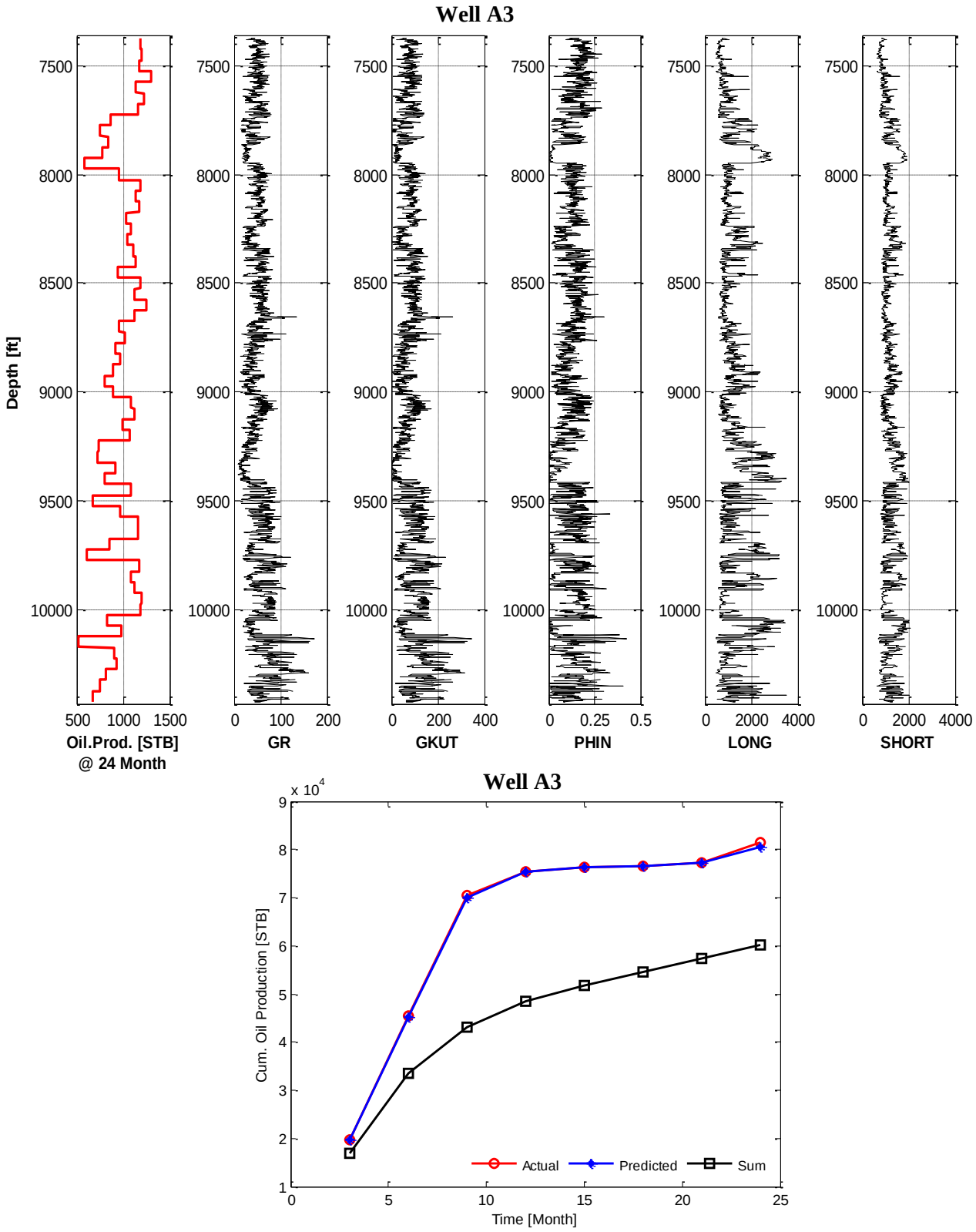

Figure 6.24: Typical results of high resolution approach, top figure: production versus depth versus well logs, bottom figure: total cumulative production profiles; worst result

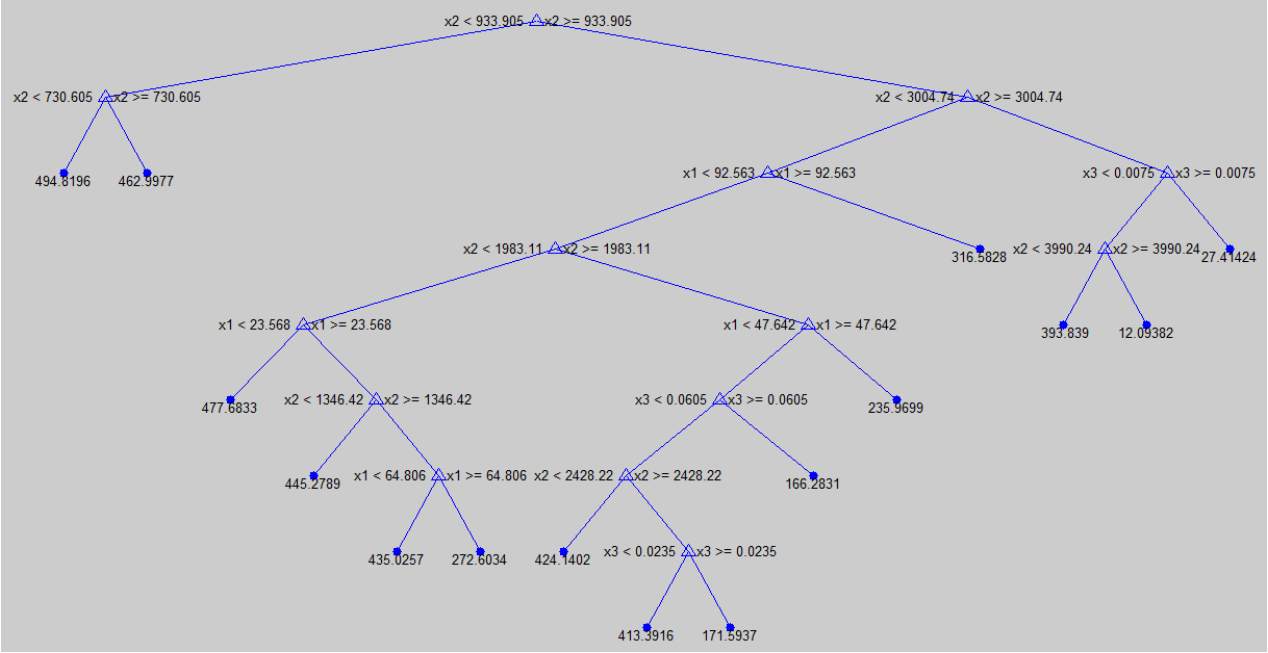

Figure 6.25: Regression tree analysis of production data and well logs (x1: GR, x2: LONG, x3: PHIN)

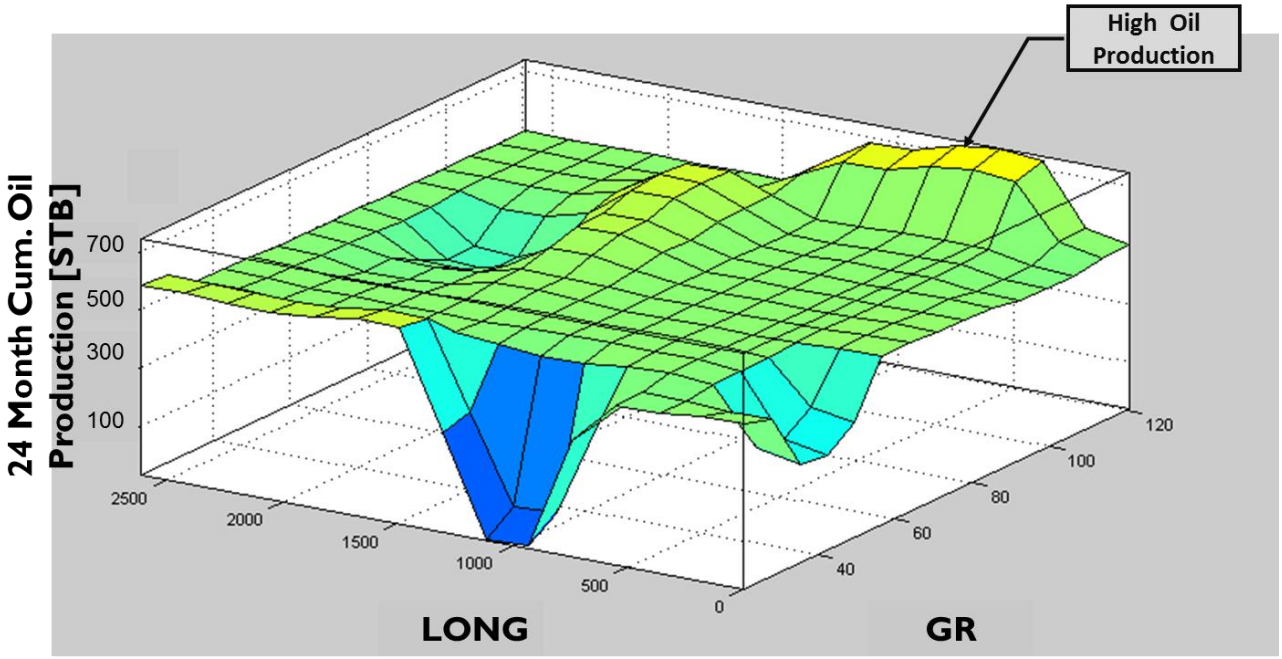

Figure 6.26: Fuzzy surfaces of oil production data and mineralogy logs

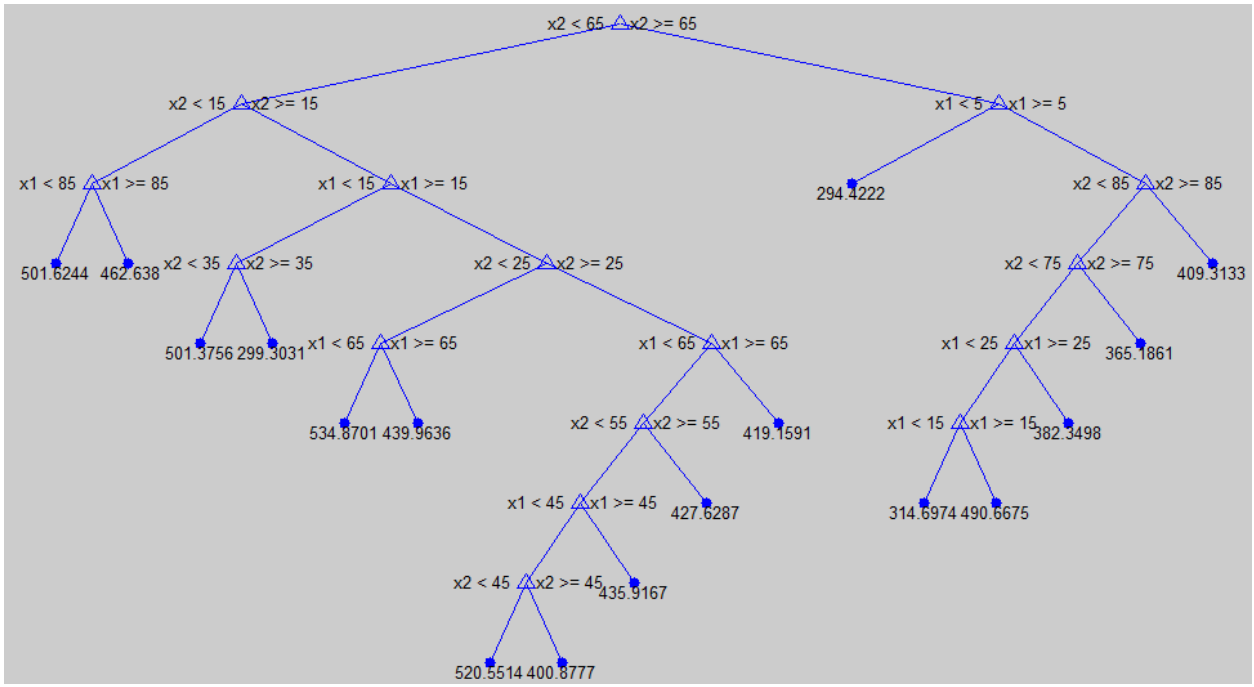

Figure 6.27: Regression tree analysis of production data and mineralogy well log (x1: Shale, x2: Lime)

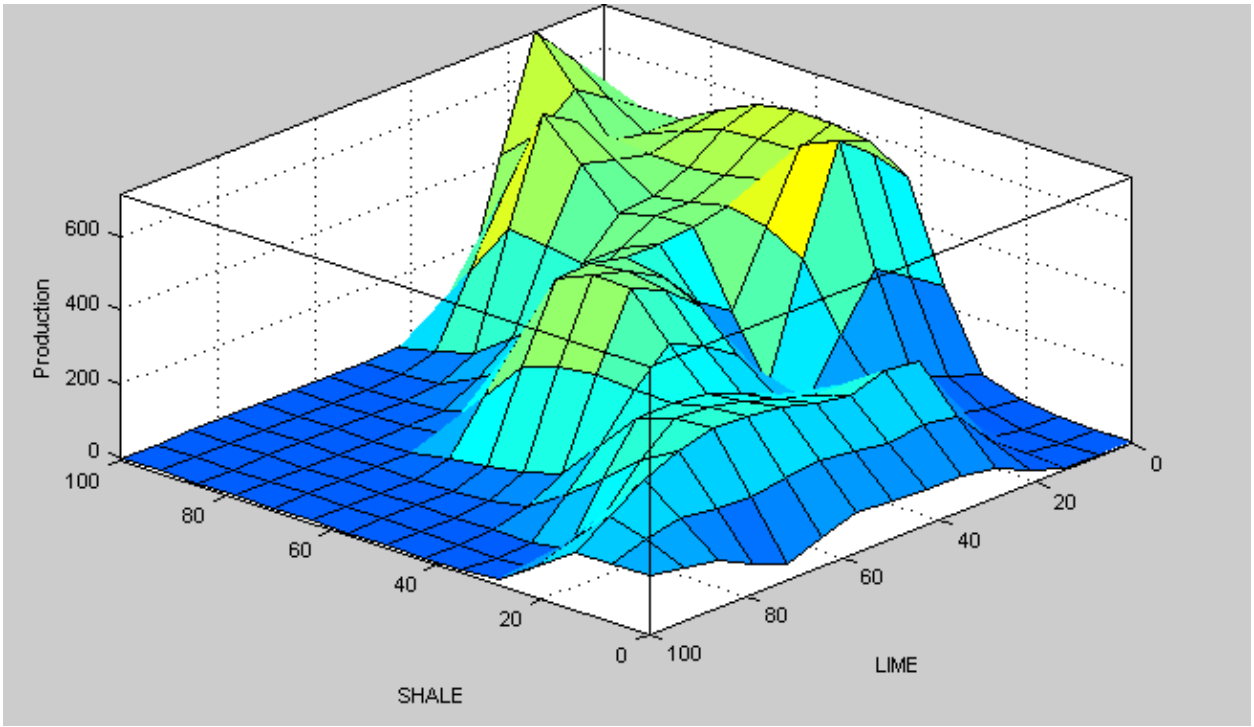

Figure 6.28: Fuzzy surfaces of production data and mineralogy logs

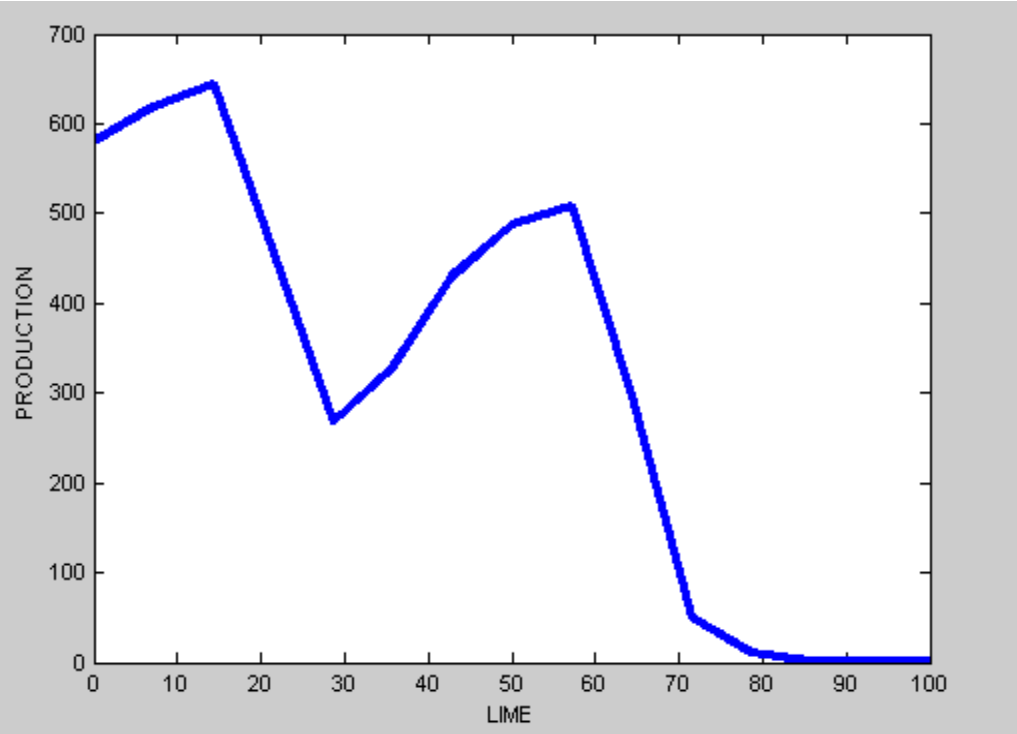

Figure 6.29: Cross-section of fuzzy surface @ Lime = 0%

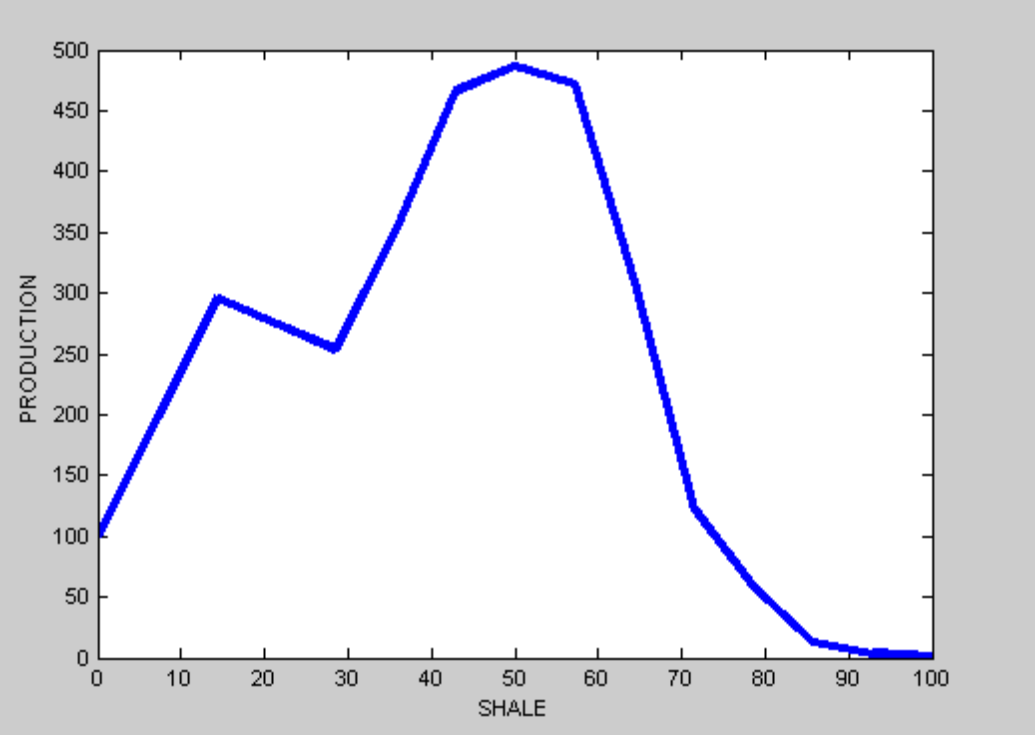

Figure 6.30: Cross-section of fuzzy surface @ Shale = 0%

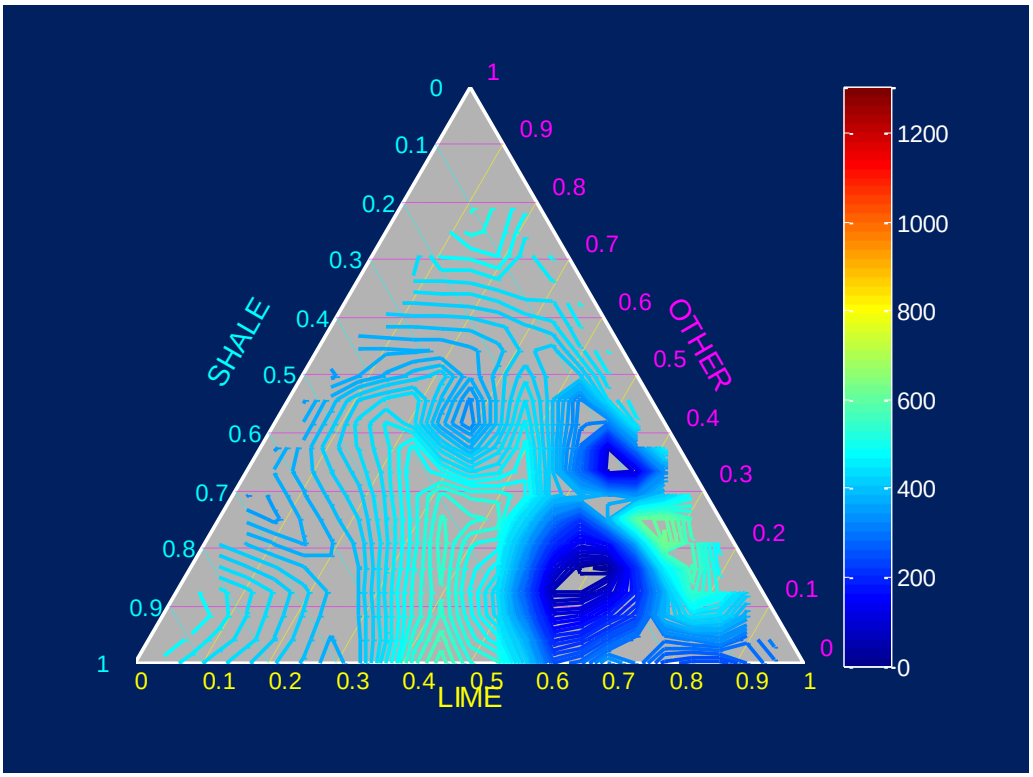

Figure 6.31: Ternary classification of oil production data and mineralogy logs

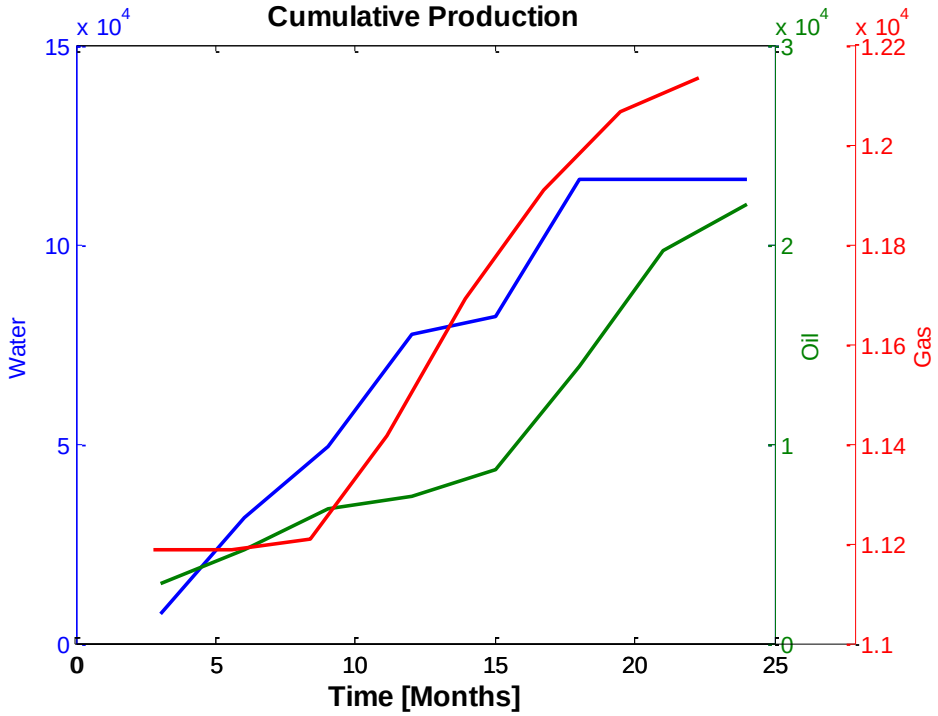

Figure 6.32: Cumulative oil, gas, and water production profiles

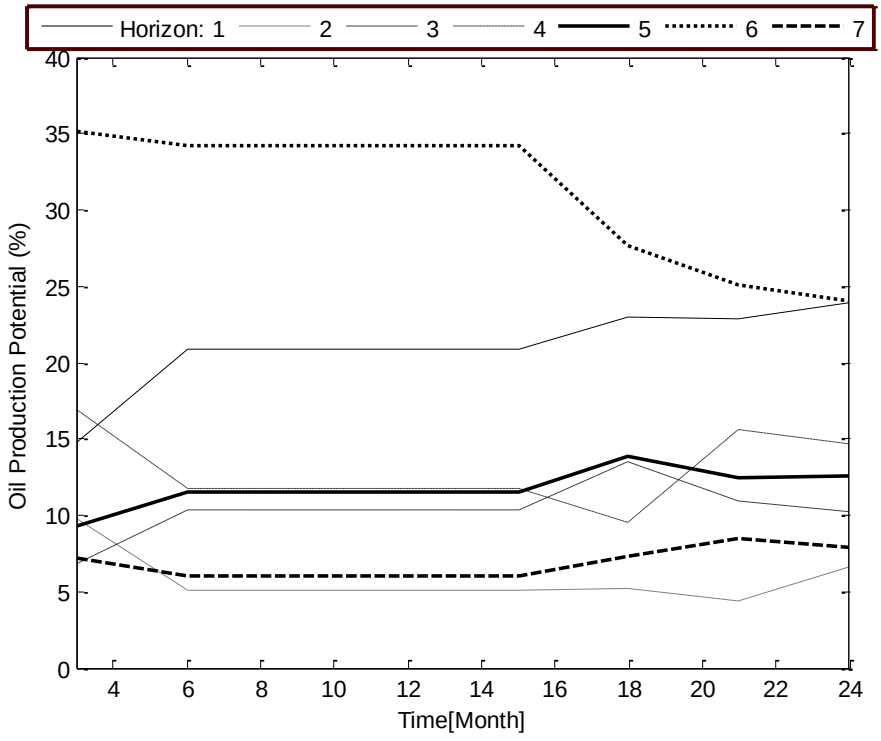

Figure 6.33: Oil production potentials for a selected location

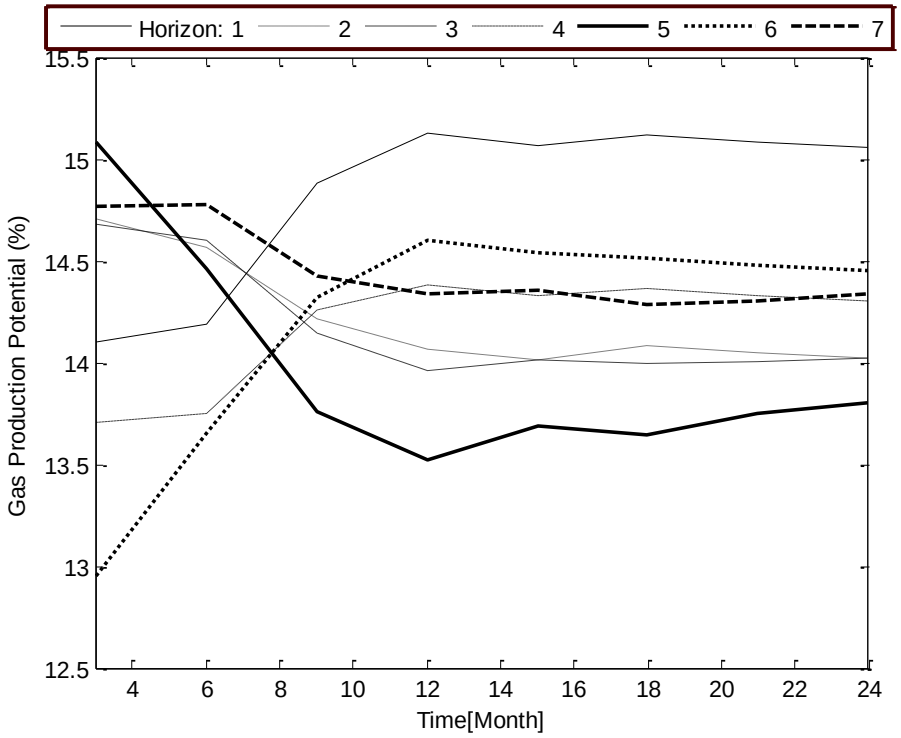

Figure 6.34: Gas production potentials for a selected location

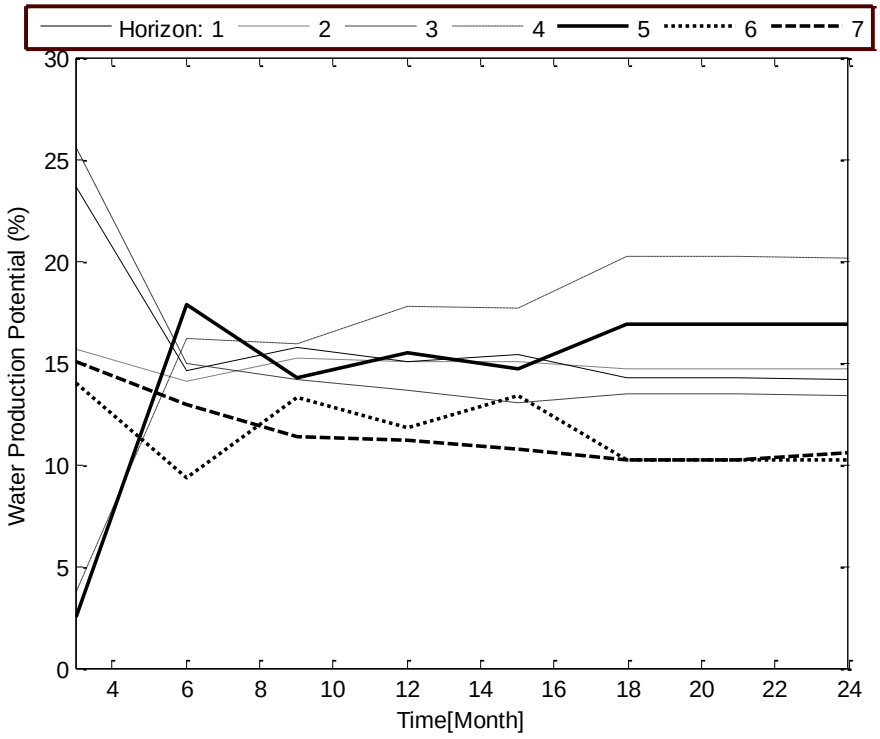

Figure 6.35: Water production potentials for a selected location

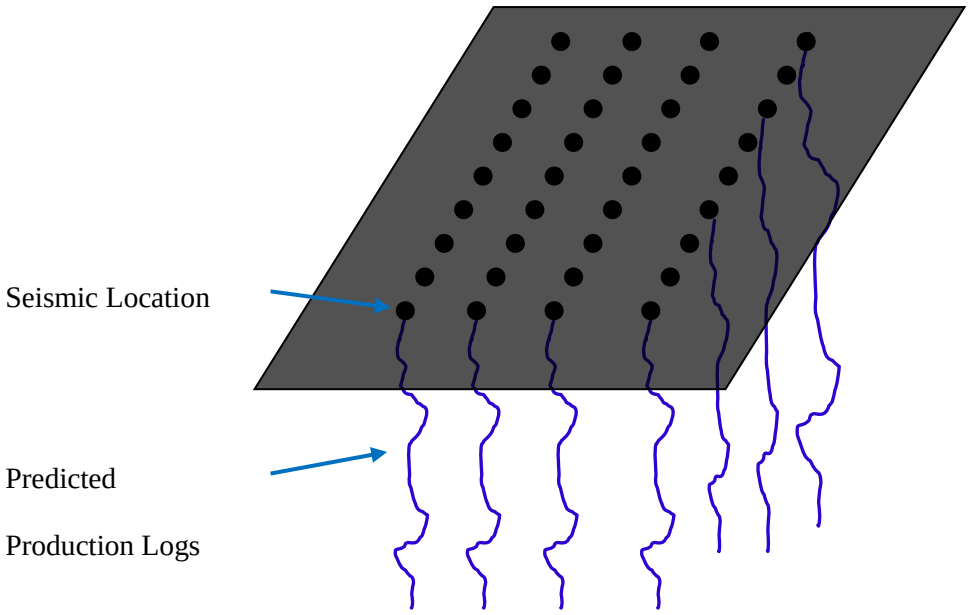

Figure 6.36: Schematic of seismic locations and production logs

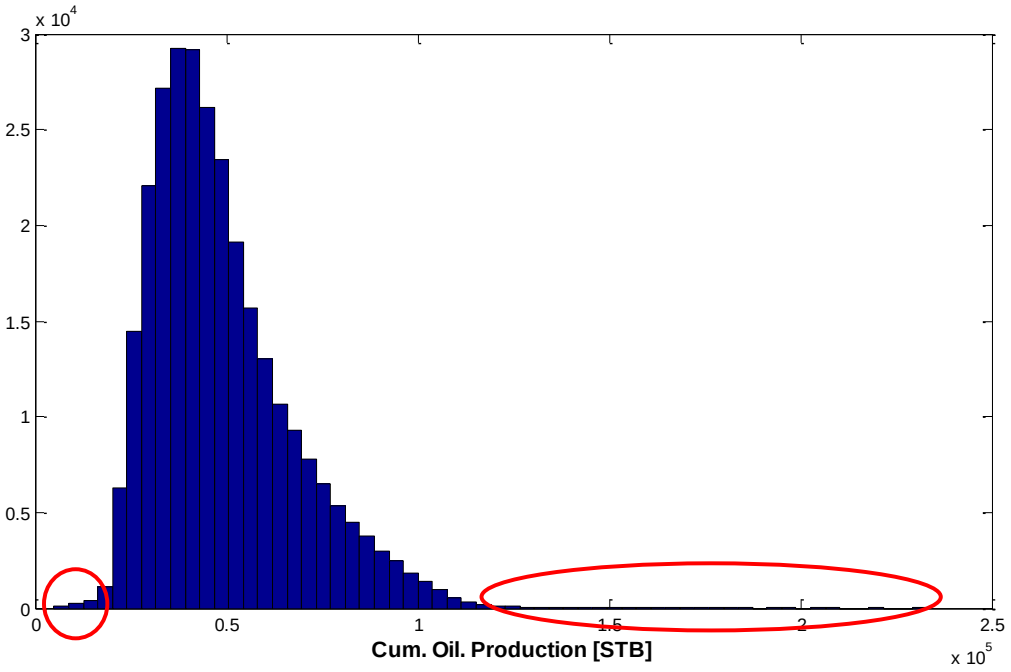

Figure 6.37: Histogram of predicted production logs

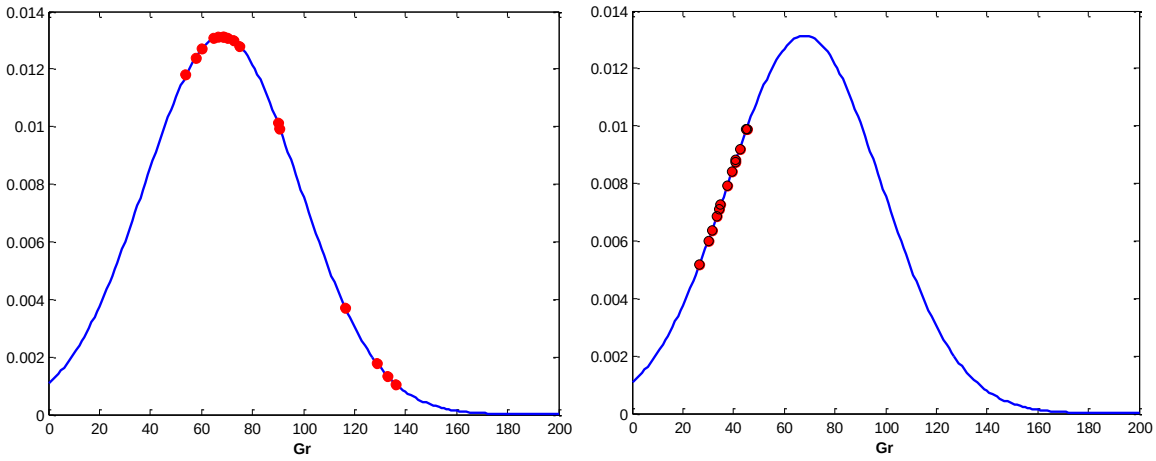

Figure 6.38: Comparison of well log points corresponding to production data: *Left:* lowest producing point, *Right:* highest producing points (blue lines: fitted well log histogram, red dots: well log points corresponding to production data)

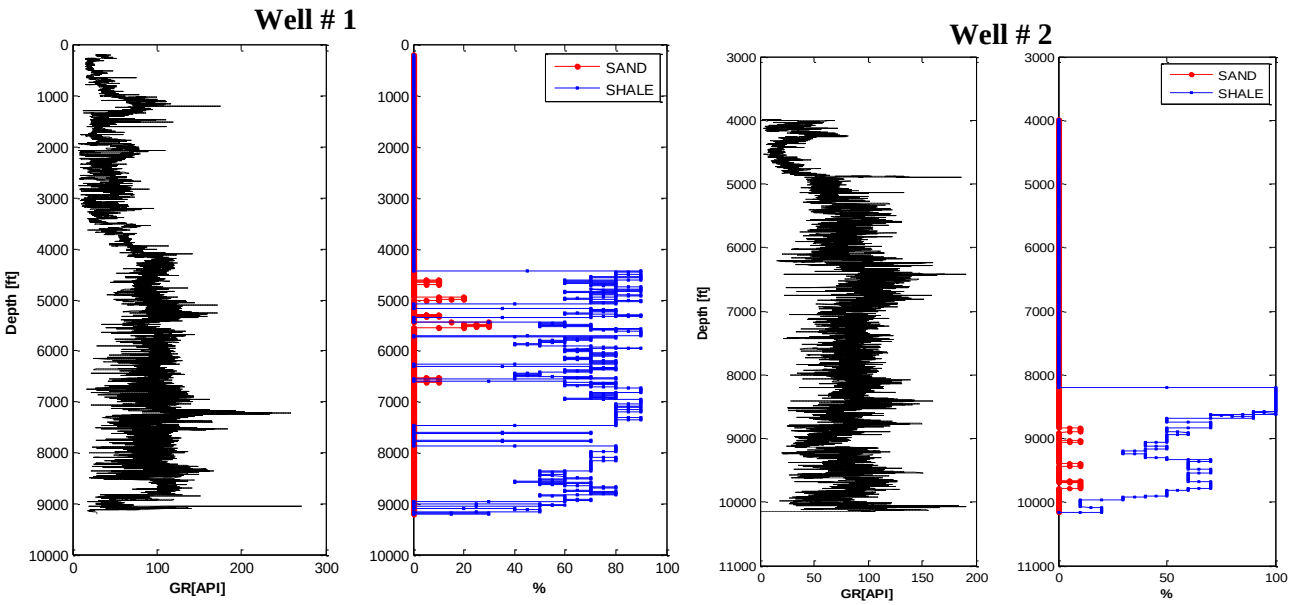

Figure 6.39: Comparison of mud log lithologies and gamma ray log for two typical wells

Comparison with Field Data

Comparison of the outcome of the artificial expert systems with field data is very important. During the development of neural networks, predicted results were compared against actual data in order to assess the performance of each network. The final stage of the comparison is done by comparing the surface map of predicted oil productions and that of actual production map. Actual map of production data is supplied at the end of this research to validate the networks. This map is constructed by interpolation of production rates of more than 340 wells. Predicted and actual surface maps are demonstrated in Figure 6.40. As it can be seen from this figure, the locations of hot spots in two maps are comparable suggesting that networks successfully captured the high production zones of the field. On the other hand, in terms of cold spots (demonstrated with blue color in predicted map, and by bright green in actual map), there is a good correlation between two maps. This is particularly important because the cold spot locations are low production zones and are recommended not to drill.

One of the most important outcomes of this study is the ability to suggest new locations for infill drilling wells. Infill drilling well locations is obtained by picking the points with highest predicted production rates. At any location where seismic data is available, well log and completion information is predicted and fed to well performance networks which predict production data (oil, water, and gas). Then, by studying the variation of the production rates spatially, one can pick best locations to drill. Map of suggested infill drilling wells is presented in Figure 6.41. These points are selected based on one year cumulative oil production. As it can be seen, most of the infill drilling wells are located in the center of the field which corresponds to high production rates at these location.

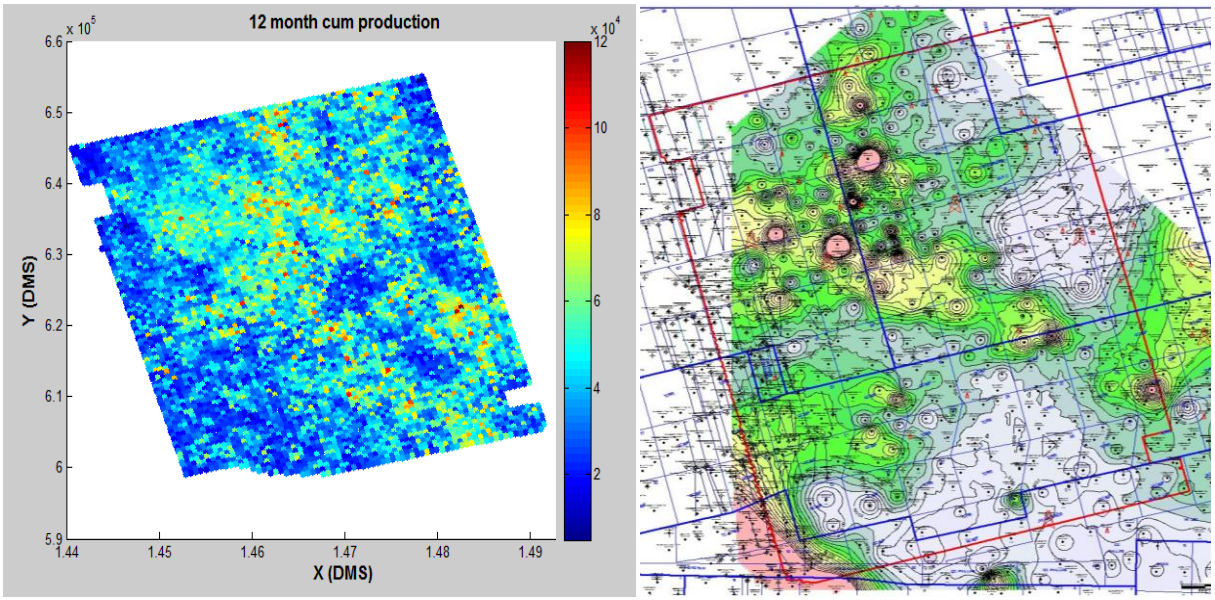

Figure 6.40: Comparison of predicted (left image) and actual (right image) surface maps

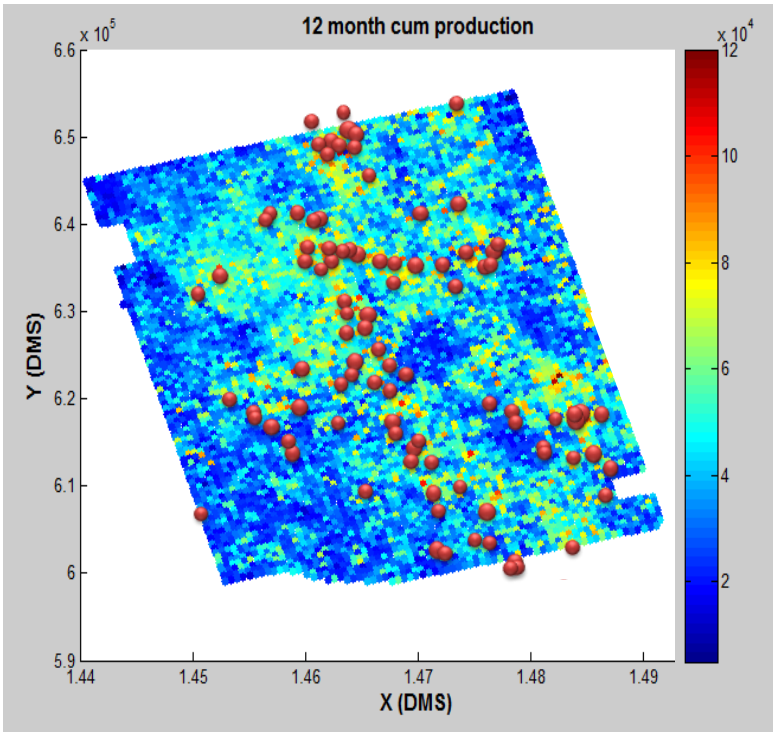

Figure 6.41: Map of predicted infill drilling locations (locations are demonstrated by red circles)

Chapter 7

CONCLUSIONS AND RECOMMENDATIONS

The focus of this research is to study and to characterize tight oil reservoir. This research is carried out in two modules. The first module is to generate synthetic well logs using seismic data, and the second module is to identify prolific reservoir segments (i.e. payzone identification). Two types of synthetic well logs are generated using different seismic data. Low-resolution well logs are predicted using averaged seismic attribute, whereas high-resolution well logs are generated using 3D seismic data.

The major issue in predicting low-resolution well logs is the inability of networks to capture the sharp variations of the well logs. This issue tested using over exercises and they confirmed that 1) predicted error behavior for different network structures and different training/testing datasets are approximately the same 2) the highest error values are related to the peaks of the well logs. Therefore, the use of two types of neural networks is proposed: trend networks and error adjustment networks. Trend networks predict the overall behavior of the well logs and error adjustment networks adjust improve the predictions of the trend networks. Using error adjustment networks significantly improved the well log predictions and correlation coefficients between network outputs and actual well logs

The second family of synthetic well logs is called as high resolution well logs. Using the sampled time-volume seismic data, well logs are predicted for each seismic interval (seven intervals are identified in ATM area). Contrary to the low resolution well log prediction, using time-volume seismic data, neural network predictions have high correlation coefficient with actual well logs and error adjustment networks are not required in this case. However, the number of neural networks is increased from 10 networks (two networks for each well log; trend and error networks) to 35 networks (seven networks for each well log corresponding to seven seismic intervals).

The main challenge in payzone identification is the lack of field data to train neural networks. Three approaches are proposed to perform payzone identification: low resolution, high resolution, and

intervals approaches. In the low-resolution approach, gross pay thickness is divided into four intervals and using the trained well performance networks (oil, water and gas) and sampled well logs of each layer, respective productions are predicted. Low-resolution approach provided the foundation for next approach, high-resolution approach. In this method, one-foot sampled actual well logs are used for performance predictions. This results productivity estimates (synthetic production logs) for every 50 feet gross thickness of reservoir. High-resolution approach is only applicable for the existing wells however classification of production logs and well logs can potentially add more insights about the reservoir.

Fuzzy logic is used to study the correlation between oil production and well logs (wireline well logs and mineralogy well logs). High oil production segments are correlated to GR values higher than 80 and LONG values less than 1000. Based on mineralogy analysis, high oil production segments are correlated to 40% to 70% shale (low lime) and 20% limestone (low shale). Also, studying on the histograms of well logs and production logs resulted that high production points are correlated to the gamma ray values of 60 or more. Formation in the ATM region is mainly dominated by shales; this is confirmed by careful analysis of lithology logs obtained from mud logging.

High-resolution approach has more accuracy than low resolution approach but it cannot be used in the locations with no wells. Therefore, the third approach is devised such that production profiles are estimated for the entire field. Using seismic and high resolution well logs of each interval, production profiles are predicted. With this approach it is possible to rank all intervals based on their productivity and identify the more prolific intervals. Predicted oil productions of third and fifth seismic intervals are consistently higher than other intervals.

Incorporating well logs, seismic, and completion data to the performance networks, it is possible to predict oil, water, and gas productions for entire field. Then, locations of infill drilling wells are identified by comparing the production at each point. In this study, 100 infill drilling wells are identified based on their respective one year cumulative oil productions.

This study has shown the applications of neural networks in the reservoir characterization of unconventional reservoirs. The recommendations for further studies and analysis are summarized below:

- The developed methodologies are greatly affected by the data availability and quality. Therefore, based on availability of different types of data, one can expand the developed algorithms. Using 3D seismic information resulted networks with higher accuracy than averaged seismic attributes. Therefore, it is recommended to use 3D seismic information because 3D seismic data has higher quality and captures more details of formation than that of averaged seismic attributes. In case of pay zone identification, if the data of production rates versus formation depth exists, it is possible to train the network to identify pay zones. On the other hand, if the core analysis data is available (only 1 core data is available in the supplied data set); it is possible to test the conventional pay zone identification methods and to identify new cut off values to pick the pay zones (the only marker that is currently used is gamma ray values less than 75 API representing clean sand segments).
- Expanding the methodologies to different parts of the Wolfcamp field is another potential extension for this work. First, performance of the network at different location should be evaluated. Then, depending on the prediction error at new locations, re-training of the networks may be required in order to increase the expertise of the networks at new locations. However, the methodologies and training procedures remain the same.
- Extension of the developed methodologies to other unconventional resources such as shale gas is recommended for further studies. Shale gas plays crucial rule in supplying world energy and production from shale gas field such as Marcellus, Bakken, and Barnett are increasing. The proposed workflow is applicable on the shale gas fields however, depending on the field properties; different types of data may be required for network training procedure. For example, because of existence of natural fractures in many shale

gas reservoirs, the use of NMR (nuclear magnetic resonance) well logs are suggested to characterize the natural fracture networks.

- Finally, prediction of infill drilling wells for the newly discovered fields is another potential of this study. New fields have seismic data; thus, it is possible to predict the well logs. Then, by using the most common completion data (e.g. well properties such tubing, pump, and completion parameters); it is possible to predict the production surfaces. Then by comparing spatial variations of productions, one can pick infill drilling locations for new field. However, the production surface should be updated once new wells are drilled and more data becomes available.

REFERENCES

Abbaszadeh, M., Fujii, H. and Fujimoto, F., 1996. Permeability Prediction by Hydraulic Flow Units - Theory and Applications. SPE Formation Evaluation(12).

Anguiano-Rojas, P., Dorantes-Huerta., D., Mejia-Olvera, A. and Spurlin, J.H., 2003. NEURAL NETWORKS FOR THE MODELING OF ELECTRICAL AND INDUCTION LOGS, Annual Logging Symposium. Society of Petrophysicists & Well Log Analysts.

Arbib, M.A., 2003. The handbook of brain theory and neural networks. The MIT Press.

Archie, G., 1942. The electrical resistivity log as an aid in determining some reservoir characteristics. Inst. Mining Metall. Trans, 146: 54-62.

Artun, E., Mohaghegh, S.D., Toro, J., Wilson, T. and Sanchez, A., 2005. Reservoir Characterization Using Intelligent Seismic Inversion, SPE Eastern Regional Meeting, Morgantown, West Virginia.

Ayala, L. F. and Ertekin, T., 2007. Neuro-simulation analysis of pressure maintenance operations in gas condensate reservoirs. Journal of Petroleum Science and Engineering, 58(1-2): 207-226.

Azalgara, C. and Floricich, M., 2001. Estimation of Reservoir Net Thickness Using Seismic Facies and Well Data in Middle Miocene Incised Valley Deposits of the Oficina FM. Oritupano Area, Eastern Venezuela, SPE Latin American and Caribbean Petroleum Engineering Conference, Buenos Aires, Argentina.

Bacon, M., Simm, R. and Redshaw, T., 2003. 3-D seismic interpretation. Cambridge Univ Pr.

Balch, R.S., Stubbs, B.S., Weiss, W.W. and Wo, S., 1999. Using Artificial Intelligence to Corellate Multiple Seismic Attributes to Reservoir Properties, SPE Annual Technical Conference and Exhibition, Houston, Texas.

Bansal, Y., 2011. Predicting the Performance of Wells Located in Tight Oil Plays Using Artificial Expert Systems. The Pennsylvania State University, PhD dissertation thesis.

Barhen, J., Reister, D. and Protopopescu, V., 1999. DeepNet: an ultrafast neural learning code for seismic imaging. IEEE, pp. 3779-3784 vol. 6.

Basbug, B. and Karpyn, Z.T., 2007. Estimation of Permeability from Porosity, Specific Surface Area, and Irreducible Water Saturation using an Artificial Neural Network, Latin American & Caribbean Petroleum Engineering Conference, Buenos Aires, Argentina.

Bassiouni, Z. et al., 1994. Theory, measurement, and interpretation of well logs. SPE.

Berger, B. and Anderson, K., 1981. Modern petroleum: a basic primer of the industry.

Bhatt, A., 2002. Reservoir properties from well logs using neural networks. Doctor Thesis Department of Petroleum Engineering and Applied Geophysics, Norwegian University of Science and Technology.

Bouffin, N. and Jensen, J.L., 2009. Efficient Detection of Productive Intervals in Oil and Gas Reservoirs, Canadian International Petroleum Conference, Calgary, Alberta.

Brown, A.R., 2001. Understanding seismic attributes. Geophysics, 66(1): 47.

Brown, D., 2008. Texas 'playgrounds' attract action. AAPG explorer.

Cabrera, I., Cordero, P. and Ojeda-Aciego, M., 2009. Fuzzy logic, soft computing, and applications. Bio-Inspired Systems: Computational and Ambient Intelligence: 236-244.

Carpenter, G.A. and Grossberg, S., 1991. Pattern recognition by self-organizing neural networks. The MIT Press.

Centilmen, A., Ertekin, T. and Grader, A.S., 1999. Applications of Neural Networks in Multiwell Field Development, SPE Annual Technical Conference and Exhibition, Houston, Texas.

Chartier, S., Giguère, G. and Langlois, D., 2009. A new bidirectional heteroassociative memory encompassing correlational, competitive and topological properties. Neural Networks, 22(5-6): 568-578.

Chen, Q. and Sidney, S., 1997. Seismic attribute technology for reservoir forecasting and monitoring. The Leading Edge, 16: 445.

Cobb, W.M. and Marek, F.J., 1998. Net Pay Determination for Primary and Waterflood Depletion Mechanisms, SPE Annual Technical Conference and Exhibition, New Orleans, Louisiana.

Cooke, D.A. and Schneider, W.A., 1983. Generalized linear inversion of reflection seismic data. Geophysics, 48: 665.

D'Windt, A., 2007. Reservoir Zonation And Permeability Estimation: A Bayesian Approach.

Doraisamy, H., Ertekin, T. and Grader, A., 2000. Field development studies by neuro-simulation: an effective coupling of soft and hard computing protocols. Computers & Geosciences, 26(8): 963-973.

Egbele, E., Ezuka, I. and Onyekonwu, M., 2005. Net-To-Gross Ratios: Implications in Integrated Reservoir Management Studies, Nigeria Annual International Conference and Exhibition, Abuja, Nigeria.

EIA, 2010. International Energy Outlook, 2010. Energy Information Administration.

Elshafei, M. and Hamada, G., 2009a. Neural Network Identification of Hydrocarbon Potential of Shaly Sand Reservoirs. Petroleum Science and Technology, 27(1): 72-82.

Elshafei, M. and Hamada, G.M., 2009b. Petrophysical Properties Determination of Tight Gas Sands From NMR Data Using Artificial Neural Network, SPE Western Regional Meeting, San Jose, California.

Elsharkawy, A.M., 1998. Modeling the Properties of Crude Oil and Gas Systems Using RBF Network, SPE Asia Pacific Oil and Gas Conference and Exhibition, Perth, Australia.

Ershaghi, I., Ortega, A., Lee, K.-H. and Mohammadnejad, A., 2008. A Method for Characterization of Flow Units Between Injection-Production Wells Using Performance Data, SPE Western Regional and Pacific Section AAPG Joint Meeting, Bakersfield, California, USA.

Flamm, D.S., 2008. MIDLAND BASIN, GLASSCOCK, STERLING, AND REAGAN COUNTIES, TEXAS, Brigham Young University.

Gadallah, M.R., 1994. Reservoir Seismology: Geophysics in Nontechnical Language. PennWell Books, Tulsa, Oklahoma.

Giles, C.L., Lawrence, S. and Tsoi, A.C., 2001. Noisy time series prediction using recurrent neural networks and grammatical inference. Machine Learning, 44(1): 161-183.

Glossary, O.F., 2010. Schlumberger Oilfield Glossary.

Gorucu, F.B. et al., 2005. A Neurosimulation Tool for Predicting Performance in Enhanced Coalbed Methane and CO2 Sequestration Projects, SPE Annual Technical Conference and Exhibition, Dallas, Texas.

Gouveia, W.P. and Scales, J.A., 1998. Bayesian seismic waveform inversion: Parameter estimation and uncertainty analysis. JOURNAL OF GEOPHYSICAL RESEARCH-ALL SERIES-, 103: 2759-2779.

Grossberg, S., 1987. Competitive learning: From interactive activation to adaptive resonance**. Cognitive science, 11(1): 23-63.

Guler, B., Ertekin, T. and Grader, A., 2003. An artificial neural network based relative permeability predictor. Journal of Canadian Petroleum Technology, 42(4).

Guo, S. et al., 2010. Hydraulic Flow Unit Based Permeability Characterization and Rapid Production Prediction Workflow for an Offshore Field, South China Sea.

Hebb, D.O., 1949. The organisation of behaviour. New York: Wiley.

Hebb, D.O., 1961. The organization of behavior: A neuropsychological theory. Science editions.

Hecht-Nielsen, R., 1990. Neurocomputing. Addison-Wesley.

Hegeman, P., Dong, C., Varotsis, N. and Gaganis, V., 2009. Application of Artificial Neural Networks to Downhole Fluid Analysis. SPE Reservoir Evaluation & Engineering, 12(1): 8-13.

Helander, D.P., 1983. Fundamentals of formation evaluation. OGCI Publications, Tulsa.

Holditch, S., 2006. Tight gas sands. Journal of Petroleum Technology, 58(6): 86-93.

Holditch, S.A., 2009. SS: Unlocking the Unconventional Oil and Gas Reservoirs: Stimulation of Tight Gas Sands.

Holstein, E.D., 2007. Petroleum Engineering Handbook, Volume 5: Reservoir Engineering and Petrophysics. Society of Petroleum Engrs.

Honarpour, M.M., Djabbarah, N.F. and Sampath, K., 2003. Whole Core Analysis - Experience and Challenges, Middle East Oil Show, Bahrain.

Hopfield, J.J., 1982. Neural networks and physical systems with emergent collective computational abilities. Proceedings of the national academy of sciences, 79(8): 2554.

Jain, A.K., Mao, J. and Mohiuddin, K.M., 1996. Artificial neural networks: A tutorial. Computer, 29(3): 31-44.

James, H., 2009. Visualizing 3D features in 3D seismic data. First Break, 27: 57–62.

Jensen, J.L. and Menke, J.Y., 2006. Some Statistical Issues in Selecting Porosity Cutoffs for Estimating Net Pay. PetroPhysics.

Johnston, J. and Lee, W., 1992. Identification of productive layers in low-permeability gas wells. Journal of Petroleum Technology, 44(11): 1240-1248.

Kohonen, T., 1988. An introduction to neural computing. Neural Networks, 1(1): 3-16.

Lake, L.W., Carroll, H.B. and Wesson, T.C., 1991. Reservoir characterization II. Academic Press.

Lawrence, S., Giles, C.L., Tsoi, A.C. and Back, A.D., 1997. Face recognition: A convolutional neural-network approach. Neural Networks, IEEE Transactions on, 8(1): 98-113.

Le Cun, B.B. et al., 1990. Handwritten digit recognition with a back-propagation network. Citeseer.

Lee, K.-H., Ortega, A., Mohammadnejad, A. and Ershaghi, I., 2011. An Active Method for Characterization of Flow Units Between Injection/Production Wells by Injection-Rate Design. SPE Reservoir Evaluation & Engineering(08).

Lee, K.-H., Ortega, A., Mohammadnejad, A., Jafroodi, N. and Ershaghi, I., 2009. A Novel Method for Mapping Fractures and High Permeability Channels in Waterfloods Using Injection and Production Rates, SPE Western Regional Meeting, San Jose, California.

Lewis, F.L., 1996. Neural network control of robot manipulators. IEEE Expert, 11(3): 64-75.

Lin, Y.-T., Ortega, A., Mohammadnejad, A. and Ershaghi, I., 2010. Waterflood Tomography: Mapping High Contrast Permeability Structures Using Injection/Production Data, SPE Western Regional Meeting, Anaheim, California, USA.

Liu, F., Mendel, J.M. and Mohammadnejad, A., 2009. Forecasting Injector/Producer Relationships From Production and Injection Rates Using an Extended Kalman Filter. SPE Journal(12).

Luthi, S.M., 2001. Geological well logs: Their use in reservoir modeling. Springer verlag.

Ma, L., Xin, K. and Liu, S., 2008. Using Radial Basis Function Neural Networks to Calibrate Water Quality Model. International Journal of Intelligent Systems and Technologies, 3(2): 90-98.

MacGregor, L., Harris, P. and Walls, J., 2008. Reservoir Characterisation Through Joint Interpretation of EM, Seismic, and Well Log Data.

Malki, H., Baldwin, J. and Kwari, M., 1996. 31010-Estimating Permeability by Use of Neural Networks in Thinly Bedded Shaly Gas Sands. SPE Computer Applications, 8(2): 58-62.

McCulloch, W.S. and Pitts, W., 1943. A logical calculus of the ideas immanent in neural nets. Bulletin of Mathematical Biophysics, 5(1): 15-137.

Merriam, C.O., 1999. Depositional history of lower Permian (Wolfcampian -Leonardian) carbonate buildups, Midland Basin, Upton County, Texas. Texas A&M University, M.S. thesis.

Minsky, M. and Seymour, P., 1969. Perceptrons.

Mohaghegh, S., Arefi, R., Ameri, S. and Rose, D., 1995. Design and development of an artificial neural network for estimation of formation permeability. SPE Computer Applications, 7(6): 151-154.

Montgomery, S.L., 1996. Permian" Wolfcamp" limestone reservoirs: Powell Ranch field, eastern Midland basin. AAPG bulletin, 80: 1349-1366.

Müller, B., Reinhardt, J. and Strickland, M.T., 1995. Neural networks: an introduction, 1. Springer Verlag.

Narendra, K.S. and Parthasarathy, K., 1990. Identification and control of dynamical systems using neural networks. Neural Networks, IEEE Transactions on, 1(1): 4-27.

Nikravesh, M. and Aminzadeh, F., 2001. Past, present and future intelligent reservoir characterization trends* 1. Journal of Petroleum Science and Engineering, 31(2-4): 67-79.

Nikravesh, M. and Hassibi, M., 2003. Intelligent reservoir characterization (IRESC). IEEE, pp. 369-373.

Oldenburg, D., Scheuer, T. and Levy, S., 1983. Recovery of the acoustic impedance from reflection seismograms. Geophysics, 48: 1318.

Omatu, S., Khalid, M. and Yusof, R., 1996. Neuro-control and its applications. Springer.

P.Dutton, S., Holtz, M.H., Tremblay, T.A. and Zirczy, H.H., 2000. The Permian Basin: proving ground for tomorrow's technologies. West Texas geological society.

Panda, M., Zaucha, D., Perez, G. and Chopra, A., 1996. Application of neural networks to modeling fluid contacts in Prudhoe Bay. SPE Journal, 1(3): 303-312.

Ramgulam, A., 2006. Utilization of Artificial Neural Networks in the Optimization of History Matching, The Pennsylvania State University.

Rojas, R., 1996. Neural networks: a systematic introduction. Springer.

Rolon, L.F., 2004. Developing intelligent synthetic logs: Application to Upper Devonian Units in PA, West Virginia University.

Rosenblatt, F., 1957. The Perceptron, a Perceiving and Recognizing Automaton Project Para. Cornell Aeronautical Laboratory.

Russum, D.A., 2010. What is unconventional oil or unconventional gas? AJM petroleum consultants.

Sampaio, T., Ferreira Filho, V.J. and Neto, A., 2009. An Application of Feed Forward Neural Network as Nonlinear Proxies for Use During the History Matching Phase.

Schatzinger, R.A. and Jordan, J.F., 1999. Reservoir characterization: recent advances, 71. Amer Assn of Petroleum Geologists.

Sejnowski, T.J., Goldstein Jr, M., Jenkins, R. and Yuhas, B., 1990. Combining visual and acoustic speech signals with a neural network improves intelligibility. Morgan Kaufmann Publishers Inc., pp. 232-239.

Serra, O. and Abbott, H.T., 1982. The Contribution of Logging Data to Sedimentology and Stratigraphy. (02).

Sheriff, R.E. and Brown, A.R., 1992. Reservoir geophysics. Society of Exploration Geophysicists.

Shokir, E.M.E.M., Alsughayer, A. and Al-Ateeq, A., 2006. Permeability estimation from well log responses. Journal of Canadian Petroleum Technology, 45(11): 41-46.

Silpngarmlers, N., Guler, B., Ertekin, T. and Grader, A., 2001. Development and Testing of Two-Phase Relative Permeability Predictors Using Artificial Neural Networks.

Silva, P.C., Maschio, C. and Schiozer, D.J., 2006. Applications of the Soft Computing in the Automated History Matching, Canadian International Petroleum Conference, Calgary, Alberta.

Simpson, P.K., 1989. Artificial neural systems: foundations, paradigms, applications, and implementations. Elsevier Science Inc.

Snyder, R.H., 1971. A Review of the Concepts and Methodology of Determining "Net Pay", Fall Meeting of the Society of Petroleum Engineers of AIME, New Orleans, Louisiana.

Soto B, R. and Holditch, S., 1999. Development of reservoir characterization models using core, well log, and 3D seismic data and intelligent software.

Tamhane, D., Wong, P., Aminzadeh, F. and Nikravesh, M., 2000. Soft computing for intelligent reservoir characterization.

Taner, M.T., Koehler, F. and Sheriff, R., 1979. Complex seismic trace analysis. Geophysics, 44: 1041.

Taner, M.T., Schuelke, J.S., O'Doherty, R. and Baysal, E., 2005. Seismic attributes revisited.

Tittman, J., 1986. Tittman (1986) Geophysical well logging. Academic Press (Orlando).

Todorov, T., Stewart, R., Hampson, D. and Russell, B., 1998. Well log prediction using attributes from 3C-3D seismic data.

Verga, F., Viberti, D. and Gonfalini, M., 2002. UNCERTAINTY EVALUATION IN WELL LOGGING: ANALYTICAL OR NUMERICAL APPROACH?, SPWLA Annual Logging Symposium. Society of Petrophysicists & Well Log Analysts.

Walls, J., Dvorkin, J. and Carr, M., 2004. Well Logs and Rock Physics in Seismic Reservoir Characterization.

Worthington, P., 2010. Net Pay--What Is It? What Does It Do? How Do We Quantify It? How Do We Use It? SPE Reservoir Evaluation & Engineering, 13(5): 812-822.

Worthington, P.F. and Cosentino, L., 2003. The Role of Cut-offs in Integrated Reservoir Studies, SPE Annual Technical Conference and Exhibition, Denver, Colorado.

Yao, T. and Journel, A.G., 2000. Integrating seismic attribute maps and well logs for porosity modeling in a west Texas carbonate reservoir: addressing the scale and precision problem. Journal of Petroleum Science and Engineering, 28(1-2): 65-79.

Zadeh, L.A., 1994. Soft computing and fuzzy logic. Software, IEEE, 11(6): 48-56.

Zhang, G. and Hu, M.Y., 1998. Neural network forecasting of the British pound/US dollar exchange rate. Omega, 26(4): 495-506.

Zirilli, J.S., 1997. Financial prediction using neural networks, 254. International Thomson Computer Press.

Appendix A

GRAPHICAL USER INTERFACE

In order for field engineers to efficiently take advantage of the developed methodologies, it is essential to integrate the networks in one user friendly graphical user interface (GUI). The interface has the capabilities of providing valuable information for asset managers, geologist, production and completion engineers. Schematic of the developed GUI is illustrated in the Figure A.0.1. ATM characterization toolbox consists of four panels:

1. Workspace panel: workspace panel consists of main controls of the software. It is also used to demonstrate the outputs and results.
2. Navigation panel: consisting of 8 tabs, each tab represents a page of the workspace panel in which the results and command are available.
3. Menu panel: General controls such as zooming and panning the graphs, selecting data points from a plot and help files are all located on menu panel.
4. Status panel: status of the program when either neuro-simulation is in progress or generating the reports for the user is demonstrated in this panel.

The toolbox also consists of 8 tabbed pages containing the input controls and outputs of the program. In order to run the neuro-simulator, first it is required to select one set of coordinates from the *Main* page of toolbox. Coordinates can be selected either by manual input or by selecting any point from the map of available data points. *Location summery* button provides the four closest wells to the selected point with their respective information such as production, API number, etc. Depending on the availability of well logs ate the selected, user can import well log to the program or let the program to predict the logs. Completion tab enables user to override the prediction of any parameter by inputting the respective value of that parameter. Layout of completion tab is presented in Figure A.0.2. After providing the necessary information, by

clicking on the *Run* button, neuo-simulators prediction for the selected point starts. On average depending on the PC computational power, neu-simulation procedure takes less than 30 seconds. Reading seismic data and extracting information from binary seismic files corresponds to two third of the CPU time. Well logs are the first outputs of the neuro-simulation, present in tabs number 3 and 4, namely *Low Res. Logs* and *High Res. Logs* (refer to Figure A.0.3). *Production data* page contains the cumulative and flowrates of oil, water, and gas production at the selected location. *Payzone* tab contains the production potentials of seven seismic intervals.

It is possible to create report files of all the predicted parameters using *Report* page. Reports are divided into two categories:

1. Well scale: report of predicted parameters for the selected point.
2. 2. Field scale: report of all parameters for entire field.

The names of the report files are the same as the user supplied name, however depending on the requested data type, suffixes added to the end of file name. For example, if user requested low resolution log and entered ‘Check’ as the file name and LAS as file format, generated file name will be “Check_LR.SGY”. Table A-1 contains definition of file name extensions and formats. The last tab of the navigation panel is *Surface Maps* tab containing the predicted maps. Many information are available in this section including the payzone maps (please refer to Figure A.0.7).

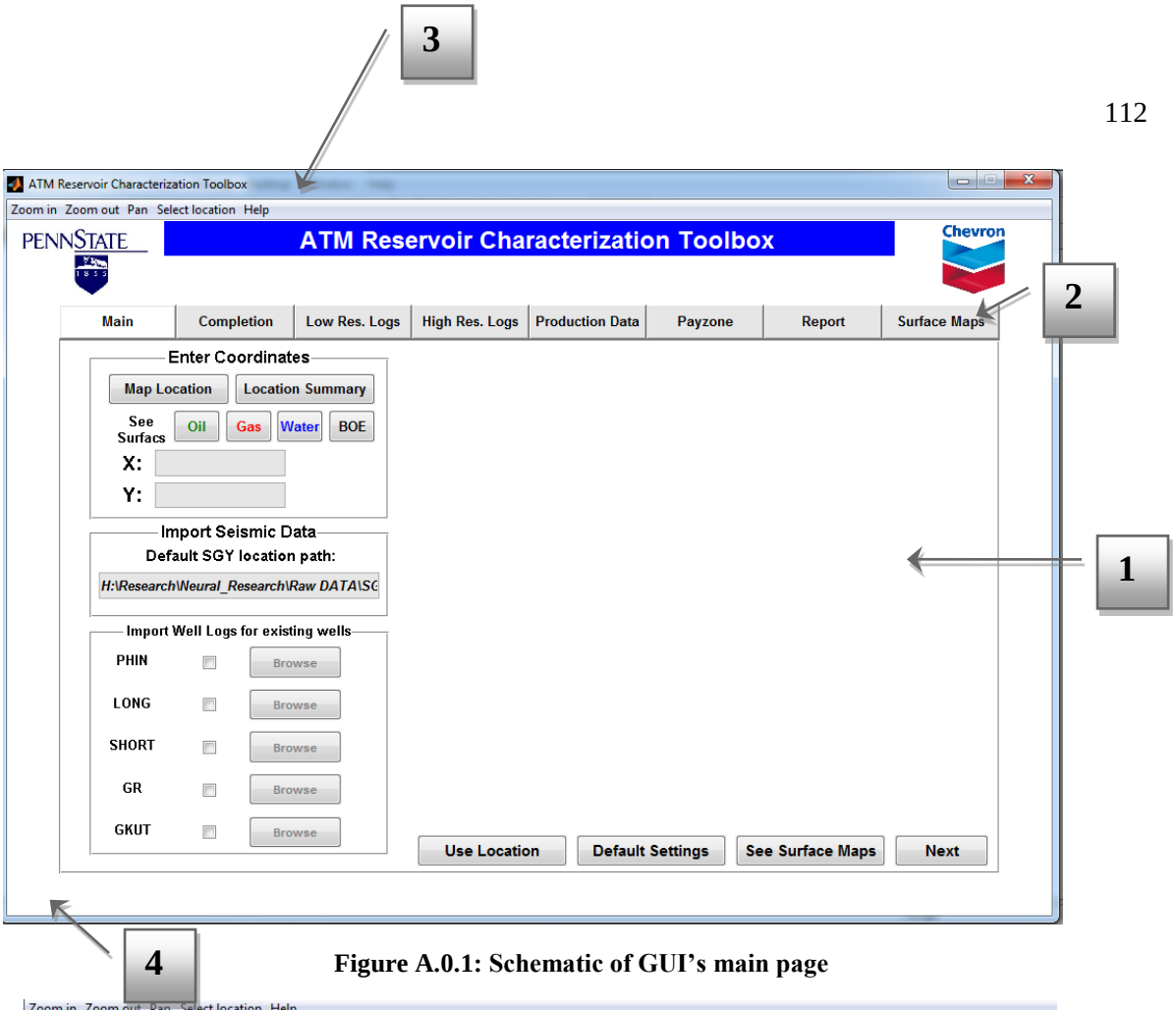

Figure A.0.1: Schematic of GUI's main page

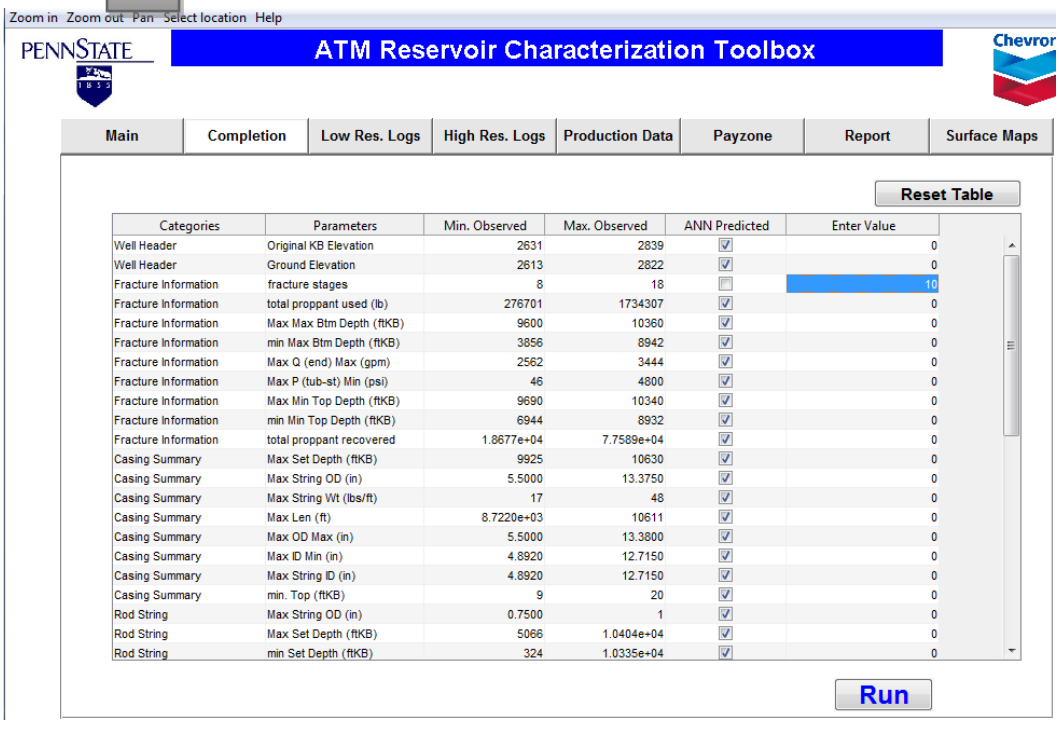

Categories	Parameters	Min. Observed	Max. Observed	ANN Predicted	Enter Value
Well Header	Original KB Elevation	2631	2839	☑	0
Well Header	Ground Elevation	2613	2822	☑	0
Fracture Information	fracture stages	8	18	☐	10
Fracture Information	total proppant used (lb)	276701	1734307	☑	0
Fracture Information	Max Max Btm Depth (ftKB)	9600	10360	☑	0
Fracture Information	min Max Btm Depth (ftKB)	3856	8942	☑	0
Fracture Information	Max Q (end) Max (gpm)	2562	3444	☑	0
Fracture Information	Max P (tub-st) Min (psi)	46	4800	☑	0
Fracture Information	Max Min Top Depth (ftKB)	9690	10340	☑	0
Fracture Information	min Min Top Depth (ftKB)	6944	8932	☑	0
Fracture Information	total proppant recovered	1.8677e+04	7.7589e+04	☑	0
Casing Summary	Max Set Depth (ftKB)	9925	10630	☑	0
Casing Summary	Max String OD (in)	5.5000	13.3750	☑	0
Casing Summary	Max String Wt (lbs/ft)	17	48	☑	0
Casing Summary	Max Len (ft)	8.7220e+03	10611	☑	0
Casing Summary	Max OD Max (in)	5.5000	13.3800	☑	0
Casing Summary	Max ID Min (in)	4.8920	12.7150	☑	0
Casing Summary	Max String ID (in)	4.8920	12.7150	☑	0
Casing Summary	min. Top (ftKB)	9	20	☑	0
Rod String	Max String OD (in)	0.7500	1	☑	0
Rod String	Max Set Depth (ftKB)	5066	1.0404e+04	☑	0
Rod String	min Set Depth (ftKB)	324	1.0335e+04	☑	0

Figure A.0.2: Completion parameters options

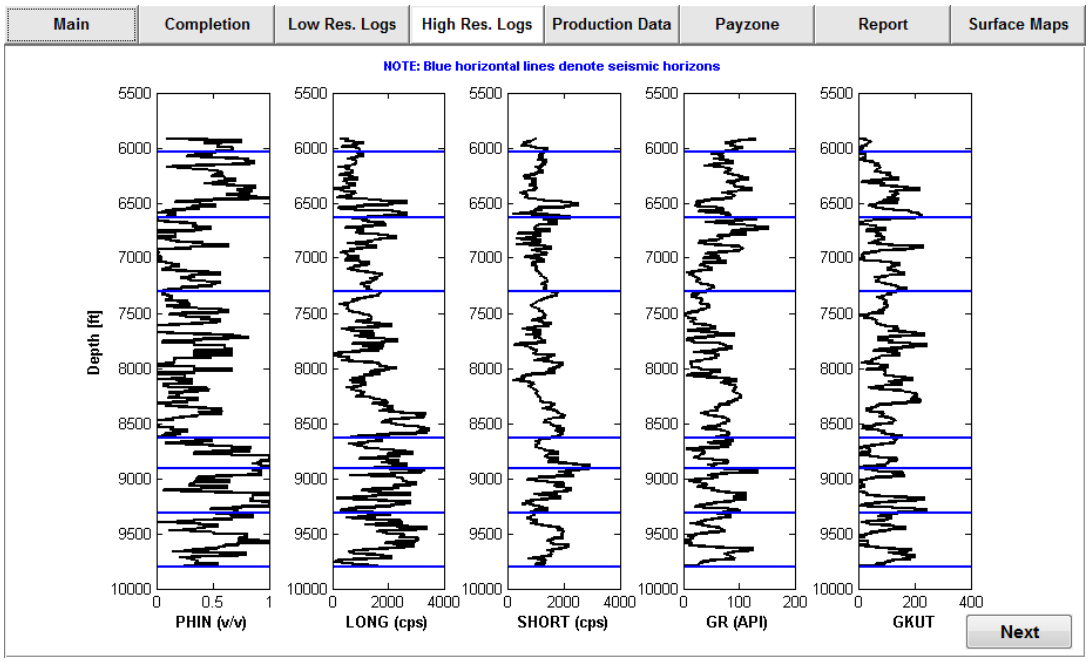

Figure A.0.3: Prediction results: High-resolution logs

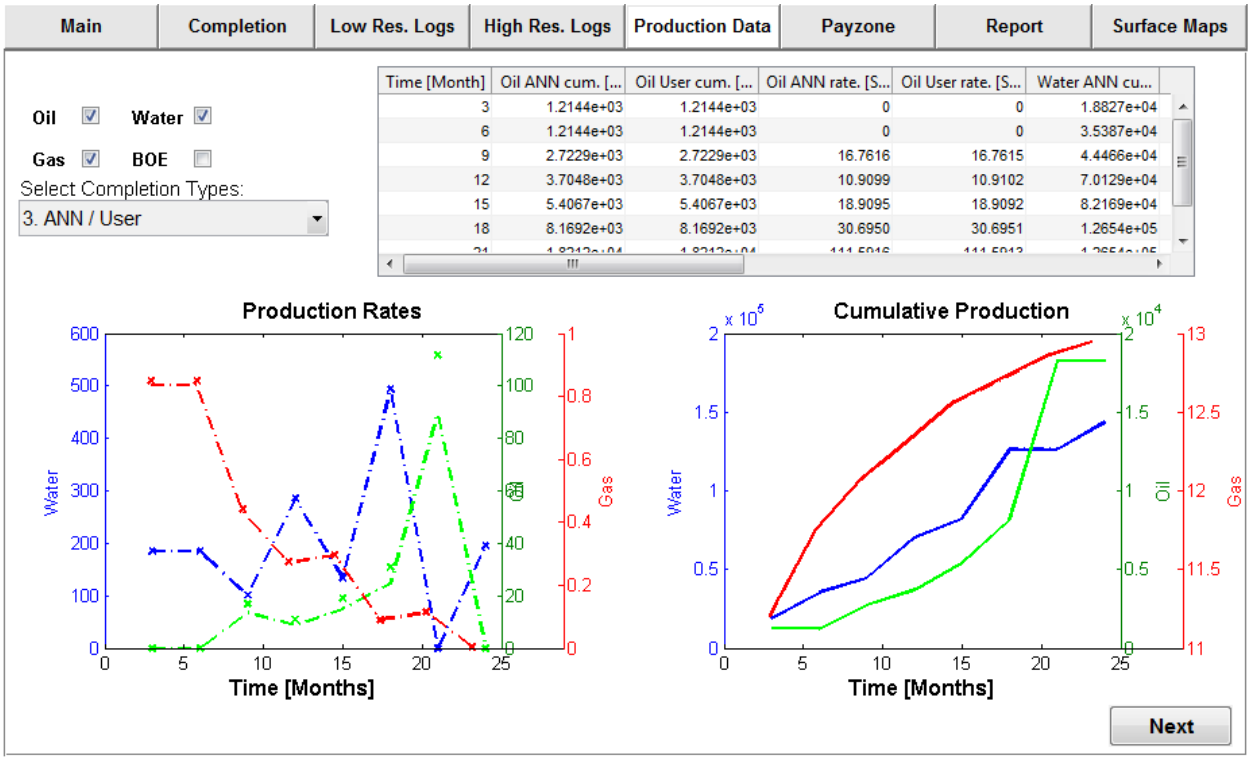

Figure A.0.4: Prediction results: Production data

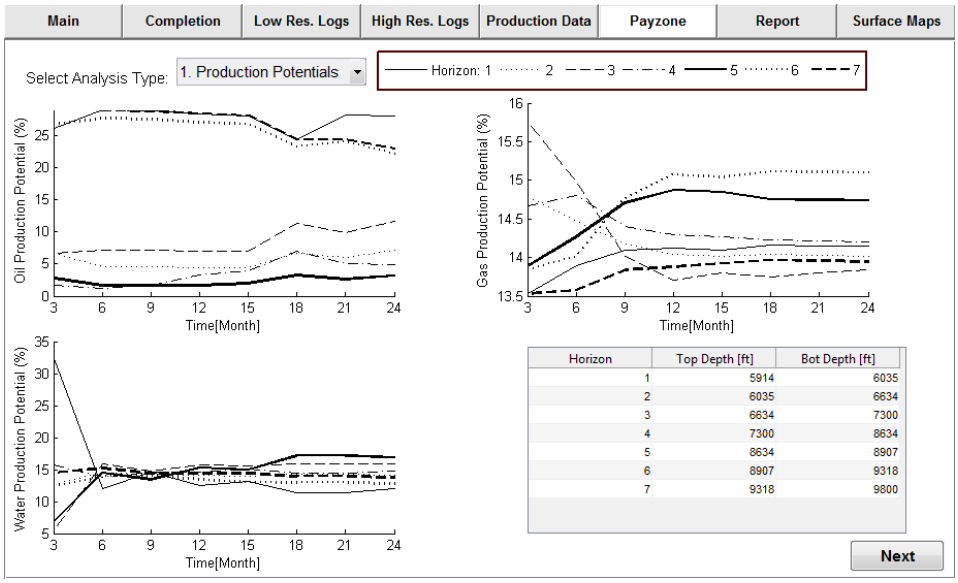

Figure A.0.5: Prediction results: Payzone data

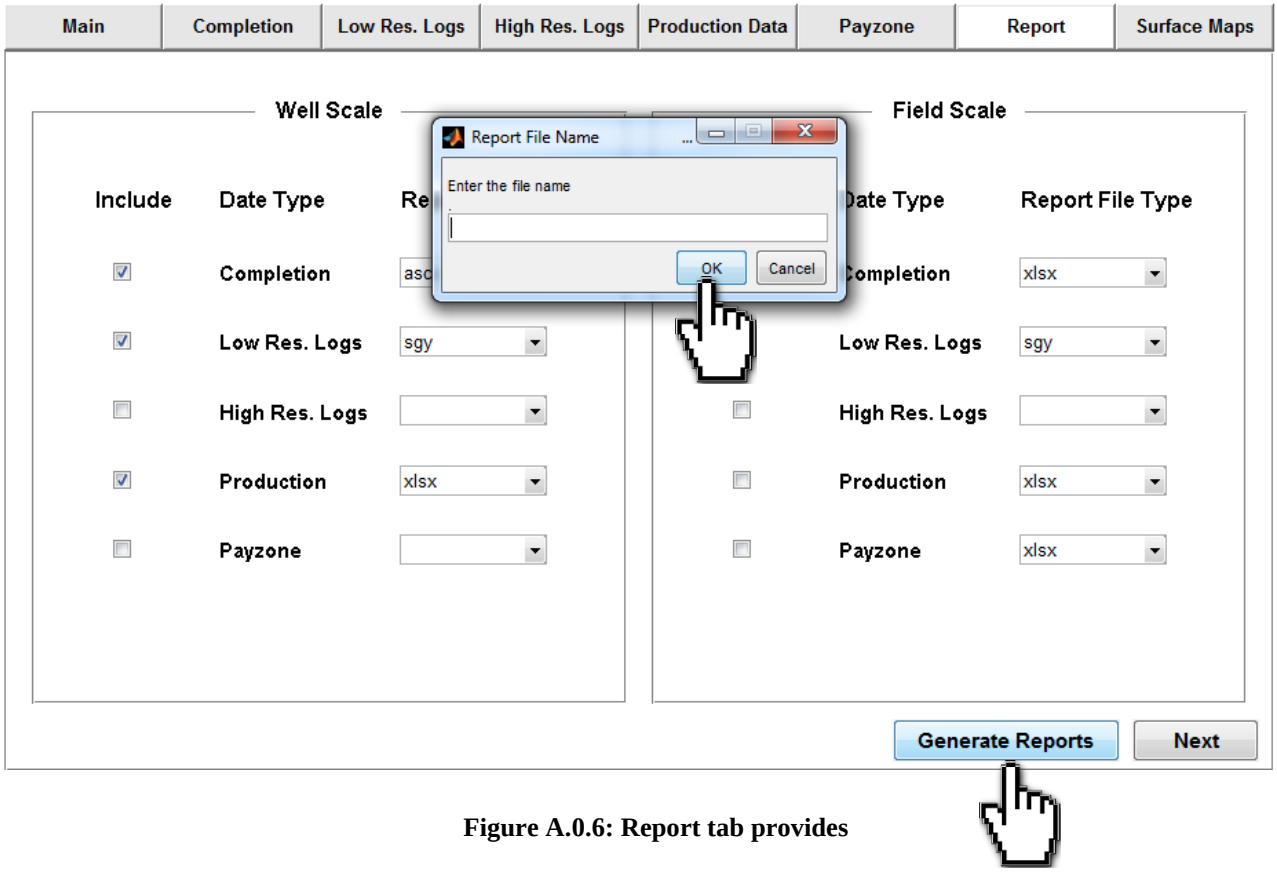

Figure A.0.6: Report tab provides

Table A-1: Report files definitions and formst

Well Scale		
Suffix	**Definition**	**Report Formats**
_LR	Low resolution log	Ascii, xlsx, LAS, SGY
_HR	High resolution log	Ascii, xlsx, LAS, SGY
_completion	Completion data	Ascii, xlsx
_prod	Production data	Ascii, xlsx, doc
_payzone	Payzone potentials	Ascii, xlsx, doc
Field Scale		
Suffix	**Definition**	**Report Formats**
_LR_field	Low resolution log	xlsx, SGY
_HR_field	High resolution log	xlsx, SGY
_completion_field	Completion data	xlsx
_Production_field	Production data	xlsx
_payzone_field	Payzone potentials	xlsx

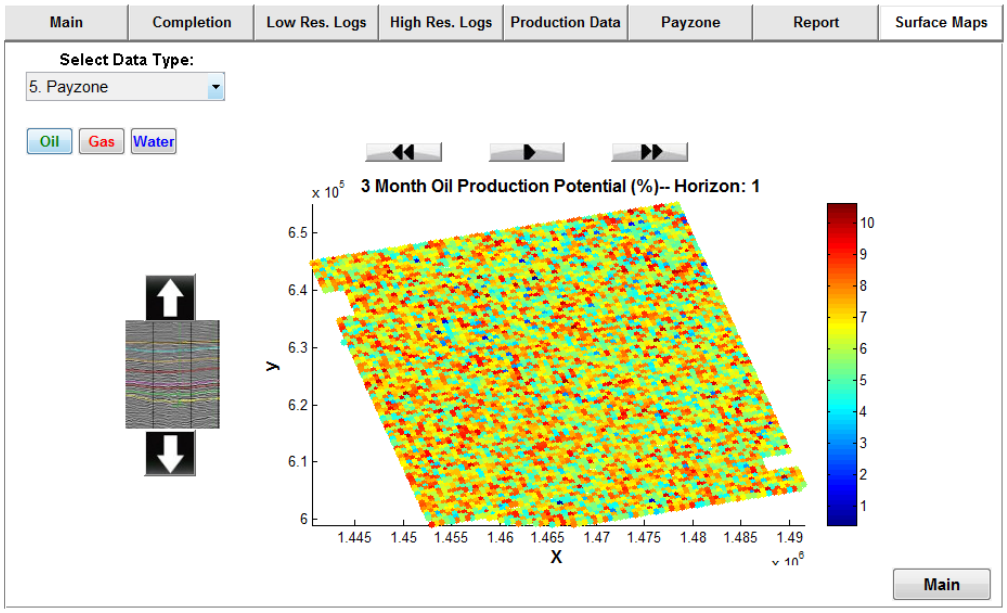

Figure A.0.7: Surface maps page

Appendix B

SEISMIC ATTRIBUTES DEFINITIONS

Attribute 1: RMS Amplitude (sliding time window 50 ms)

RMS amplitude provides a scaled estimate of the time envelope. Like energy half time and arc length, it is computed in a specific time window. RMS is calculated with the following equation:

$$x_{RMS} = \sqrt{\frac{1}{N}\sum_{i=1}^{N} x_i^2} \tag{B-1}$$

Attribute 2: Amplitude Acceleration

Instantaneous amplitude acceleration (t) is defined as the second derivative of the logarithm of the reflection strength. It is scaled to have units of Hz/s. Like all second-order attributes, it is widely variable and hence should be interpreted qualitatively and not quantitatively. In particular it can have huge values and tends to spike at the same places where instantaneous frequency spikes. As a result, scaling this attribute can be difficult.

Attribute 3: Dominant Frequency (average over 100 ms)

Instantaneous dominant frequency $f_a(t)$ is defined as the square root of the sum of the squares of the instantaneous frequency$f(t)$ and the instantaneous bandwidth $\sigma(t)$:

$$f_d(t) = \sqrt{f^2(t) + \sigma^2(t)} \quad \text{(B-2)}$$

Dominant frequency has units of Hertz values that range from 0 to Nyquist frequency and occasionally larger. It is always positive and at least as large as instantaneous frequency.

Attribute 4: Instantaneous Frequency (average over 100 ms)

Frequency represents the rate of change of instantaneous phase as a function of time. It is a measure of the slope of the phase trace and is obtained by taking the derivate of the phase. Instantaneous frequency ranges from –Nyquist to + Nyquist frequency.

Attribute 5: Reflection Strength

Reflection strength is the square root of the total energy of the seismic at an instant of time. For each time sample, reflection strength is calculated as follows:

$$R = \sqrt{trace^2 + quadrature^2} \quad \text{(B-3)}$$

Attribute 6: Quadrature Trace

Quadrature component of the trace is obtained by performing Hilbert transform on the recorded trace:

$$h(t) = \frac{1}{\pi t} * f(t) \quad \text{(B-4)}$$

$h(t)$ is obtained by convolution of recorded trace $f(t)$ and phase.

Attribute 7: Thin Bed Indicator (window length 100 ms)

Thin bed indicator is a hybrid complex attributes obtained by the difference between the instantaneous frequency and weighted average instantaneous frequency.

Attribute 8: Bandwidth (average in a 200 ms window)

Instantaneous bandwidth $\sigma(t)$ is defined as absolute value of the time rate of change of the natural logarithm of the instantaneous amplitude $a(t)$ divided by 2π:

$$\sigma(t) = \frac{1}{\pi t}\left|\frac{d}{dt}(\ln a(t))\right| \tag{B-5}$$

Attribute 9: Response Frequency

Response frequency attempts to extract physical meaningful frequency information about the localized seismic wavelet. Response frequency is defined by the instantaneous frequency calculated at the peak of amplitude envelope.

Attribute 10: Instantaneous Q Factor (average over 200 ms window)

Generally Q is determined in term of the ratio of energy stored in the resonator to that of the energy being lost in one cycle:

$$Q(t) = 2\pi\frac{f_r}{\Delta f} \tag{B-6}$$

Where $\frac{f_r}{\Delta f}$ denotes the ratio of resonant frequency to its bandwidth.

Attribute 11: Amplitude Change (average over 100 ms)

Amplitude change employs the same computation as instantaneous bandwidth but presents it as a signed measure.

Attribute 12: Energy Half-Time (average over 100 ms)

Energy half tie is he relative measure of where seismic energy is concentrated within a time window. In any given window, the average time of the trace power can computed by:

$$t_a = \frac{\sum_{n=1}^{N} t_n x_n^2}{\sum_{n=1}^{N} x_n^2} \quad \text{(B-7)}$$

Where x_n are the windowed trace samples. Letting t_c as the time at the window center and t_l as the total window length, energy half time becomes:

$$E_{ht} = 200\% \frac{t_a - t_c}{t_l} \quad \text{(B-8)}$$

Attribute 13: Energy Half-Time (average over 50 ms)

Please refer to attribute 12 for attribute definition.

Attribute 14: Thin Bed Indicator (50 ms window length)

Please refer to attribute 7 for attribute definition.

Attribute 15: Differentiation

This attribute is defined by differentiating the trace using Fourier transform.

Attribute 16: Integration

This attribute is defined by integrating the trace using Fourier transform.

Attribute 17: RMS Amplitude (25 ms sliding window)

Please refer to attribute 1 for attribute definition.

Attribute 18: Reflection Curvature

Reflective curvature is obtained using instantaneous mean curvature.

Attribute 19: Absolute Amplitude

Calculated simply using the absolute value of the amplitude of original sample.

Attribute 20: Amplitude Change (average over 50 ms)

Please refer to attribute 11 for attribute definition.

Attribute 21: Amplitude Change (average over 200 ms)

Please refer to attribute 11 for attribute definition.

Attribute 22: RMS Amplitude (100 ms sliding window)

Please refer to attribute 1 for attribute definition.

Attribute 23: Cosine of Phase

The recorded trace is the product of amplitude and phase:

$$f(t) = A(t)\cos\theta(t) \tag{B-9}$$

Thus, cosine of phase can be described as:

$$\cos\theta(t) = \frac{f(t)}{A(t)} \tag{B-10}$$

In other words, the cosine of phase is described by the ratio of the recorded trace $f(t)$ to the reflection strength $A(t)$.

Attribute 24: Bandwidth (average over 100 ms window)

Please refer to attribute 8 for attribute definition.

Attribute 25: Instantaneous Q Factor (average over 100 ms window)

Please refer to attribute 10 for attribute definition.

Attribute 26: Dominant Frequency (average over 50 ms window)

Please refer to attribute 3 for attribute definition.

Attribute 27: Arc Length (50 ms sliding window)

Arc length is a scaled measure of total excursion of a seismic trace in a window. It only measures the distance from sample to trace using the following formula:

$$S = \frac{1}{NT}\sum_{i=1}^{N}\sqrt{|a(i+1)-a(i)|^2 + T^2} \quad \text{(B-11)}$$

Attribute 28: Arc Length (100 ms sliding window)

Please refer to attribute 27 for attribute definition.

Attribute 29: Amplitude Variance (3 traces, 3 lines, 5 samples)

Amplitude variance is how much seismic amplitude varies from average amplitude within an analysis window.

Attribute 30: Amplitude Variance (7 traces, 7 lines, 5 samples)

Please refer to attribute 29 for attribute definition.

Appendix C

TRANSFER FUNCTIONS

Transfer functions are mathematical relationships between input and output. They help mapping non-linear problem and stabilize the network during the training process. Many types of transfer functions are available depending on the nature of problem. In this study the following transfer functions are used:

Tansig: Hyperbolic tangent sigmoid transfer function

$$f(x) = \frac{2}{1 + \exp(-2x)} - 1 \tag{C-1}$$

Softmax: Softmax transfer function

$$f(x) = \frac{\exp(x)}{sum(\exp(x))} \tag{C-2}$$

Radbas: Radial basis transfer function

$$f(x) = \exp(-x^2) \tag{C-3}$$

Stalins: Symmetric saturating linear transfer function

$$f(x) = \begin{cases} -1 & x \leq -1 \\ x & -1 \leq x \leq 1 \\ -1 & x \geq 1 \end{cases} \tag{C-4}$$

Appendix D

HIGH RESOLUTION NETWORKS PREDICTION RESULTS

Gamma Ray Logs (GR)

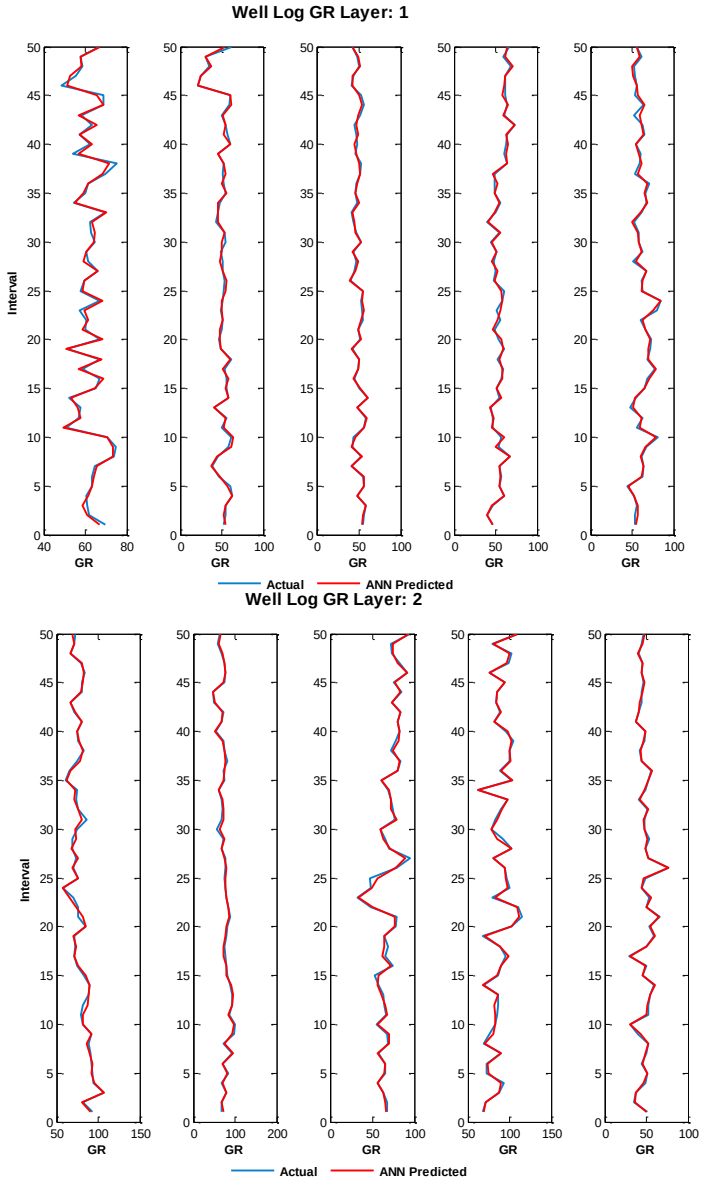

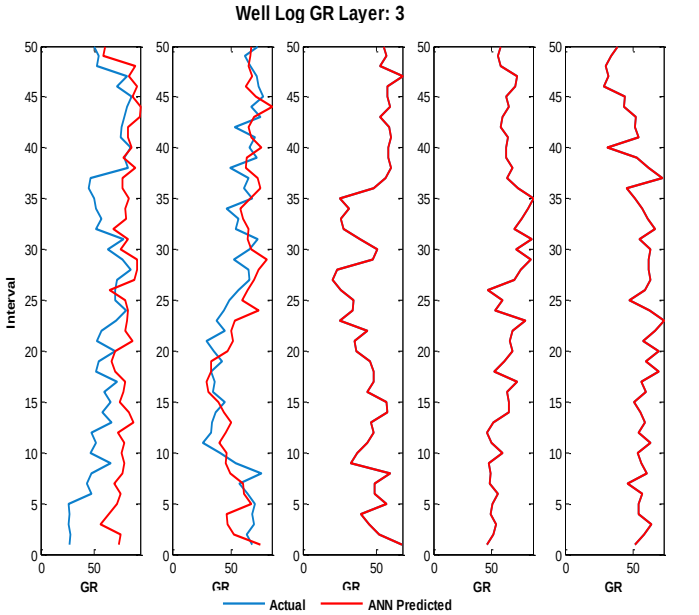
Well Log GR Layer: 3
Interval
GR
Actual
ANN Predicted

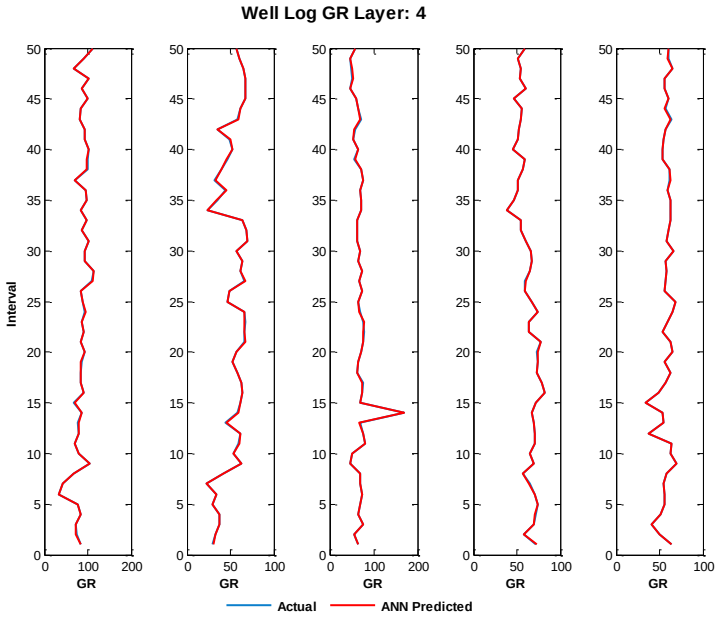
Well Log GR Layer: 4
Interval
GR
Actual
ANN Predicted

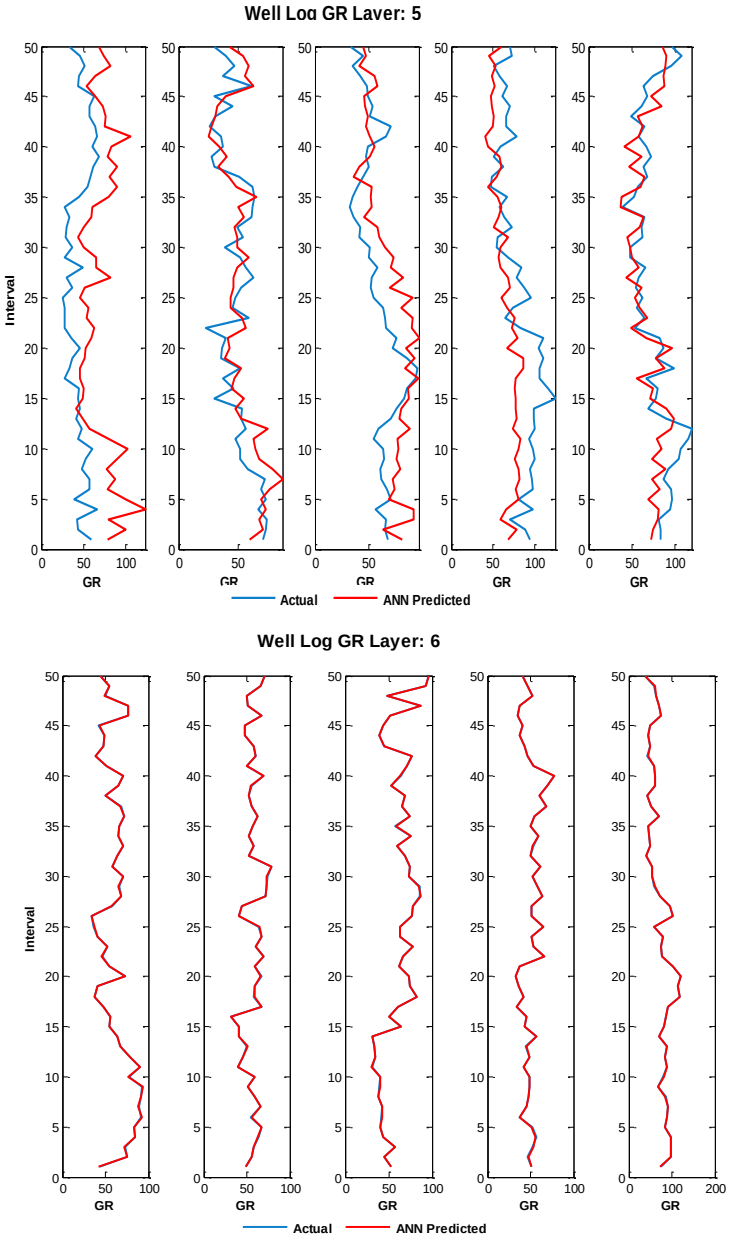
Well Log GR Layer: 5
Interval
GR
Actual
ANN Predicted
Well Log GR Layer: 6
Interval
GR
Actual
ANN Predicted

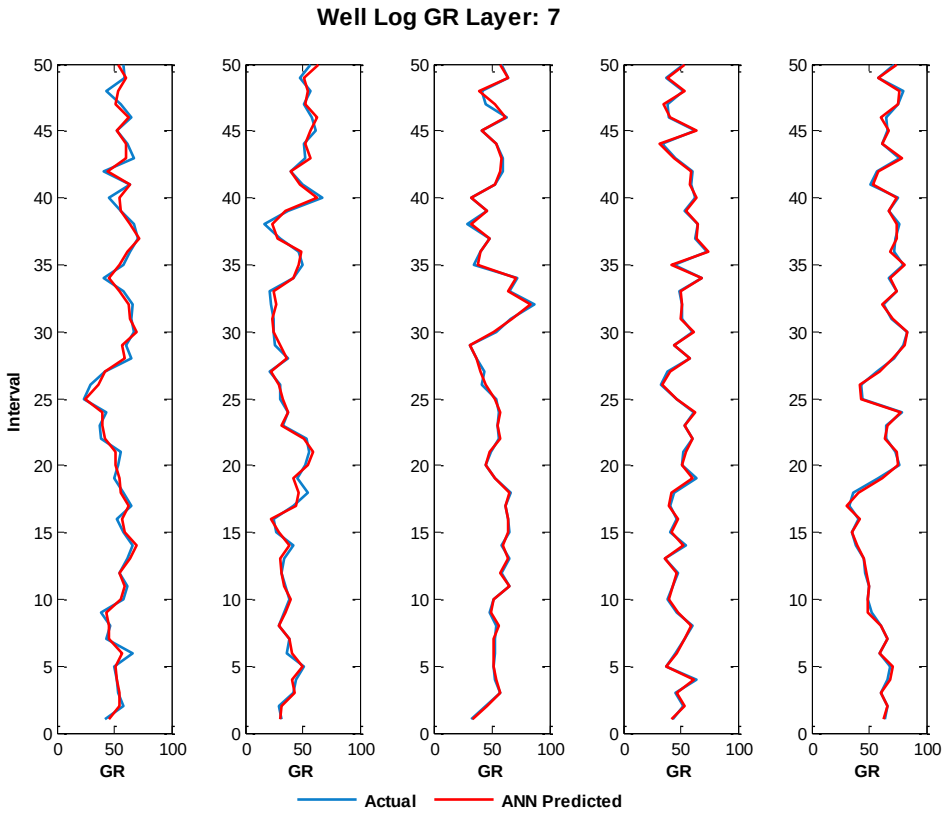

Normalized Gamma Ray Logs (GKUT_NRM)

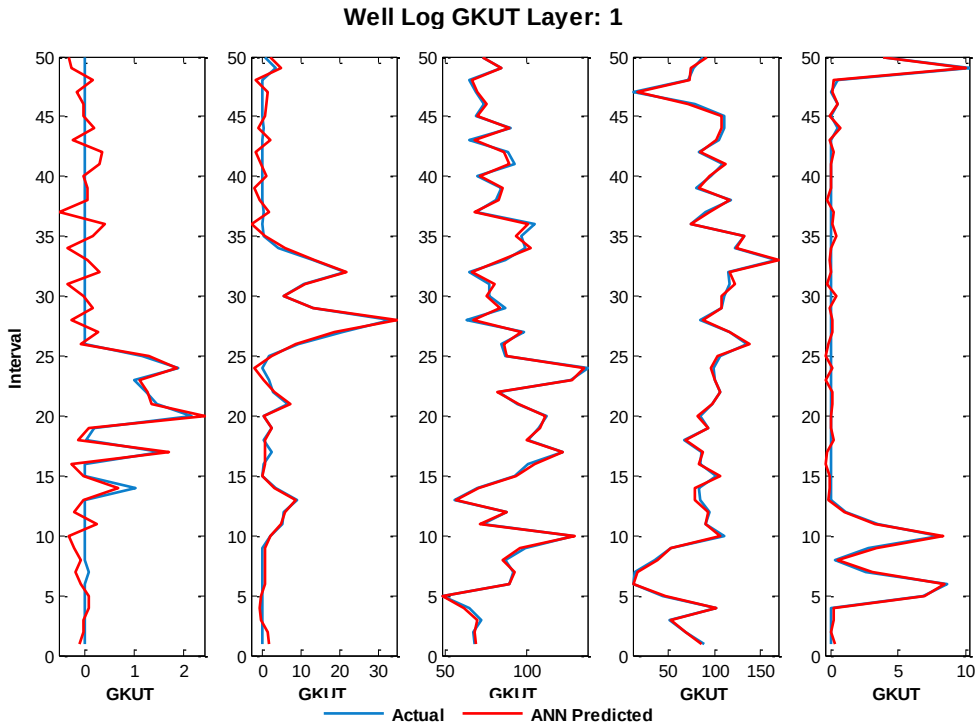

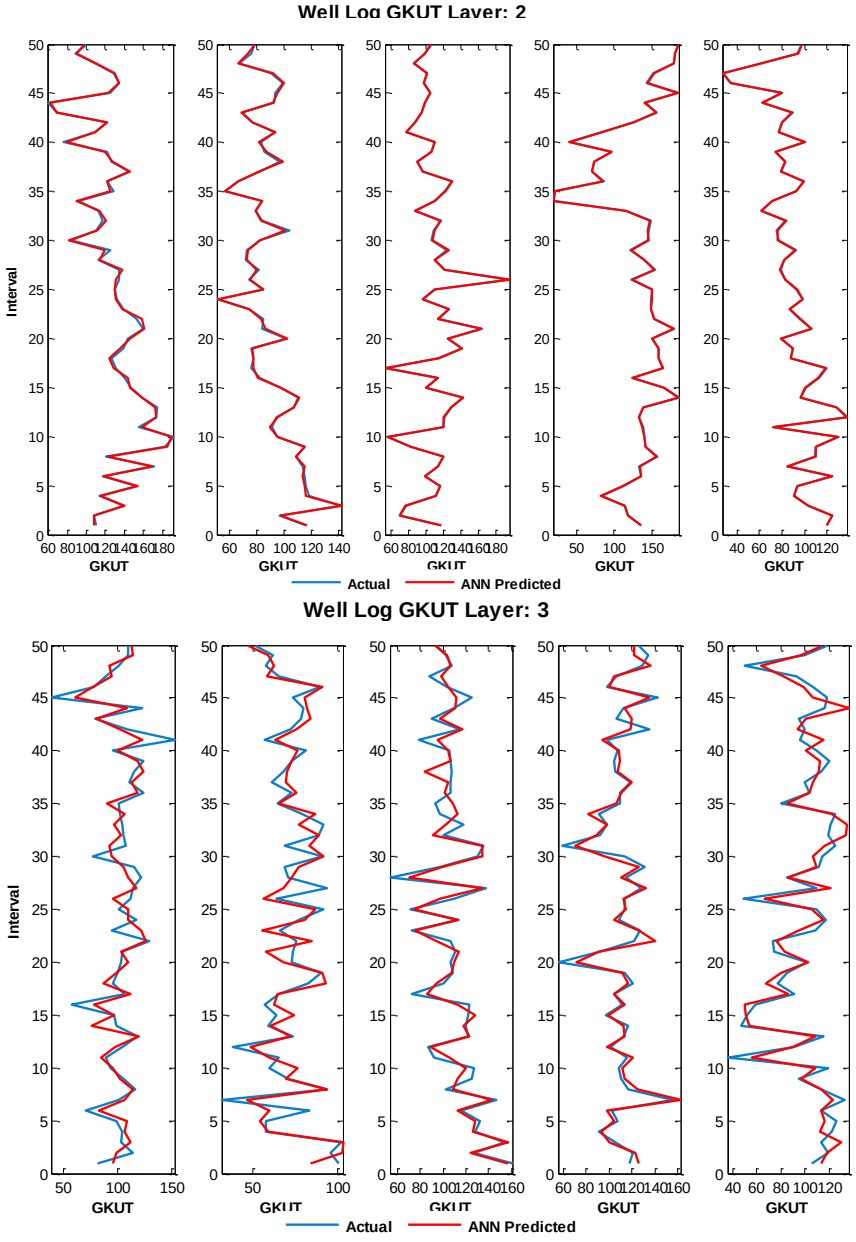
Well Log GKUT Layer: 2
Interval
GKUT
Actual
ANN Predicted
Well Log GKUT Layer: 3
Interval
GKUT
Actual
ANN Predicted

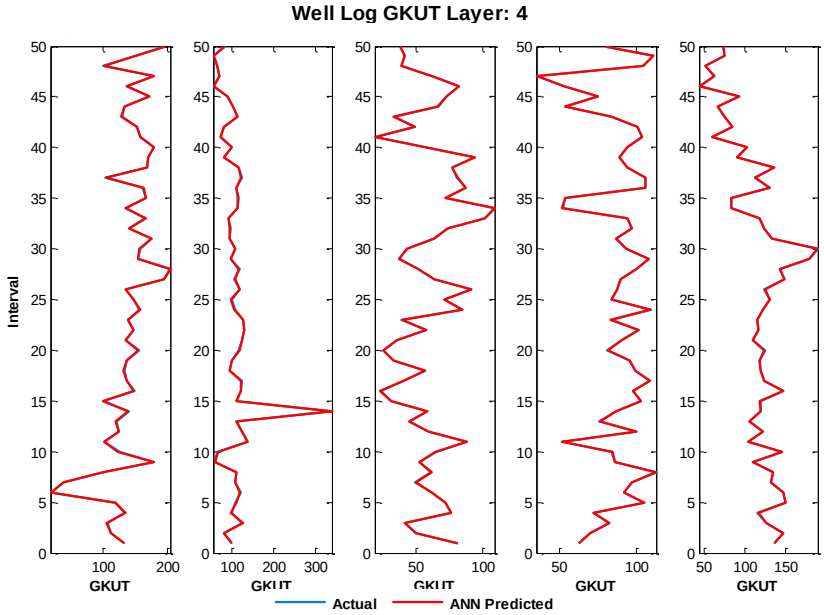
Well Log GKUT Layer: 4
Interval
GKUT
Actual
ANN Predicted

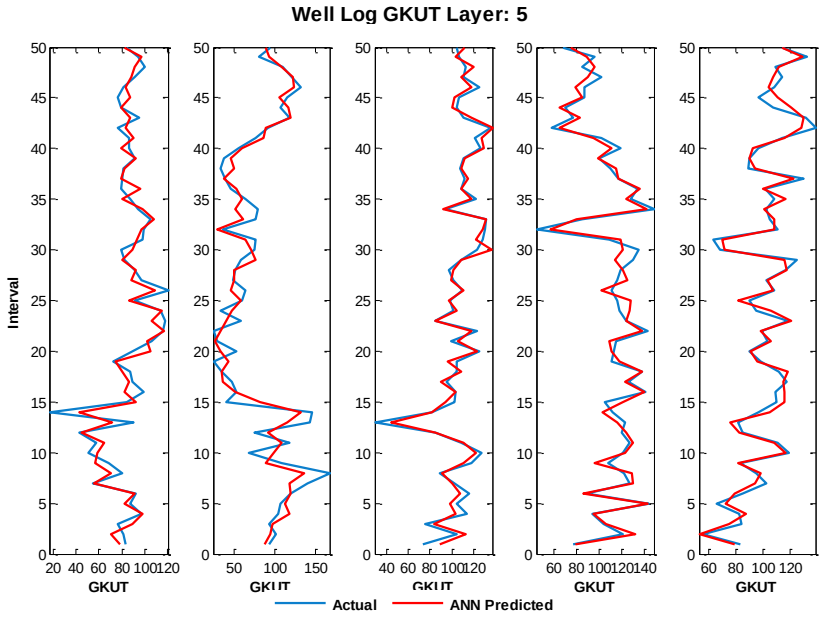
Well Log GKUT Layer: 5
Interval
GKUT
Actual
ANN Predicted

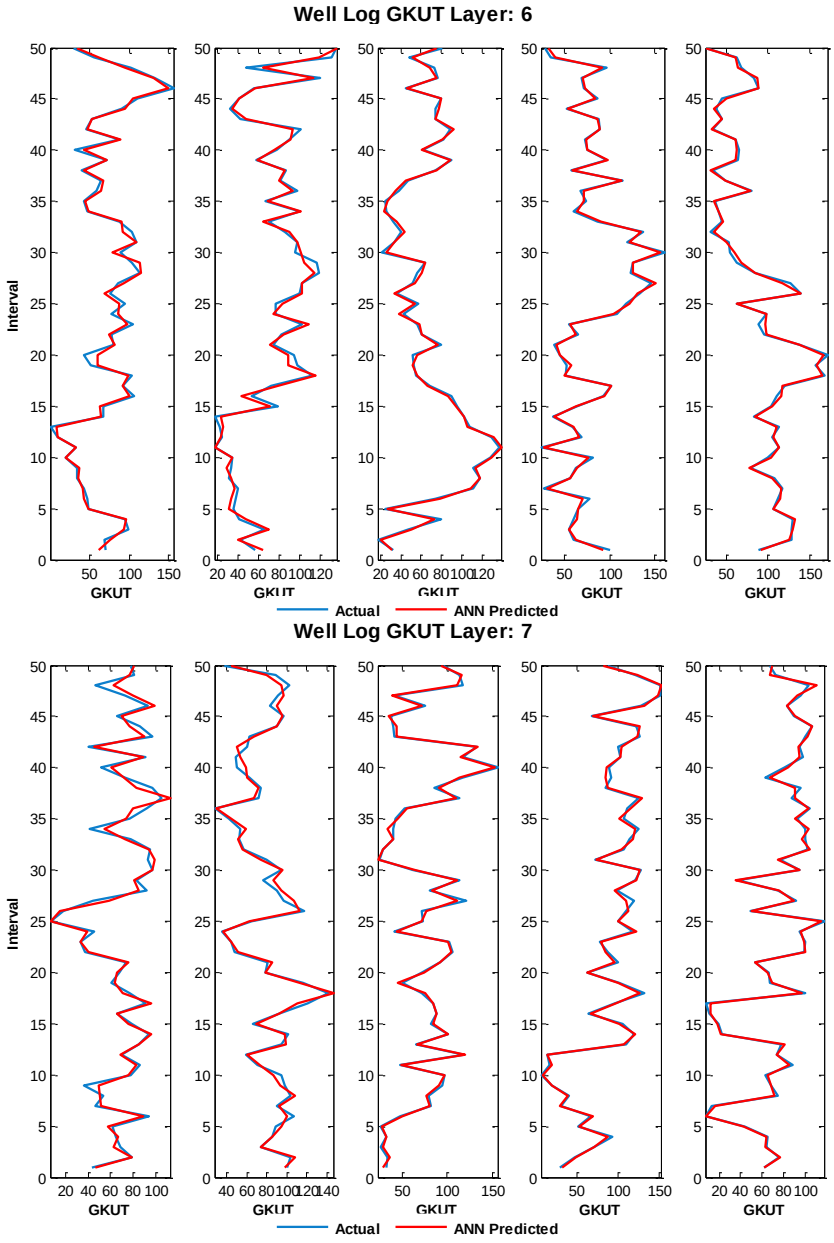
Well Log GKUT Layer: 6
Interval
GKUT
Actual
ANN Predicted
Well Log GKUT Layer: 7
Interval
GKUT
Actual
ANN Predicted

Neutron Porosity Logs (PHIN)

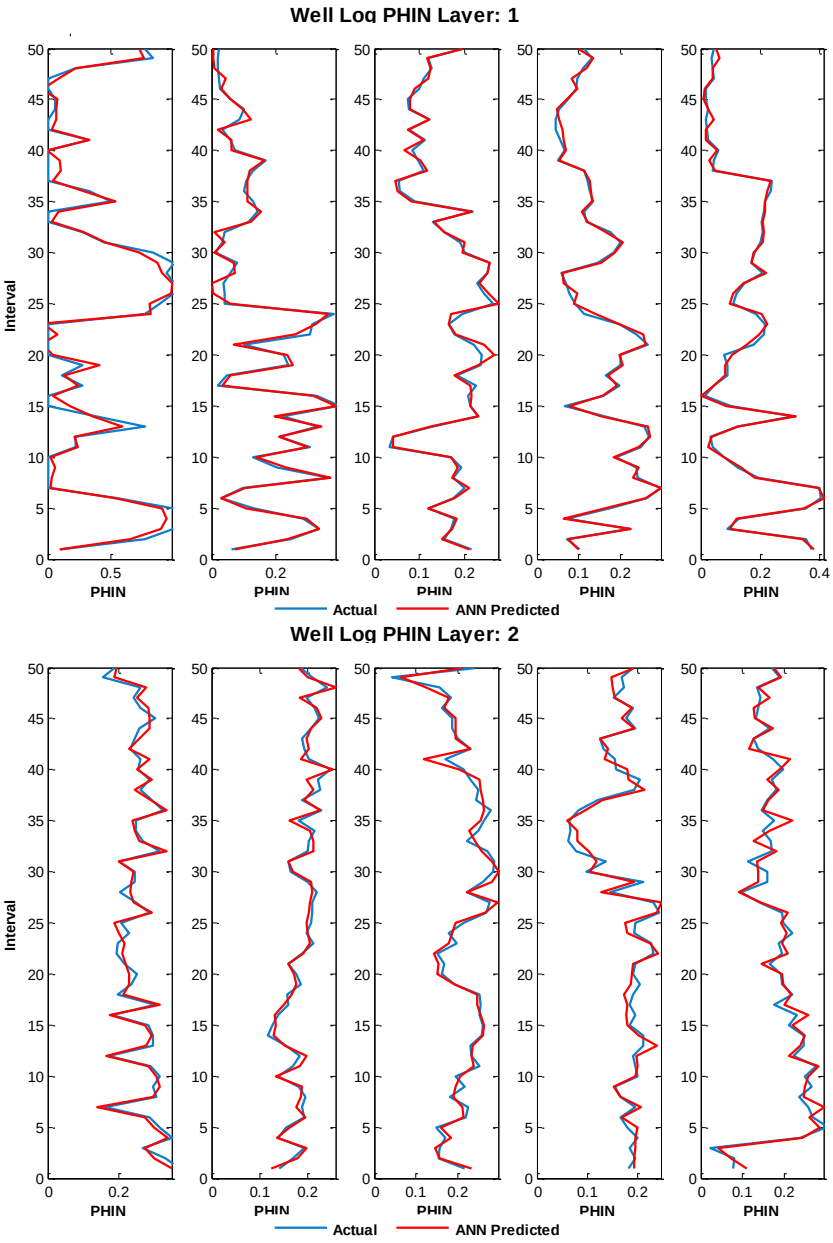

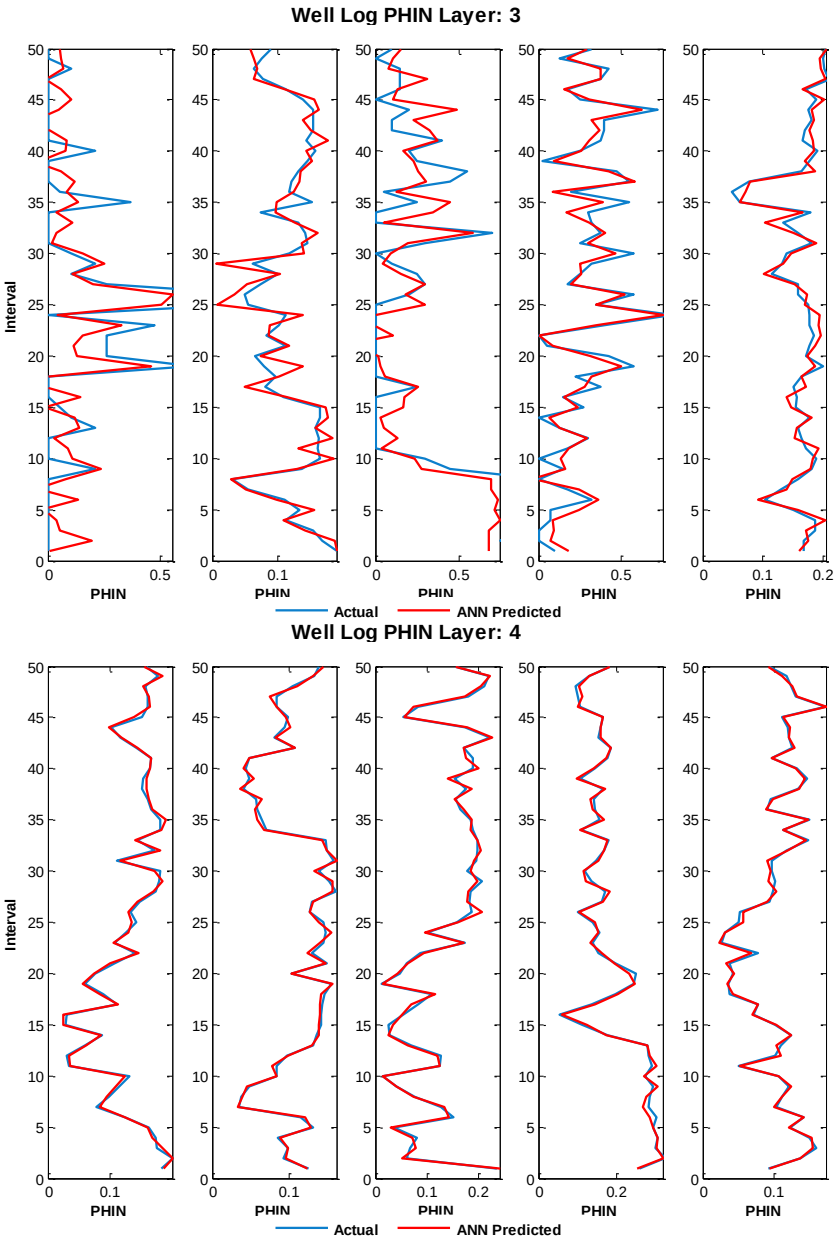
Well Log PHIN Layer: 3
Interval
PHIN
Actual
ANN Predicted
Well Log PHIN Layer: 4
Interval
PHIN
Actual
ANN Predicted

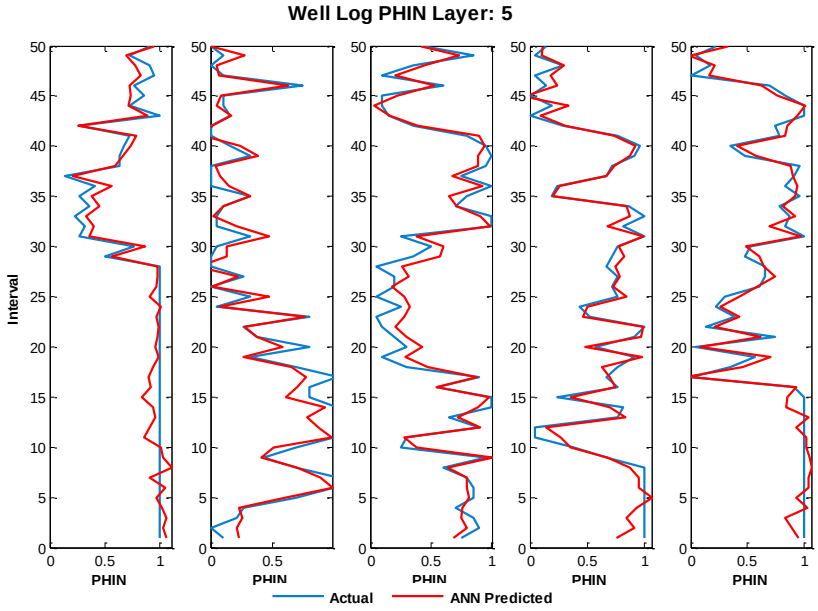
Well Log PHIN Layer: 5
Interval
PHIN
Actual
ANN Predicted

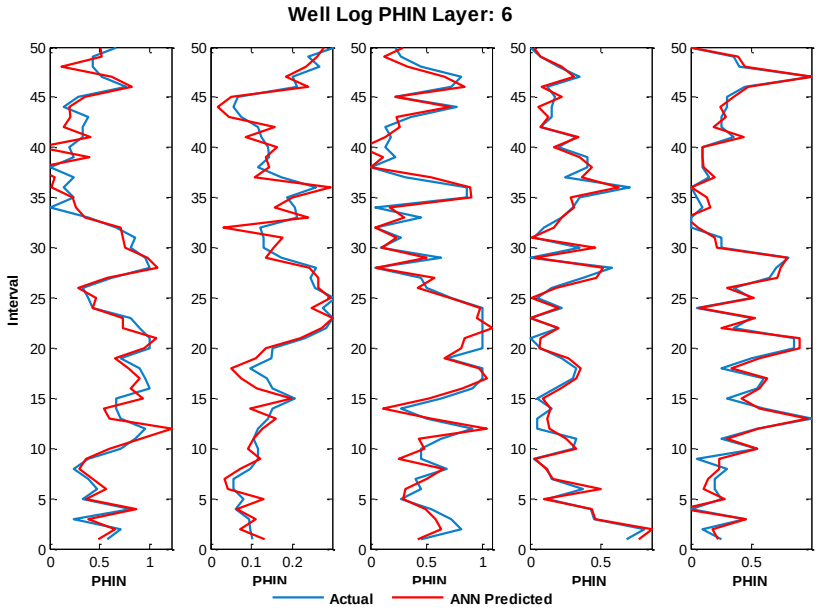
Well Log PHIN Layer: 6
Interval
PHIN
Actual
ANN Predicted

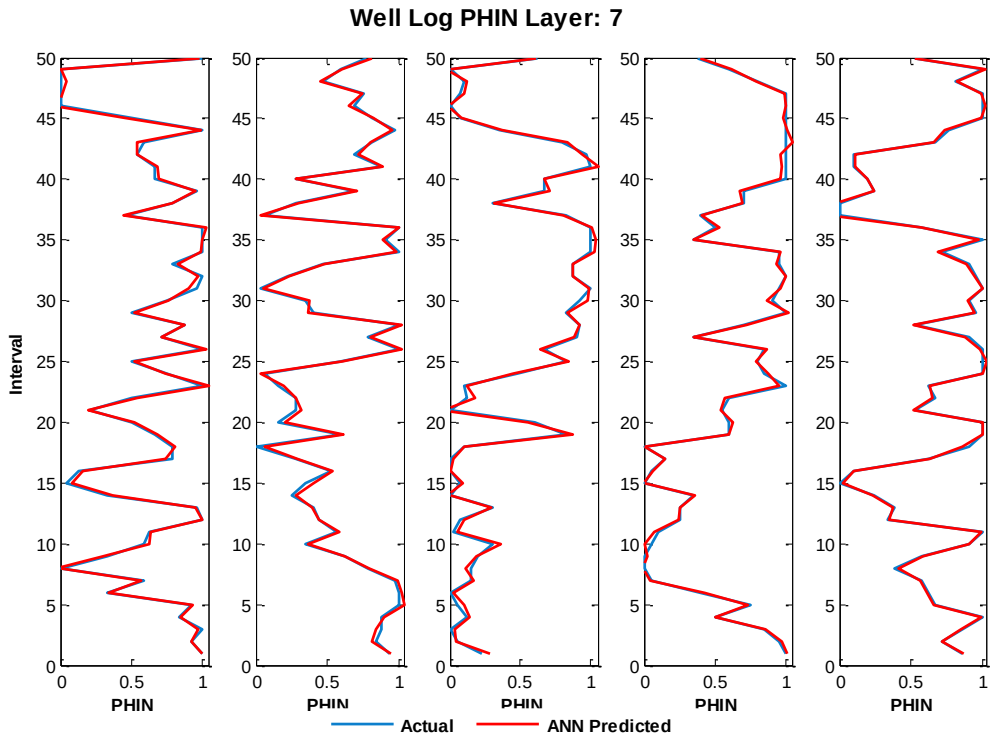

Long Space Neutron Count Rate Logs (LONG)

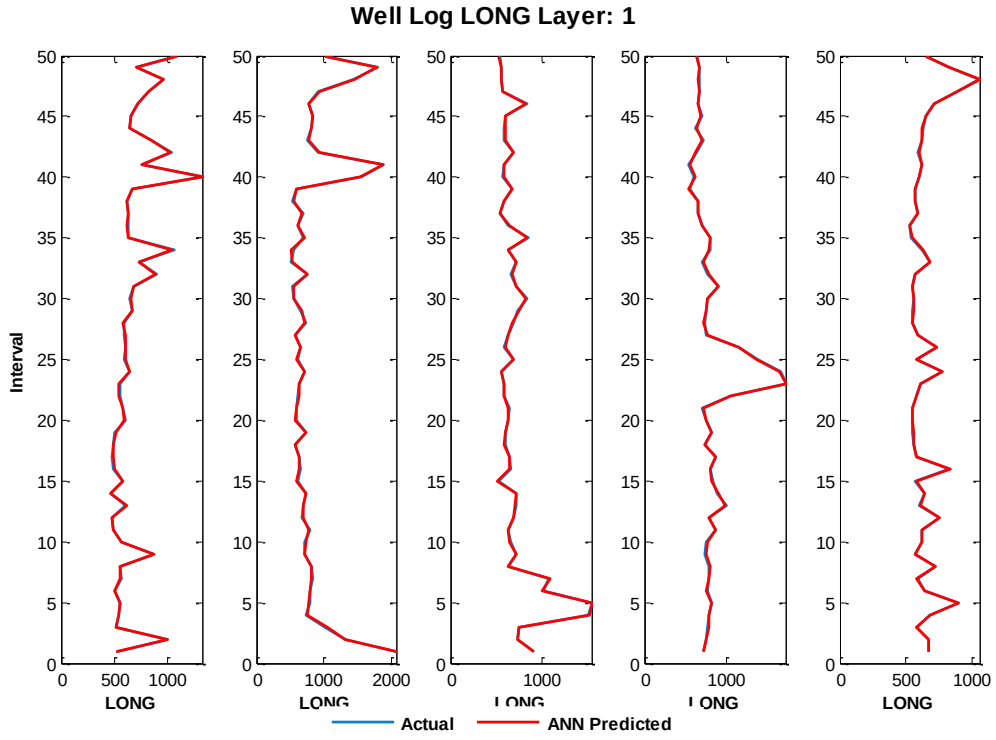

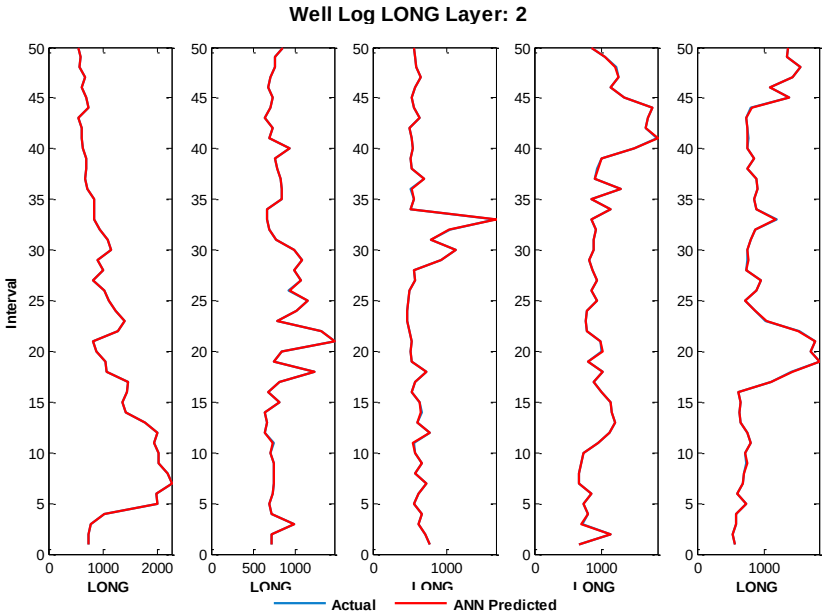
Well Log LONG Layer: 2
Interval
LONG
Actual
ANN Predicted

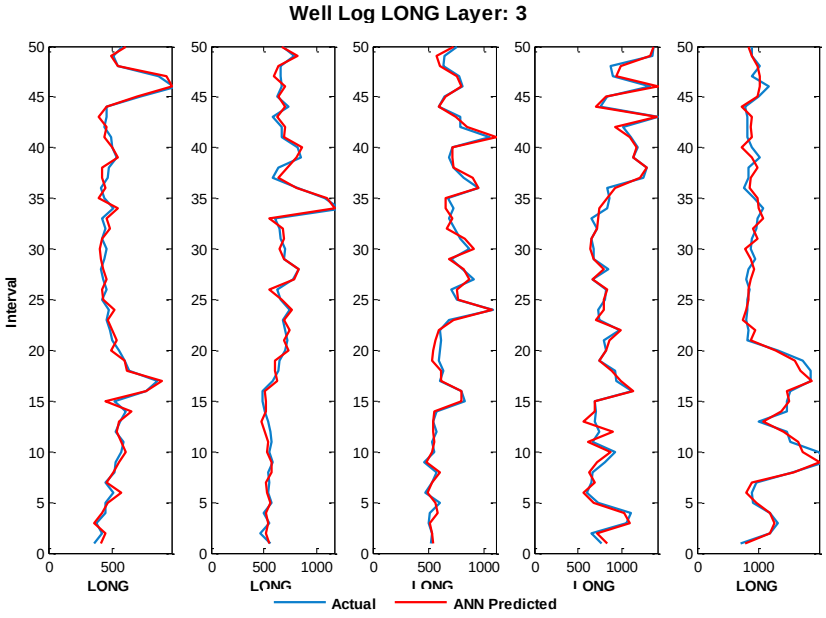
Well Log LONG Layer: 3
Interval
LONG
Actual
ANN Predicted

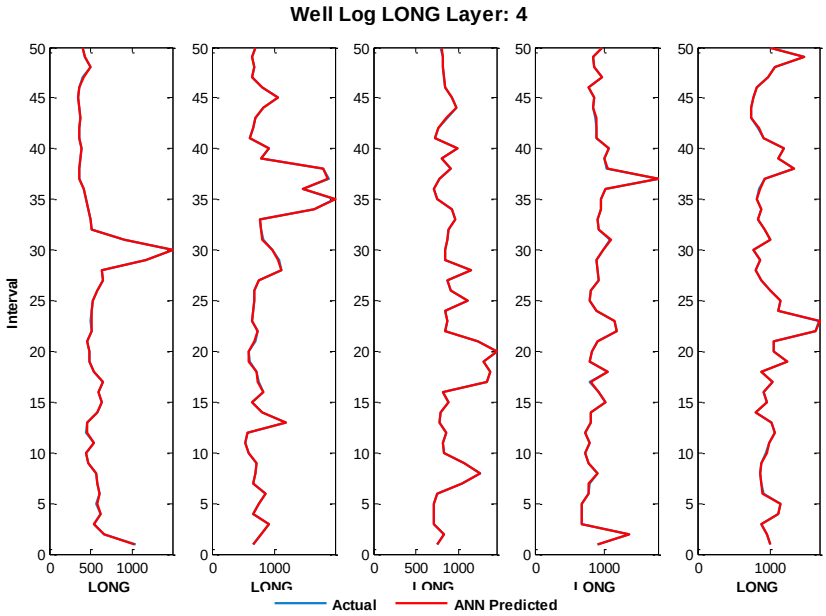
Well Log LONG Layer: 4
Interval
LONG
Actual
ANN Predicted

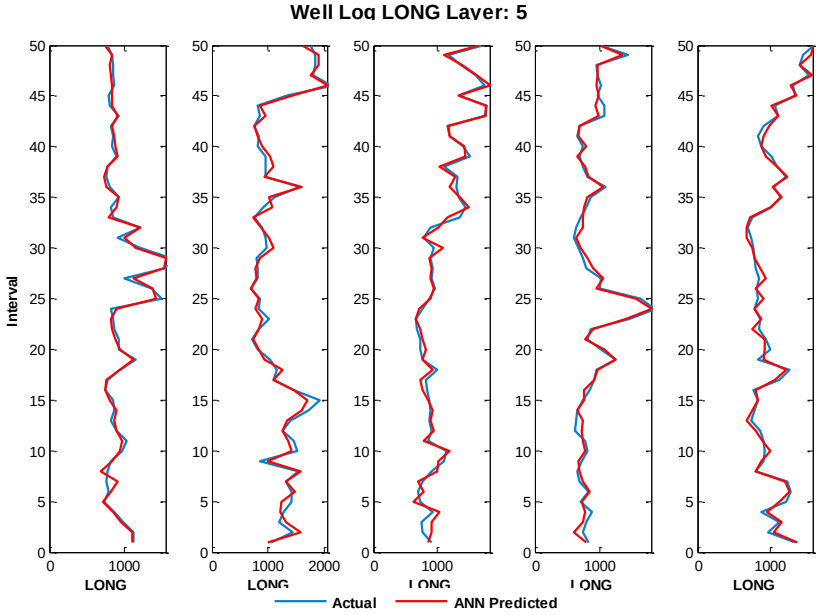
Well Log LONG Layer: 5
Interval
LONG
Actual
ANN Predicted

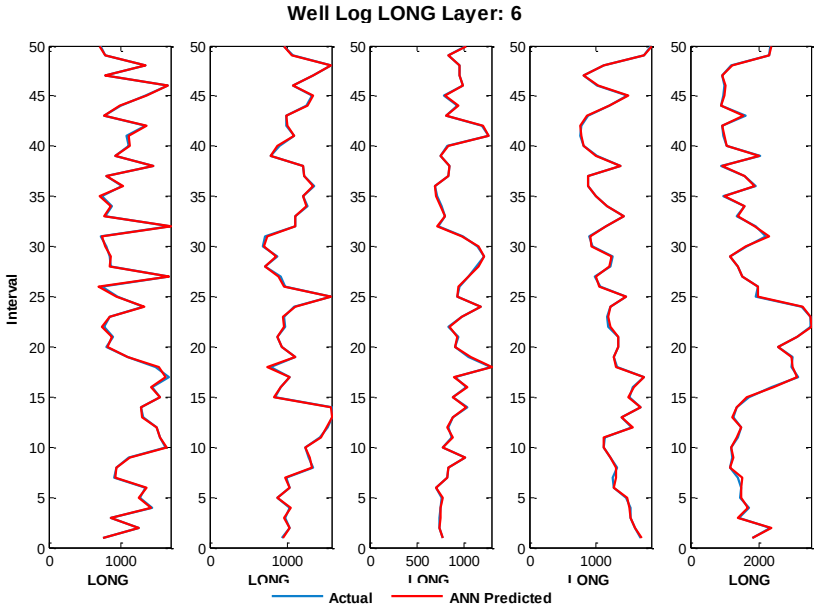
Well Log LONG Layer: 6
Interval
LONG
Actual
ANN Predicted

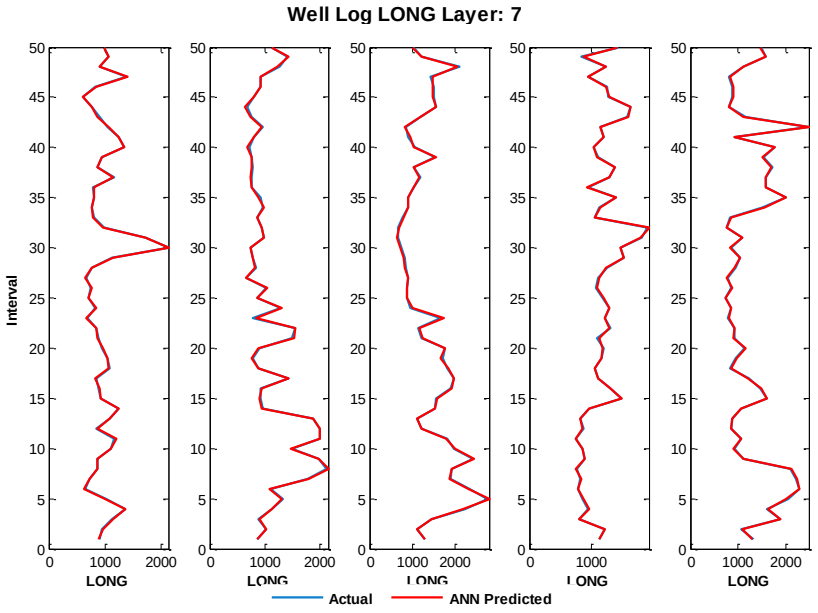
Well Log LONG Layer: 7
Interval
LONG
Actual
ANN Predicted

Short Space Neutron Count Rate Logs (SHORT)

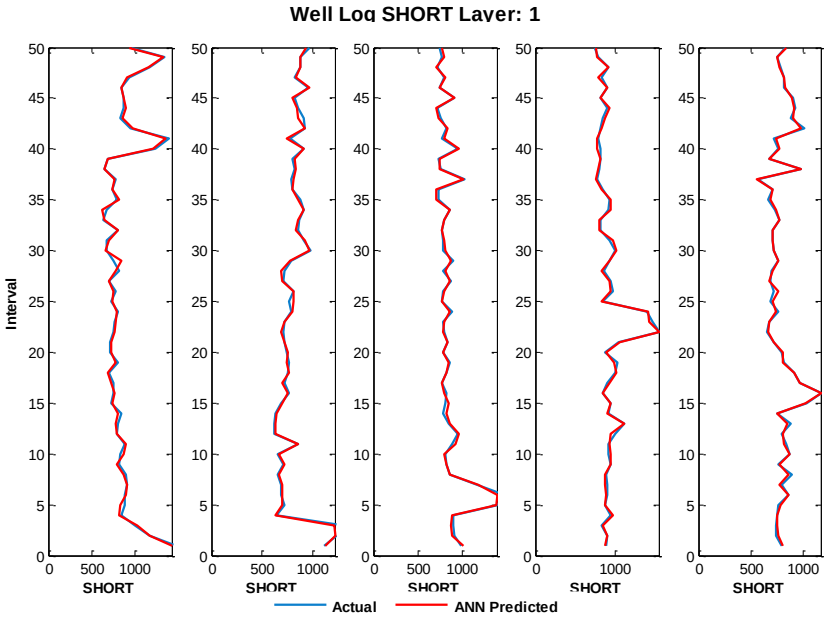

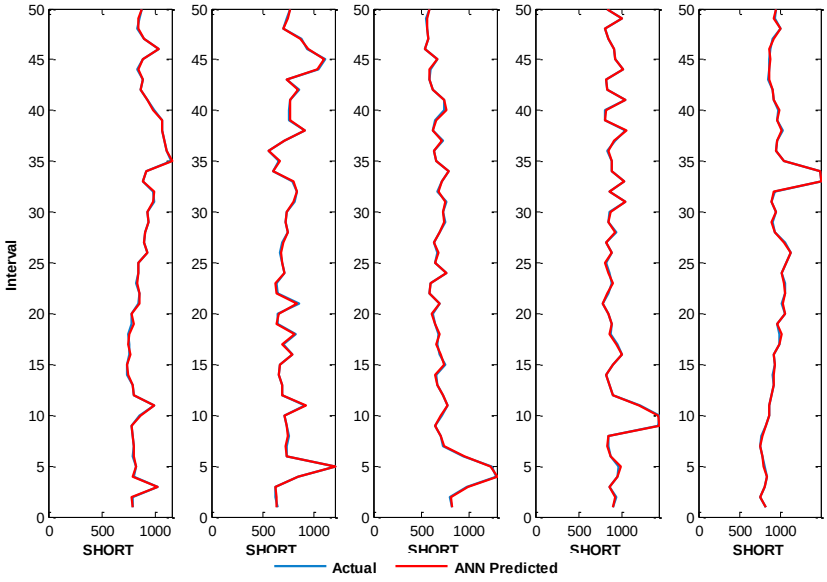

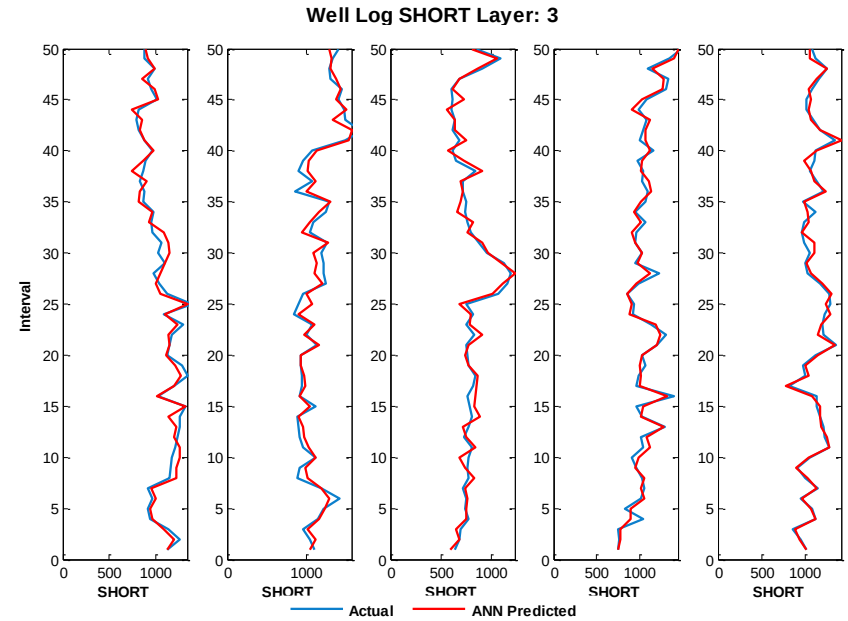
Well Log SHORT Layer: 3
Interval
SHORT
Actual
ANN Predicted

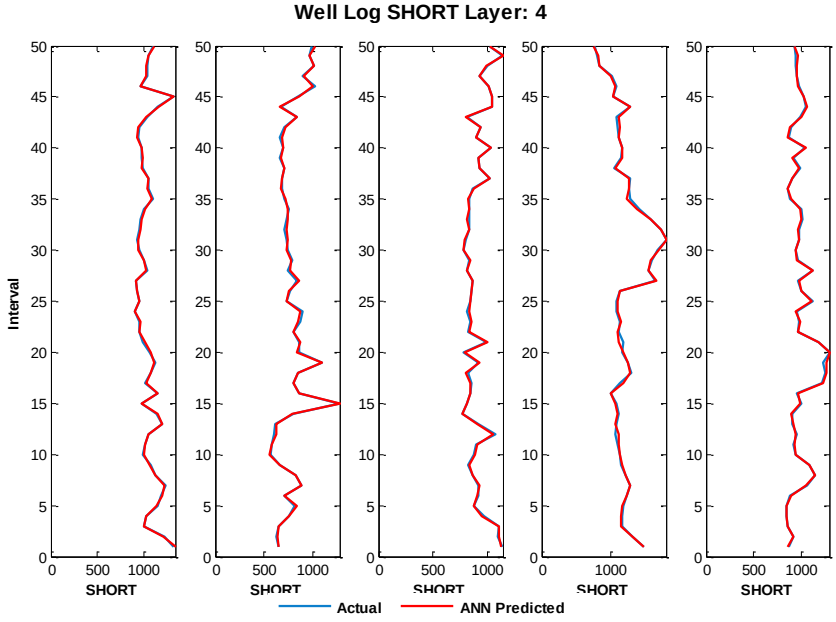
Well Log SHORT Layer: 4
Interval
SHORT
Actual
ANN Predicted

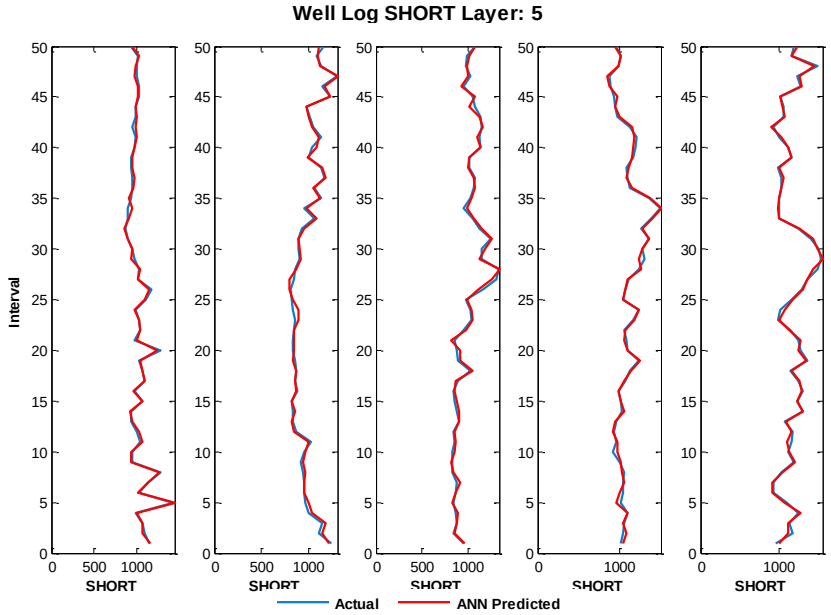
Well Log SHORT Layer: 5
Interval
SHORT
Actual
ANN Predicted

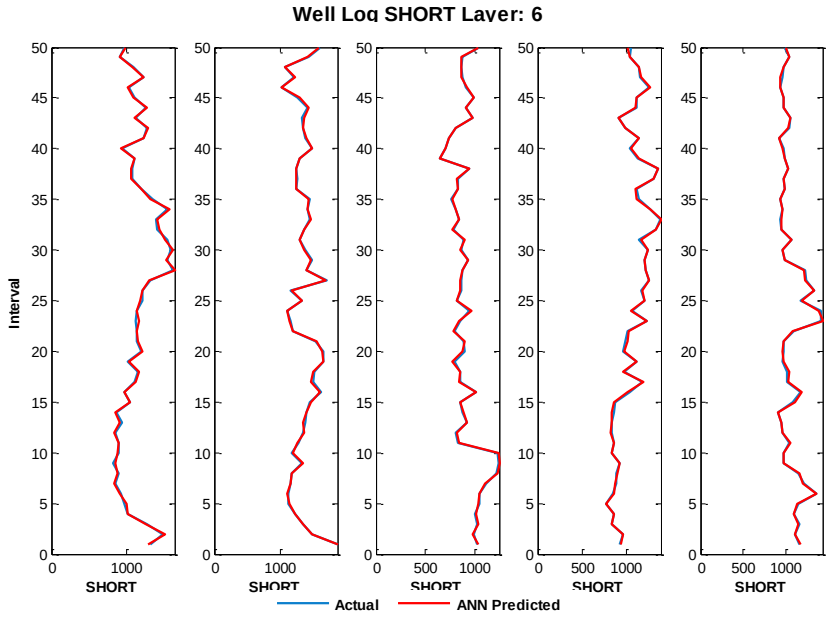
Well Log SHORT Layer: 6
Interval
SHORT
Actual
ANN Predicted

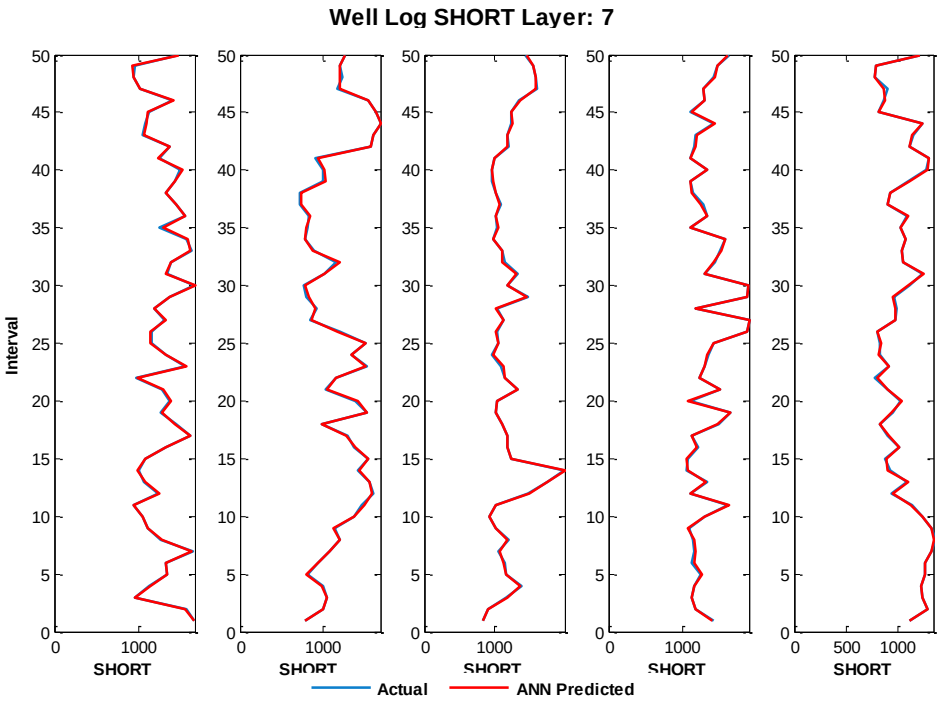
Well Log SHORT Layer: 7
Interval
SHORT
Actual
ANN Predicted

VITA

Amir Mohammadnejad Gharehlo

Amir Mohammad Nejad Gharehlo was born in Iran on January 1980. He graduated with bachelors in Chemical Engineering from Iran. After graduation, he came to Canada to study and work in University of Calgary. He received his masters in chemical engineering from that university. He then came to United State of America to study at University of Southern California. He worked in the center for smart oilfield technologies (CiSOFT) and learned IT aspect of oil exploration and production. After earning his master's degree in petroleum engineering, he then came to Pennsylvania State University to pursue his doctorate degree. He successfully defended his PhD on Dec 6, 2011 and he accepted reservoir-engineering position in CARBO Ceramics Company, located in Houston, Texas.